Mobile Sediments in a Karst Aquifer

Approved by
Dissertation Committee:

[redacted]

Philip Bennett, Supervisor

[redacted]

Mobile Sediments in a Karst Aquifer

by

Barbara June Mahler, B. Mus., M.A.

Dissertation

Presented to the Faculty of the Graduate School of

The University of Texas at Austin

in Partial Fulfillment

of the Requirements

for the Degree of

Doctor of Philosophy

The University of Texas at Austin

May, 1997

Dedication

To Barton Springs

Acknowledgements

A very long list of people helped make this research possible. To any whom I have inadvertantly forgotten, I apologize. I thank all my committee members for editorial assistance. In addition, Phil Bennett offered invaluable help throughout the project, from laboratory wizardry (which included making sure that the injectorator and spargeroo were operating properly) to general perspective. Special thanks to David Johns and Nico Hauwert for tips on local geology and offerings of dirt. Leo "Claynac" Lynch, king of XRD, contributed hugely to the research with data, ideas, and exhortations. MaryLynn Musgrove was a superb student editor. Many thanks to particle-counting stars Annika Van Gelder, Jie "Jessie" Li, and Desmond Lawler. The hard-working field cohort included Sylvia Pope, Alisa Remington, MaryLynn Musgrove, Phil Bennett, Bill Bunch, Mike Harren, Mark Kirkpatrick, Tim Jones, and Leo Lynch. Robert Hansen and John Tyree helped make possible sample collection at Barton Springs Pool. Byron Townsend, Mike Dorsey, and the staff of the City of Sunset Valley helped in collection of well samples. Laboratory whizzes Todd Minehardt and Mitch Zimmerman kept the HPLC fed and happy. Todd Minehardt, in addition, gave vast moral support, along with Jim Mayer, over Quax cappuccinos. Finally, none

of this would even have been dreamed of, let along embarked upon and brought to the finish line, without Mark Kirkpatrick, who celebrated small victories, took seriously epiphanies, listened in times of discouragement, provided perspective in times of faux-crises, and provided more understanding, encouragement, and support than could possibly be expected of any husband.

Mobile Sediments in a Karst Aquifer

Publication No._____

Barbara June Mahler, Ph.D.

The University of Texas at Austin, 1997

Supervisor: Philip Bennett

In karst aquifers, mobile sediments may play a fundamental role in determining water quality by concentrating and transporting contaminants. This study investigates spatial characteristics of sediment in a karst aquifer, examines temporal characteristics of sediment discharging from a karst spring, and describes a new method for tracing sediment in karst terrane.

Sediment samples were collected from different compartments of a karst aquifer (the Edwards Aquifer, Central Texas) and analyzed for mineralogy, grainsize distribution, organic carbon content, and specific surface area. Suspended sediment samples discharging from a karst spring in response to two storms were analyzed for mineralogy and grainsize distribution. To test the hypothesis that allochthonous sediment can move through karst systems, a sediment tracer—montmorillonite clay homoionized to the lanthanide form—was developed.

Statistical analysis of sediment characteristics separated the sampling sites into three groups: 1) streambeds, sinkholes, and small springs; 2) wells; and 3) caves. Characteristics of sediments from Barton Springs (the main spring in the region) showed a mixture of the characteristics of these three groups. The mineralogic signature of sediments discharging from Barton Springs in response to storms was initially allochthonous and then became more autochthonous. Temporal changes in aqueous chemistry of Barton Springs varied in response to rainfall, seasonal changes in aquifer level, and draining of the pool over the spring.

The results indicate that some sediments, containing calcite and a high organic carbon content, are allochthonous, and others, containing dolomite and a low organic carbon content, are autochthonous. Sediments issuing from Barton Springs contain a mix of both allochthonous and autochthonous sediments. Based on geochemical characteristics, allochthonous sediments have a greater potential to sorb and transport contaminants than do autochthonous sediments. Development and testing of the sediment tracer verified that allochthonous sediments can be transported through karst.

Sediments, particularly allochthonous sediments, can play a crucial role in contaminant transport in karst; the volume of these sediments will increase with increasing urbanization. Because those sediment characteristics which determine contaminant transport potential vary both spatially and temporally, determination of sediment volume and type is critical to evaluating its impact on water quality.

Table of Contents

List of Tables xi

List of Figures xii

Preface 1

Chapter 1. Characteristics of Mobile Sediment in an Urbanizing Karst Aquifer 4

Introduction 4

Geology and Hydrogeologic Framework 11

Methodology 16

Results 20

Discussion 30

Allochthonous vs. Autochthonous Sediments 36

Contaminant Transport Potential 46

Implications 49

Conclusion 52

Chapter 2. Muddy Waters: Temporal Changes in Characteristics of Sediment Discharging from a Karst Spring 55

Introduction 55

Study Area: Hydrogeologic Setting 59

Methods 68

Sample Collection 68

Analyses 71

Results 74

Precipitation and Discharge 74

Particulates 74

Aqueous Chemistry 83

Discussion 85

Suspended Solids 86
Aqueous Chemistry 91
Implications 95
Conclusions 98

Chapter 3. Lanthanide clay: A New Sediment Tracer for Use in Karst Terranes 101
Introduction 101
Materials and Methods 105
Preparation of the Lanthanide Montmorillonite 105
Laboratory Batch Tests 107
Lanthanide Detection and Quantification 108
Field Tracer Tests 109
Results 113
Tracer stability and detection 113
Surface Water Sediment Tracing 115
Subsurface Sediment Tracing 118
Discussion 120
Chemistry of Lanthanide-clays 121
Field Sediment Traces 123
Lanthanide-Clays as Particle Tracers 125
Implications 128
Conclusions 129

Appendix A. Barton Springs Aquifer Sample Descriptions 131

Appendix B. Geochemistry of Barton Springs Aquifer Samples 134

Appendix C. Geochemistry of Barton Springs Suspended Sediment Samples .. 141

Appendix D. Aqueous Chemistry of Barton Springs Water Samples 143

Bibliography 159

Vita 168

List of Tables

Table 1.1. Total petroleum hydrocarbon (TPH) concentrations for selected samples. 28

Table 1.2. Correlation coefficients for sediment characteristics grouped by site type. 31

Table 1.3. Results of discriminant function analysis. 33

Table 1.4. Between-groups significance from discriminant function analysis. 34

Table 1.5. Changes in the hydrologic cycle associated with urbanization. 50

Table 3.1. Extant particle tracers and characteristics 103

Table 3.2. Physical characteristics of the montmorillonite, Swy-2, used in the tracer experiments. 106

Table 3.3. Chemistry of the solutions used to test stability of the lanthanide-clay in batch experiments. 108

Table 3.4. Travel-time data for water and particle tracers in Waller Creek, Austin, Texas. 117

List of Figures

Figure 1.1. Location of the three segments of the Edwards Aquifer in Central Texas. 10
Figure 1.2. The Barton Springs watershed and aquifer. 12
Figure 1.3. Conceptual cross-section and hydrostratigraphy of the Barton Springs Aquifer. 14
Figure 1.4. Locations of sampling sites. 17
Figure 1.5. Whole rock mineralogy of samples. 21
Figure 1.6. Ternary diagram of Edwards rock and Del Rio Clay whole rock mineralogy. 23
Figure 1.7. Box plots of sediment characteristics. 25
Figure 1.8. Results of Kruskal-Wallis test for differences in populations. 26
Figure 1.9. Comparison of sediment sample organic carbon content and specific surface area. 27
Figure 1.10. Gas chromatograms for TPH analysis. 29
Figure 1.11. Conceptual diagram of sediment compartments and flow systems in the Barton Springs Aquifer. 35
Figure 1.12. Scanning electron microscope photomicrograph of a "hollow box" dolomite grain from a well in the unconfined zone. 37
Figure 1.13. Comparison of arithmetic sample skewness (SkA) and median diameter to grainsize deviation (SA). 44
Figure 2.1. The three segments of the Edwards Aquifer, Texas. 60
Figure 2.2. The zones of the Barton Springs Aquifer and watershed. 62

Figure 2.3. Schematic cross-section of the Barton Springs Aquifer and the hydrogeologic stratigraphy of the members. 63
Figure 2.4. Potentiometric surface of the Barton Springs Aquifer under contrasting aquifer conditions..... 66
Figure 2.5. Schematic diagram of Barton Springs Pool. 67
Figure 2.6. Discharge from Barton Springs for Storm 1 (November, 1995) and Storm 2 (May-June, 1996). 75
Figure 2.7. Changes in total suspended solids and mineralogy in response to storm events. 76
Figure 2.8. Sediment flux from Barton Springs in response to Storms 1 and 2...77
Figure 2.9. Particulates discharged from Barton Springs after a storm. 79
Figure 2.10. Changes in the mineralogic composition of sediments discharging from Barton Springs in response to Storms 1and 2. 81
Figure 2.11. Representative particle-size distributions for Storms 1 and 2. 82
Figure 2.12. Changes in volume of particles of both small- and large-size populations in response to rainfall. 83
Figure 2.13. Changes in aqueous chemistry in response to rainfall and pool draining. 84
Figure 2.14. Depiction of conditions of sediment deposition and transport..... 88
Figure 2.15. Creek discharge at Barton Creek and Loop 360 for Storm 2. 91
Figure 2.16. Variations in the relation between sulfate and chloride concentration and strontium and sodium concentration. 93
Figure 3.1. HPLC response peaks..... 110

Figure 3.2. Locations of surface water and groundwater traces. 111

Figure 3.3. Concentration-time curves for the water and particle tracers in Waller Creek, Austin, Texas. 116

Figure 3.4. Travel-time curves for the water and particle tracers in Waller Creek, Austin, Texas 118

Figure 3.5. Breakthrough curves for groundwater tracing test. 119

Figure 3.6. Hypothetical geometry of the Salado conduit system. 124

Preface

This dissertation focuses on the phenomenon of sediment transport through karst aquifers. Although sediment transport in surface water has been well-studied, in groundwater the solid phase has generally been assumed to be limited to the immobile aquifer matrix. In addressing a mobile particulate phase, this study represents a new contribution to the concept of subsurface flow in karst. The dissertation is organized as three independent chapters, each of which addresses a different aspect of mobile sediments in karst. The first chapter presents an overview of sediment compartments in a karst aquifer, the characteristics and behavior of the sediments in those compartments, and the resulting implications for contaminant transport. The second chapter describes in detail the temporal changes in characteristics of suspended sediments discharging from a karst spring in response to a storm event. The third chapter describes a new sediment tracer with valuable potential for further investigation of sediment transport in karst.

The first chapter characterizes sediments across a karst aquifer (the Barton Springs segment of the Edwards Aquifer of Central Texas) and evaluates their potential role in contaminant fate and transport. Sediments were collected from 1) streambeds and sinkholes, representing the watershed surface; 2) wells and caves, representing the interior of the aquifer; and 3) springs, representing aquifer discharge. Based on analysis of sediment characteristics, including mineralogy, organic carbon content, and specific surface area, sediments are classified as

allochthonous (originating outside of the aquifer) or autochthonous (originating from the interior of the aquifer). The potential role of these sediments on the fate and transport of contaminants currently found in the aquifer is assessed, and the probable effect of continuing urbanization discussed.

The second chapter details temporal changes in the geochemical characteristics of both sediment and water discharging from a karst spring in response to a storm. Prior to this study, the composition and characteristics of suspended sediments discharging from a karst spring had not been investigated as thoroughly as is done here. The spring was monitored intensively after two storms, one which occurred during a period of normal rainfall and one which occurred after an extended period of low rainfall. Changes in sediment concentration, mineralogy, and particle size distribution are analyzed and used to determine sediment origin. Concommittal analyses of spring water chemistry demonstrate the importance of aquifer level on water chemistry.

The third chapter presents a new method for tracing sediment which should prove to be particularly valuable in karst aquifers. The tracer—montmorillonite clay homoionized to a lanthanide form—has several advantages over existing particle tracers: 1) its detection is automated and detection limits are extremely low; 2) its characteristics mimic those of natural sediment; 3) it is available with multiple signatures to avoid cross-interference; and 4) it is environmentally benign. Results of field tests in both surface and subsurface flow are presented. This tracer will aid in future studies to determine sediment source, travel time, and storage.

It is hoped that this work will alert the hydrogeologic community to the presence of mobile sediment in karst aquifers, to its potential importance in the fate and transport of contaminants, and to a new method for further investigating the behavior of sediment in the subsurface.

Chapter 1. Characteristics of Mobile Sediment in an Urbanizing Karst Aquifer

INTRODUCTION

This study characterizes sediments in a karst aquifer and evaluates their potential importance in contaminant fate and transport. Mobile particulates play a fundamental role in determining water quality. Sediment is itself a contaminant; it also profoundly affects the transport and fate of other contaminants. The impact of mobile sediment on contaminant transport in surface water systems is well-documented, but its importance in groundwater systems is less recognized. In porous-media aquifers the solid phase is regarded as immobile; sorption and partitioning to immobile solid phase surfaces retard contaminant transport. In the last decade, researchers have begun to include a mobile, colloidal solid phase in contaminant transport models (e.g., McCarthy and Zachara, 1989; Pankow and McKenzie, 1991; Saiers and Hornberger, 1994). In karst aquifers, sediment can be mobile: large pore diameters and rapid flow velocities result in turbulent flow and the transport of particles in a wide range of sizes (White and White, 1968; Bögli, 1980; Gale, 1984; White, 1988; Thrailkill, 1989). Mobile sediment may act as a vector for contaminant transport (Ford and Williams, 1989), particularly for poorly soluble compounds, including from metals and hydrocarbons (McCarty et al., 1981; Smith, 1988; Schwarzenbach et al., 1993).

Karst aquifers are an important source of potable water worldwide: 20% of the U.S. is underlain by soluble, primarily carbonate rock (Mull et al., 1988),

and it is estimated that karst aquifers supply drinking water to 25% of the global population (Ford and Williams, 1989). Groundwater in karst, however, is more susceptible to pollution than is groundwater in any other geologic terrane. This sensitivity of karst to human activity, in particular landuse, is a result of 1) thin overlying soils, which are poor filtering agents and allow rapid infiltration, 2) lack of granular texture within the aquifer, which inhibits mechanical filtration as a self-purification mechanism, and 3) a short residence time for flow, which reduces the time possible for biological purification processes (White, 1988). The highly localized, heterogeneous, and anisotropic permeability of karst combined with turbulent flow make karst systems notoriously difficult to model (Yevjevich, 1981).

Researchers have long been intrigued by the presence of mobile sediments in karst aquifers (e.g., Bretz, 1942). White and White (1968) postulate that gravel and sand are transported through cave systems as bedload while clay is transported as suspended load. White (1988) suggests that rapid facies changes in cave sediments are evidence of stream flow "subject to large annual fluctuations," and states that "transport in caves is highly episodic ... little is known of the actual transport rates [of sediments] or how the loads are distributed among flood pulses of various magnitudes." Ford and Williams (1989) report the transport of pebbles up to 10 cm in diameter up a 7.5 m vertical shaft. Thrailkill (1989) suggests that shallow conduit-flow carbonate aquifers may both transport and store surface sediments, and that these sediments may play a role in the fate of contaminants.

Despite this interest in mobile sediments in carbonate aquifers, only a few researchers have characterized the actual sediment material. Gale (1984) used hydraulically transported sediments in caves to determine the hydraulic conditions in groundwater conduits during flood flow. He used the particle size distribution of the sediments to calculate mean values for a variety of hydraulic parameters. White (1977) used infrared spectroscopy to group different surface and cave sediments based on their spectral reflectance, which is influenced by their iron content. He found that differences in sediments in Mammoth Cave suggested two different sources, but he was unable to determine if the cause was a major change in source area during a point in cave development or the back-flooding of the cave by the adjacent Green River. Frank (1965) studied sediments from eleven Central Texas caves. He noted the presence of red clay, composed primarily of quartz and kaolinite, and a fine, moderately-sorted dolomite silt. He later investigated sediments in a small (50 m^2) cave in Australia (Frank, 1969), analyzing clay mineralogy in fourteen samples to interpret variations in climate affecting surface soils.

No studies have been undertaken to characterize sediments in karst from the standpoint of environmental impact. Mobile sediments in karst aquifers are of concern for several reasons: their deposition within the aquifer may decrease aquifer permeability, fill in wells, and cause pumps to seize; their deposition at spring mouths may destroy species habitat; their presence impairs the esthetic appearance of spring water; and they may act as vectors for nutrient or contaminant transport. Sediments in karst originate both at the surface

(allochthonous) and within the aquifer (autochthonous). Allochthonous sediments filter in through small crevices and openings at the surface, wash in through sinking streams, and are in some cases even pushed into the system during backflooding (White and White, 1968; Ford and Willaims, 1989). Autochthonous sediments, in contrast, are derived from weathering within the subsurface as the dissolution network is enlarged.

Sediments may transport contaminants into and through the aquifer. Many contaminants sorb onto solid surfaces in concentrations orders of magnitude greater than that of their equilibrium concentration in the aqueous phase. The degree to which this occurs for an individual contaminant is a function of the organic carbon content, specific surface area, and mineralogy of the sediments. Contaminants sorb to mineral particles largely through one of two mechanisms: partitioning into organic matter coating the particle, and direct sorption to the mineral surface. Both neutral and ionizable organic chemicals can partition into organic matter and adsorb to polar mineral surfaces (Smith et al., 1988; Schwarzenbach et al., 1993). Metallic ions are adsorbed into clay layers and onto oxide and carbonate surfaces by ion exchange (McCarthy and Zachara, 1989).

The capacity for sediment particles to sorb neutral organic contaminants is highly correlated with the organic carbon content of the particles. Competing sorption mechanisms are insignificant when the fraction of organic carbon of the particle (f_{oc}) is greater than 0.1% (Schwarzenbach et al., 1993). In this case, K_d, the solid-water distribution ratio, is directly porportional to f_{oc}. Particle size and organic carbon content are often but not always inversely correlated (Smith et al.,

1988). In some environments the sediment may have a very low organic carbon content, and bonding directly to the inorganic particle surface will dominate the sorption process. The importance of this phenomenon increases with the number of surface sites available for bonding, i.e. the surface area (McCarty et al., 1981).

Ionizable organics present additional sorption possibilities: in their charged form, they can form electrostatic interactions with charged mineral surfaces, and they can undergo exchange reactions with ligands that were previously bound to the surface. Their sorption is thus controlled by pH, surface charge density, and specific surface area; the product of the latter two is the cation exchange capacity (CEC) (Schwarzenbach et al., 1993). Organic acids (e.g. chlorophenols, cresols) are deprotonated as pH increases, and in the anionic form are not attracted to the negatively charged mineral surface; what sorption does occur is due to partitioning into sediment organic matter. In constrast, organic bases (e.g. atrazine, paraquat) deprotonate to a cationic form which can adsorb to particle surfaces (Smith et al., 1988). At low concentrations and a given pH, the bound-to-dissolved ratio (K_d) is directly proportional to the CEC (Schwarzenbach et al., 1993).

Trace metals also sorb onto particles. They form complexes with organic and oxide coatings, which contain surface groups that act as coordinating sites (Stumm and Morgan, 1981). Metals can also form complexes with carbonate surfaces (Stumm and Morgan, 1981; Papenguth, 1995). Sorption of lead in soils is correlated with organic carbon and clay content (Singh and Sekhon, 1977; Adb-Elfattah and Wada, 1981), and increases strongly on both materials with

increasing pH (Griffin and Shimp, 1976). At low concentrations, the Langmuir isotherm applies, and Langmuir sorption coefficients are approximately 3.6-5.3 for organic matter and 3.5-4.1 for kaolinite (Griffin and Shimp, 1976). In addition, lead readily forms carbonate complexes: lead carbonate is fairly insoluble, with a log dissolution coefficient of -13.1 (Stumm and Morgan, 1981). Arsenic, in contrast, is present in aqueous solutions as an anionic species, and its sorption to sediments decreases with increasing solution pH. The adsorption of arsenic to soils is not correlated with organic carbon content, but rather to Fe- and Al-oxides (Gupta and Chen, 1978), on which adsorption decreases as solution pH increases from 7 to 9.

The karst aquifer investigated here is the Barton Springs segment of the Edwards Aquifer (referred to here as the Barton Springs Aquifer) in central Texas (Fig. 1.1), one of the most rapidly urbanizing regions in the nation. Increased amounts of sediment in wells and springs in the Barton Springs Aquifer have been documented over the last decade, and elevated levels of arsenic, lead, and aluminum are associated with sediments in a number of well samples (Hauwert and Vickers, 1994). This chapter presents geochemical characteristics of both surface and subsurface sediments, including mineralogy, organic carbon content, specific surface area, and size distribution, and discusses their role in determining the contaminant transport potential of mobile sediments in the aquifer.

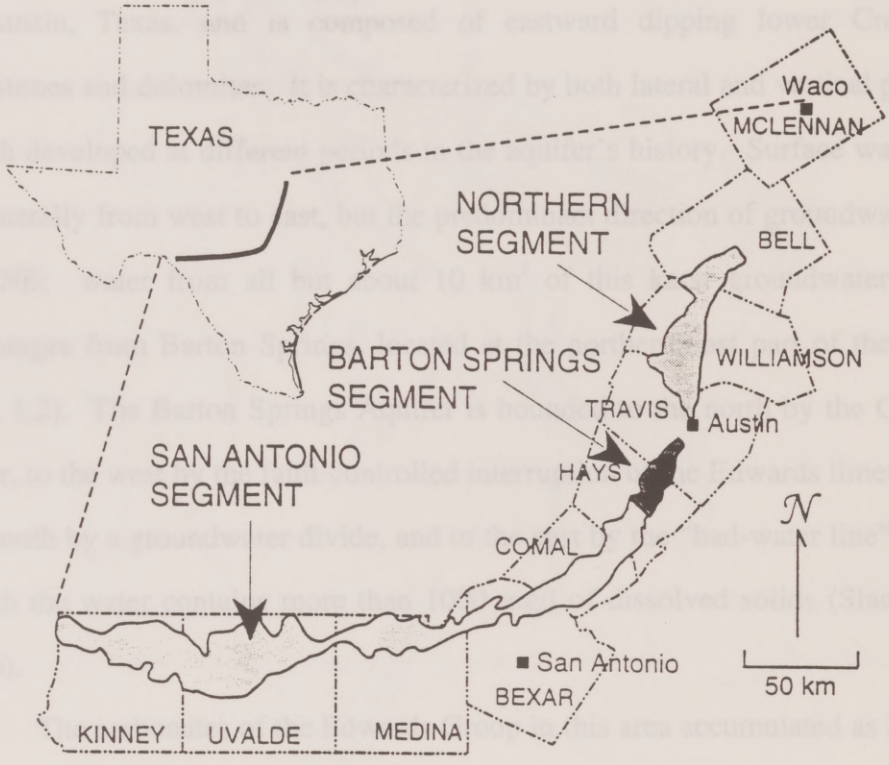

Figure 1.1. Location of the three segments of the Edwards Aquifer in Central Texas. Adapted from Senger (1983).

Geology and Hydrogeologic Framework

The depositional and structural history of the Central Texas area has shaped the unusual hydrogeologic regime of the Barton Springs segment of the Edwards Aquifer. The Barton Springs Aquifer extends across 391 km^2 southwest of Austin, Texas, and is composed of eastward dipping lower Cretaceous limestones and dolomites. It is characterized by both lateral and vertical porosity, which developed at different periods in the aquifer's history. Surface water flow is generally from west to east, but the predominant direction of groundwater flow is NNE; water from all but about 10 km^2 of this karst groundwater system discharges from Barton Springs, located at the northernmost part of the aquifer (Fig. 1.2). The Barton Springs Aquifer is bounded to the north by the Colorado River, to the west by the fault-controlled interruption of the Edwards limestone, to the south by a groundwater divide, and to the east by the "bad-water line" beyond which the water contains more than 1000 mg/l of dissolved solids (Slade et al., 1986).

The carbonates of the Edwards Group in this area accumulated as lagoonal and rudist reef deposits in the shallow inland sea which covered most of Texas in the Cretaceous Period. Karstification of these rocks during brief periods of subaerial exposure at that time created lateral porosity in the aquifer, primarily along bedding planes (Rose, 1972; Maclay and Small, 1984). Vertical porosity was created during the Oligocene - Miocene epochs, when vertical displacement

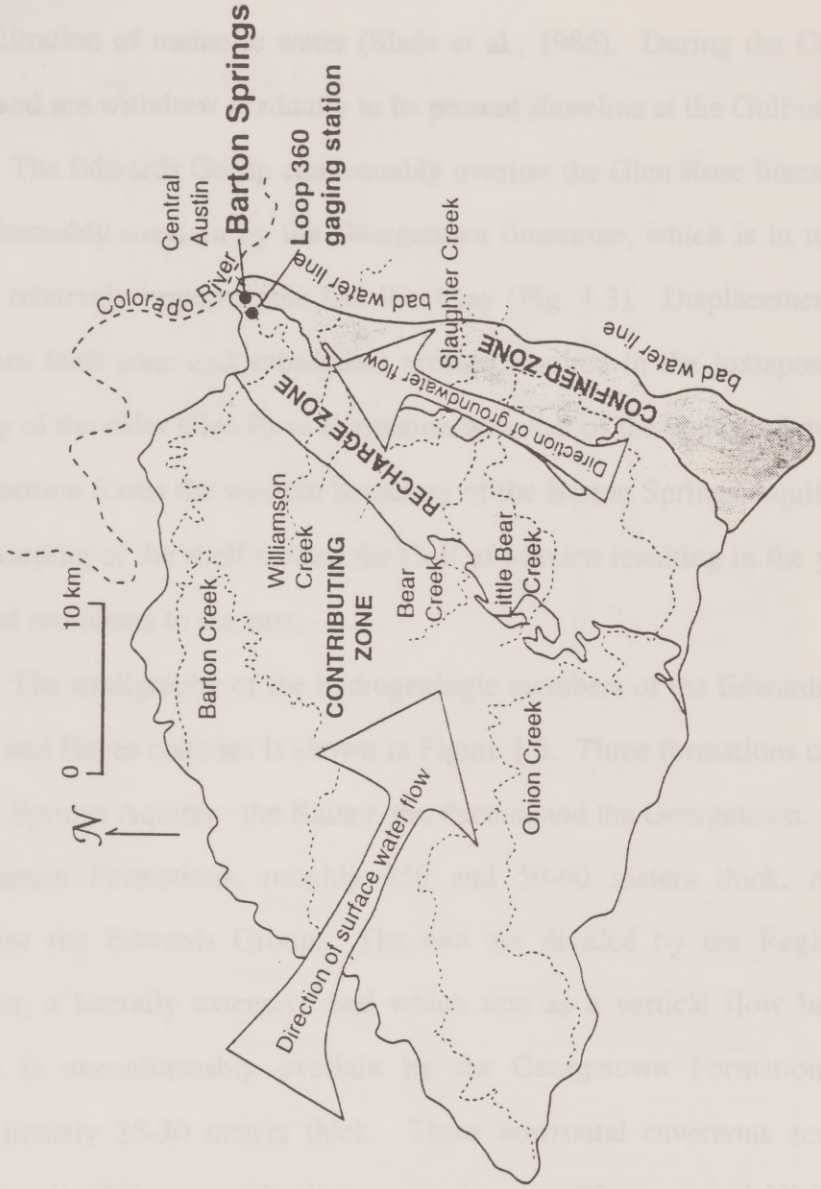

Figure 1.2. The Barton Springs watershed and aquifer.

The watershed is comprised of the Contributing and Recharge Zones, and the aquifer is comprised of the Recharge and Confined Zones.

along NNE-trending high-angle normal faults (the Balcones fault zone) allowed the infiltration of meteoric water (Slade et al., 1986). During the Cenozoic Era the inland sea withdrew gradually to its present shoreline at the Gulf of Mexico.

The Edwards Group conformably overlies the Glen Rose limestone, and is unconformably overlain by the Georgetown limestone, which is in turn overlain by the relatively impermeable Del Rio Clay (Fig. 1.3). Displacement along the Balcones fault zone and subsequent erosion resulted in the juxtaposition of the outcrop of the older Glen Rose Formation with that of the younger Edwards. This juxtaposition forms the western boundary of the Barton Springs Aquifer, with the downwarping of the shelf toward the Gulf of Mexico resulting in the younging of exposed sediments to the east.

The stratigraphy of the hydrogeologic members of the Edwards Aquifer in Travis and Hayes counties is shown in Figure 1.3. Three formations comprise the Barton Springs Aquifer: the Kainer, the Person, and the Georgetown. The Kainer and Person Formations, roughly 150 and 50-60 meters thick, respectively, comprise the Edwards Group. The two are divided by the Regional Dense Member, a laterally extensive bed which acts as a vertical flow barrier. The Person is unconformably overlain by the Georgetown Formation, which is approximately 25-30 meters thick. Three horizontal cavernous zones contain virtually all of the recognized caves in the area (Hauwert and Vickers, 1994). These are 1) an upper cavernous zone, 3 m thick, in the Marine Member; 2) a central cavernous zone, 15 m thick, in the units overlying and underlying the

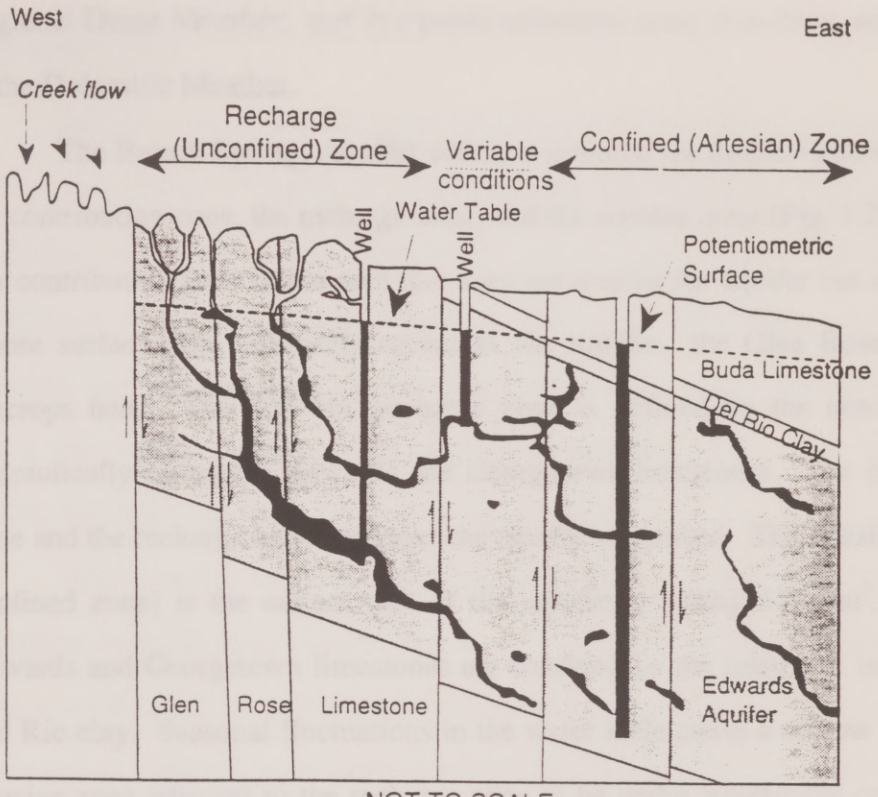

	Del Rio Formation			Principal confining bed above Edwards.
	Georgetown Formation			Dense limestone; very low matrix porosity.
Barton Springs Aquifer	Edwards Group	Person Formation	Marine Member	Reefal limestone; laterally extensive zones of significant porosity and permeability; karstified unit.
			Leached & Collapsed Member	Tidal and supratidal deposits; laterally extensive zones of honeycombed porosity.
			Regional Dense Member	Deep water limestone; negligible permeability and porosity; laterally extensive bed acts as vertical flow barrier.
		Kainer Formation	Grainstone Member	Shallow lagoonal sediments; cavernous, honeycombed layer occurs near the middle; interparticle porosity locally significant.
			Dolomitic & Kirschberg Members	Supratidal at top; tidal to subtidal below; very porous and permeable zones formed by boxwork porosity.
			Basal Nodular Member	Hard, dense, clayey limestone; negligible porosity and permeability.

Figure 1.3. Conceptual cross-section and hydrostratigraphy of the Barton Springs Aquifer.

Cross-section adapted from Slade et al. (1986) and hydrostratigraphy from Maclay and Small (1976) and Rose (1972).

Regional Dense Member; and 3) a lower cavernous zone, 6 m thick, near the base of the Dolomitic Member.

The Barton Springs Aquifer and its watershed are divided into three areas: the contributing zone, the recharge zone, and the artesian zone (Fig. 1.2). The 684 km^2 contributing zone is that area that does not overlie the aquifer but a portion of whose surface flow ultimately recharges the aquifer; the Glen Rose limestone outcrops here. The 233 km^2 recharge zone is defined by the outcrop of the hydraulically-connected Edwards and Georgetown limestones. The contributing zone and the recharge zone comprise the aquifer watershed. The artesian zone (or confined zone) is the eastern part of the aquifer, covering 158 km^2, where the Edwards and Georgetown limestones are confined by the relatively impermeable Del Rio clay. Seasonal fluctuations in the water table cause a narrow strip of the artesian zone adjacent to the recharge zone to be under water-table conditions at some times (Fig. 1.3). Surface water flows east across the contributing zone via one of six main creeks (Barton, Williamson, Slaughter, Little Bear, Bear, and Onion). Once these creeks cross onto the recharge zone, the surface water infiltrates through sinkholes and fractures in the creekbeds. Slade et al. (1986) estimate that 85% of recharge occurs through these creekbeds. The direction of groundwater flow, in contrast to that of surface flow, is NNE, following the trend of the Balcones fault zone; 96% of aquifer flow discharges at Barton Springs, while the remaining 4% discharges at small, intermittent springs.

METHODOLOGY

Sediment samples were collected from creeks, sinkholes, caves, wells, and springs, as shown in Figure 1.4. Samples were also collected from aquifer and confining unit source rocks. Sites were chosen to represent as wide an areal distribution as possible. There were some necessary limitations, however. For example, in order to collect a sediment sample from a well, it was necessary first that a well exist and second that it contain sediment. Thus those areas of the aquifer that have few wells are under-represented.

Most samples were collected between September 1995 and August 1996. Sampling methods varied depending on site. Creek, sinkhole, and cave samples were scooped with an aluminum foil-wrapped spoon into baked glass jars, Whirl-Pac bags, or ziplocs. Well samples were either collected as solid samples with a corer, or in water in 20-liter polyethylene containers. The latter were either pumped directly from the well or "vacuumed" from the bottom of collection tanks with a peristaltic pump, and the sediment fraction separated by flow-through centrifugation at the laboratory. Spring samples, with the exception of those collected at the main orifice of Barton Springs, were collected where they settled just after emerging from the spring mouth. At Barton Springs, where the concentration of suspended sediment was too low to be collected in the manner described above, a composite sediment sample was collected on three cotton string bundles secured inside a kick-net, which was secured in the spring orifice for twenty-four hours, then removed and rinsed out into a container. The sample was then passed through a 63-μm sieve to remove cotton fibers and the <63 μm

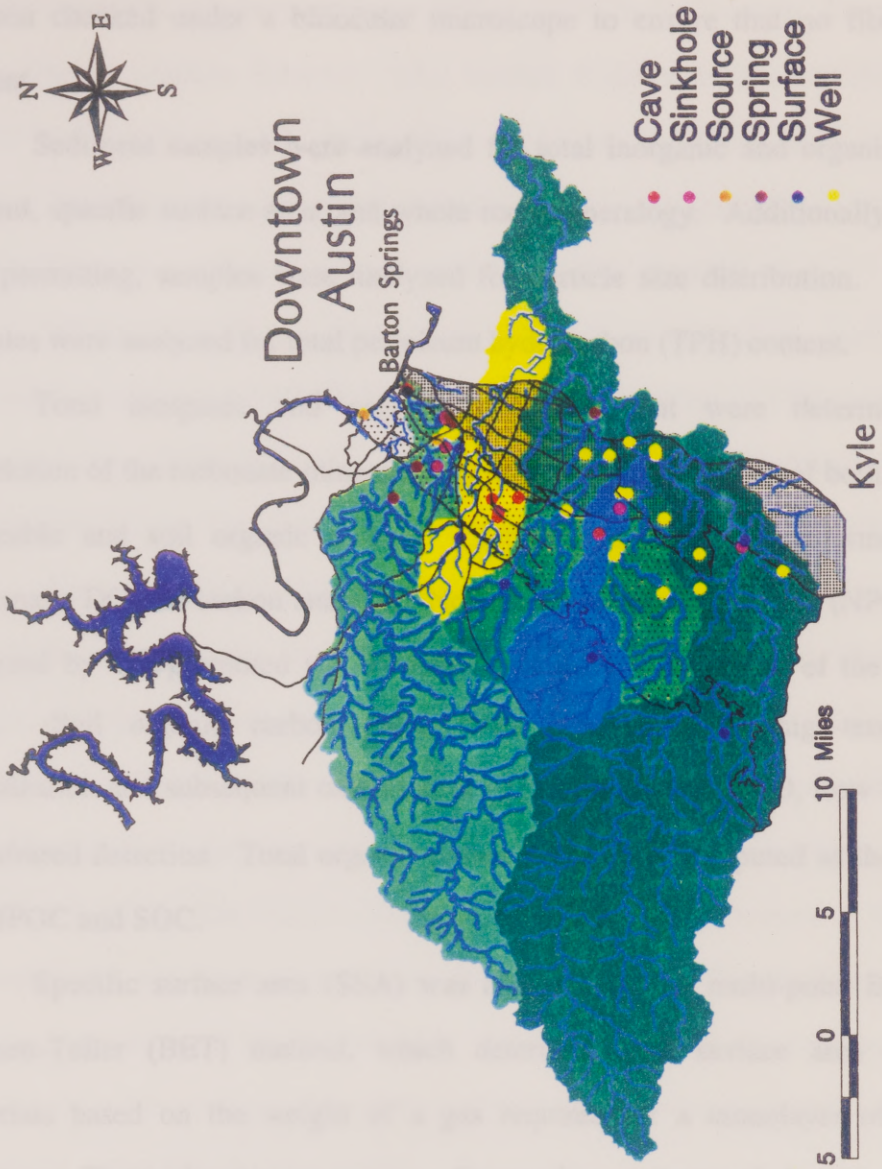

Figure 1.4. Locations of sampling sites.

The lightly-stippled area is the recharge and the heavily-stippled area is the contributing zone.

fraction checked under a binocular microscope to ensure that no fibers were present.

Sediment samples were analyzed for total inorganic and organic carbon content, specific surface area, and whole rock mineralogy. Additionally, sample size permitting, samples were analyzed for particle size distribution. Selected samples were analyzed for total petroleum hydrocarbon (TPH) content.

Total inorganic and organic carbon content were determined by dissolution of the carbonate minerals with nitric acid and analysis of both the non-purgeable and soil organic carbon. Carbon analyses were performed on a Dohrmann DC-180 carbon analyzer. Non-purgeable organic carbon (NPOC) was analyzed by UV-promoted wet-oxidation and infrared detection of the evolved CO_2. Soil organic carbon (SOC) was determined by high-temperature vaporization and subsequent oxidation of CO_2 by a continuous O_2 flow followed by infrared detection. Total organic carbon (TOC) was computed as the sum of the NPOC and SOC.

Specific surface area (SSA) was analyzed by the multi-point Brunauer-Emmett-Teller (BET) method, which determines the surface area of solid materials based on the weight of a gas required for a monolayer of surface coverage. The analyses were run on a Quantachrome Autosorb-1 using nitrogen as the absorbent.

Total petroleum hydrocarbon concentrations (TPH) were determined by thermal desorption gas chromatography. Separation was performed on a 30m SPB-1 Macrobore capillary column (0.5 mm) using hydrogen as the carrier gas.

Temperature was programmed from 40°C to 260°C at 6°C/minute. Detection was by a flame ionization detector. This method is different that USEPA Method 418.1 and results are not comparable. Sediment samples were air-dried and loaded into pre-baked glass tubes packed with silanized glass wool on both ends. A 0.2 µl injection of diesel fuel was used as the TPH standard.

Whole-rock mineralogy was analyzed by X-ray diffraction. Samples were ground to a powder and back loaded into sample holders. XRD spectra were collected on a Siemens D-500 diffractometer, using a 0.02º 2θ step and a 2-second time count. The data were interpreted as described in Lynch (1994).

Grain-size distribution was determined by sieving and ro-tapping the >63 µm fraction and by the pipette method for the ≤63 µm fraction (Folk, 1980). Cumulative percent weight was plotted versus grain size (phi scale) using a probability ordinate, and 16, 50, and 84 percentiles were graphically determined. The Graphic Mean (M_z) was computed to determine overall size, where $M_z = (\phi 16 + \phi 50 + \phi 84)/3$. The Graphic Standard Deviation (σ_G), a measure of the sorting of sediments, was computed as $\sigma_G = (\phi 84 - \phi 16) / 2$. The Graphic Skewness ($Sk_G$), a measure of the skewness as represented by the displacement of the median from the average of the ϕ 16 and ϕ 84 points, was computed as $Sk_G = (\phi 16 + \phi 84 + 2*\phi 50) / (\phi 84 - \phi 16)$.

Differences and similarities between sediment sample characteristics were analyzed statistically. Samples were divided into groups based on their origin: sinkhole, streambed, confined well, unconfined well, cave, spring, or source rock. Tested variables, as detailed above, included mineralogy (dolomite, calcite,

quartz, and clay content), organic carbon content, specific surface area, and grainsize distribution (Graphic Mean, Graphic Standard Deviation, and Graphic Skewness). For each variable, the Kruskal-Wallis non-parametric test was used to test the hypothesis that samples from different types of sites came from the same population; this was used in lieu of means testing with a standard t-test since the between-groups variances for some parameters were significantly different. The hypothesis that the sample groups came from the same population was rejected for $p < \alpha = 0.05$. Correlation coefficients between all variables were computed, both for each sample group and for all samples combined. Linear discriminant analysis was used to determine if samples could be classified into one of several mutually exclusive groups based on linear combinations of predictor variables. Variables were entered into the analysis phase in the order which maximized the Mahalanobis' distance between the two closest groups. The test of significance of separation between groups assumes equality of variances, but is not seriously affected by limited departures from this (Davis, 1973).

RESULTS

Whole-rock mineralogic analyses of the sediments show that they contain dolomite, calcite, quartz, and clay as their principal constituents. A few samples contain minor amounts of plagioclase and potassium feldspar (2% or less), and three samples contain more than 5% of either. Figure 1.5 shows the composition of sediment samples, grouped by sample type, plotted on ternary diagrams. In

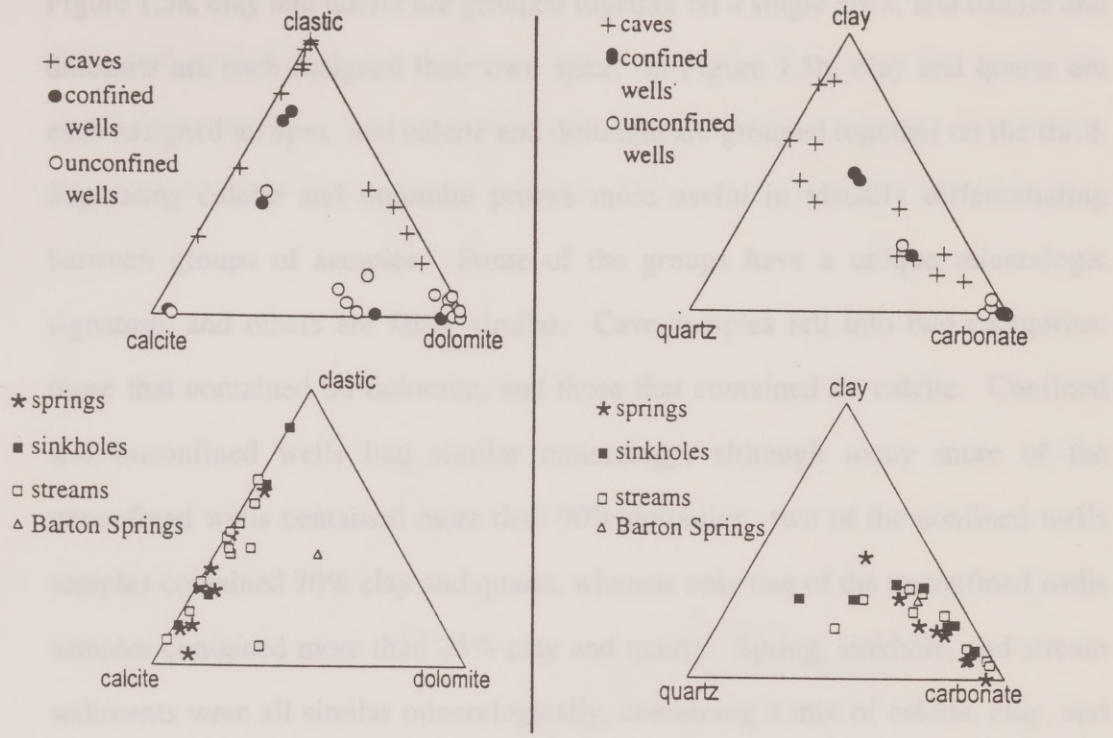

Figure 1.5. Whole rock mineralogy of samples.

Samples are grouped as follows: a) vertices of ternary diagrams are clay+quartz, calcite, and dolomite; b) vertices of ternary diagrams are clay, quartz, and carbonate (calcite + dolomite).

Figure 1.5a, clay and quartz are grouped together on a single apex, and calcite and dolomite are each assigned their own apex; in Figure 1.5b, clay and quartz are each assigned an apex, and calcite and dolomite are grouped together on the third. Separating calcite and dolomite proves more useful in visually differentiating between groups of samples. Some of the groups have a unique mineralogic signature, and others are fairly similar. Cave samples fell into two categories: those that contained no dolomite, and those that contained no calcite. Confined and unconfined wells had similar mineralogy, although many more of the unconfined wells contained more than 90% dolomite; two of the confined wells samples contained 70% clay and quartz, whereas only one of the unconfined wells samples contained more than 25% clay and quartz. Spring, sinkhole, and stream sediments were all similar mineralogically, containing a mix of calcite, clay, and quartz, but almost no dolomite.

Two things, overall, are distinctive about the mineralogy of the sediments: 1) in the ternary diagram that separates calcite and dolomite (Fig. 1.5a), samples group along the sides of the ternary diagrams (i.e., most samples are lacking in one of the constituents: calcite, dolomite, or clay and quartz); 2) in the ternary diagram that separates clay and quartz (Fig. 1.5b), the points group on a line which extends from 100% carbonate to a 60:40 mix of clay and quartz (i.e., as the carbonate content decreases, both quartz and clay content increase in a fairly fixed ratio).

Eight different samples of the Edwards Group were analyzed: rocks from the (1) Grainstone, (2) Basal Nodular, (3) Leached Collapsed, (4) upper

Dolomitic, (5) rhythmic beds of the Dolomitic; marls from the (6) Leached Collapsed and (7) Regional Dense members, and (8) pulverulite from the Kirschberg member. A sample of Del Rio Clay was also analyzed. The whole rock mineralogy of these samples is shown in Figure 1.6. With one exception, the

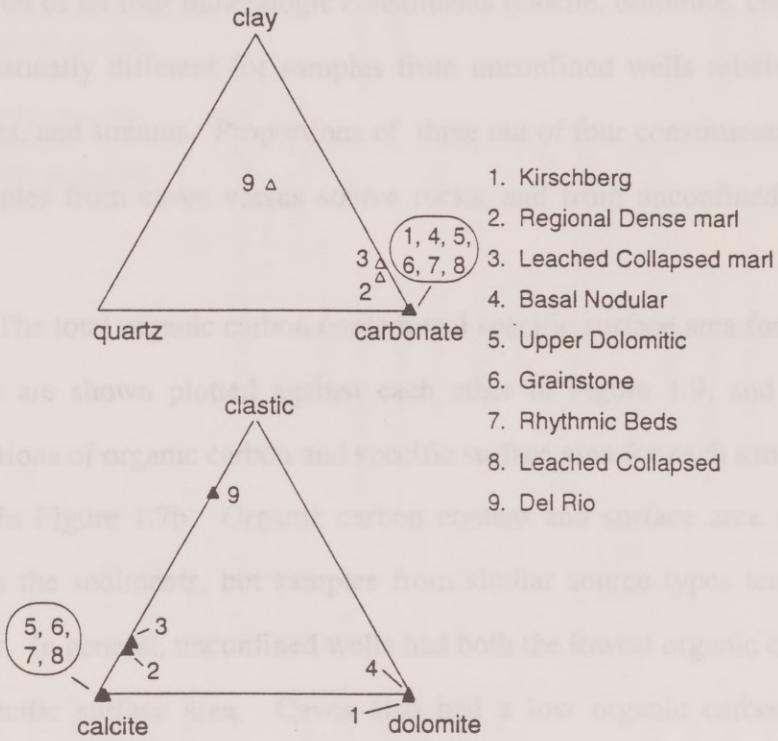

Figure 1.6. Ternary diagram of Edwards rock and Del Rio Clay whole rock mineralogy.

rocks from the Edwards Group are primarily calcite with a small amount of clay; the exception is the sample from the Kirschberg member, which is composed entirely of dolomite. The Del Rio Clay is 53% clay, 26% calcite, and 21% quartz. Box plots of mineralogic proportions for all the sample groups, including source rocks, are shown in Figure 1.7a.

The results of statistical comparison of sediment groups from different types of sample sites by the Kruskal-Wallis test are shown in Figure 1.8. The proportion of all four mineralogic constituents (calcite, dolomite, clay and quartz) are statistically different for samples from unconfined wells relative to springs, sinkholes, and streams. Proportions of three out of four constituents are different for samples from caves versus source rocks, and from unconfined wells versus caves.

The total organic carbon content and specific surface area for the sediment samples are shown plotted against each other in Figure 1.9, and box plots of distributions of organic carbon and specific surface area for each sample group are shown in Figure 1.7b. Organic carbon content and surface area varied greatly between the sediments, but samples from similar source types tended to group together. In general, unconfined wells had both the lowest organic carbon content and specific surface area. Caves also had a low organic carbon content but comprised those samples with the highest specific surface area. Sinkhole and stream samples had the highest organic carbon content, ranging from 0.5 to 4% by weight. Spring samples were intermediate for both organic carbon content and surface area.

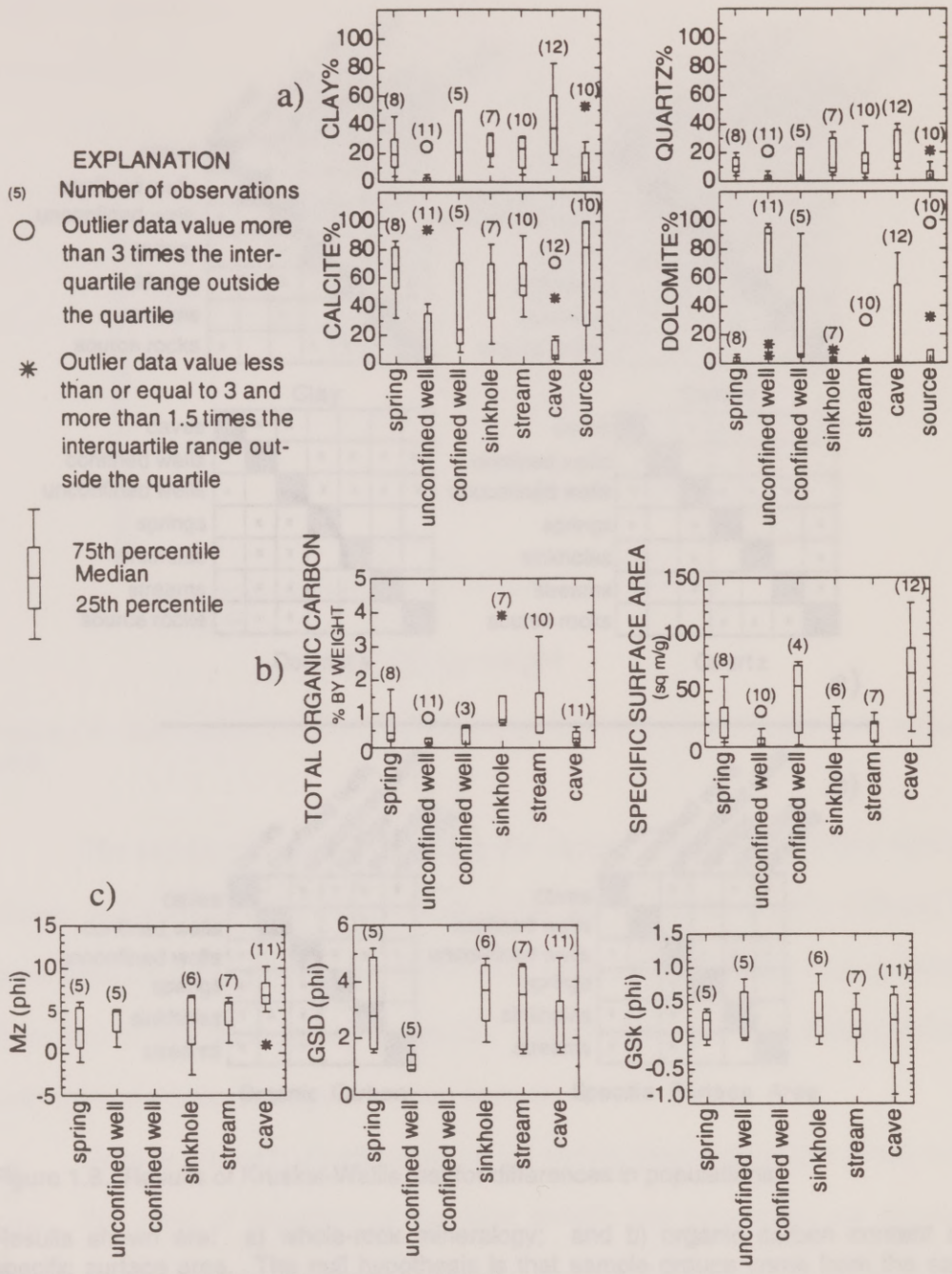

Figure 1.7. Box plots of sediment characteristics.

a) whole rock mineralogy; b) total organic carbon and specific surface area; c) grain-size distributions: Mz (graphic mean), GSD (graphic standard deviation), and GSk (graphic skewness).

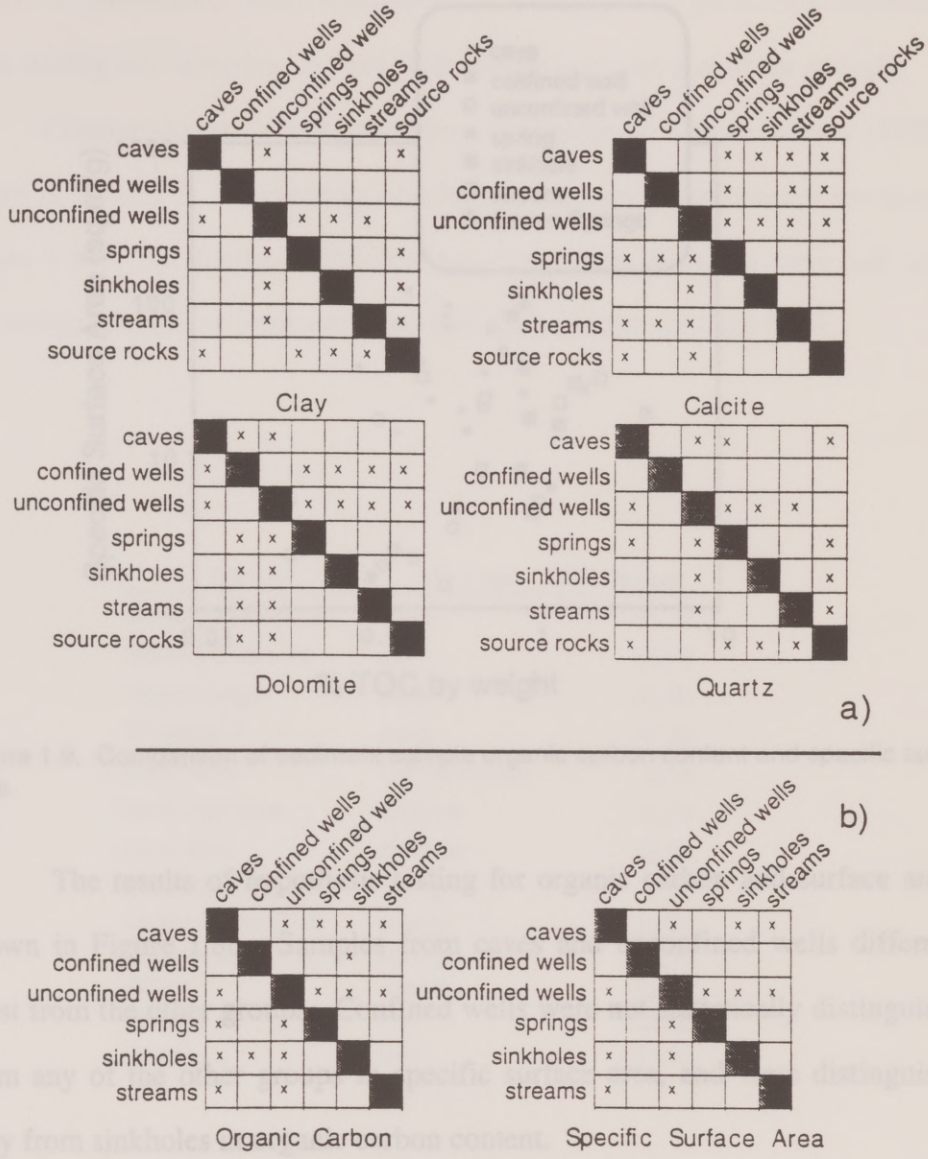

Figure 1.8. Results of Kruskal-Wallis test for differences in populations.

Results shown are: a) whole-rock mineralogy; and b) organic carbon content and specific surface area. The null hypothesis is that sample groups come from the same populations. Pairs of sample groups for which the hypothesis is rejected ($p<\alpha=0.05$) are marked with an "x".

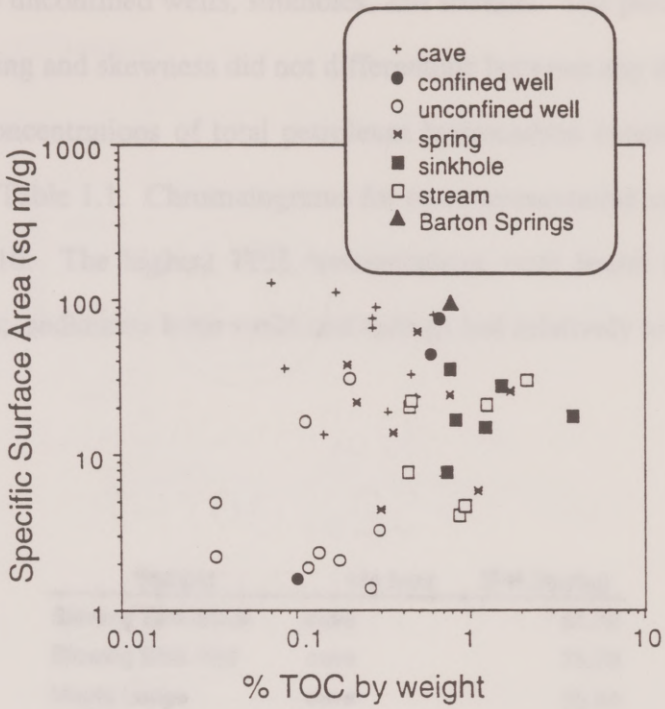

Figure 1.9. Comparison of sediment sample organic carbon content and specific surface area.

The results of hypothesis testing for organic carbon and surface area are shown in Figure 1.8b. Samples from caves and unconfined wells differed the most from the other groups. Confined wells were not statistically distinguishable from any of the other groups in specific surface area, and were distinguishable only from sinkholes in organic carbon content.

Sample grainsize distributions varied widely from one sample group to the next. Box plots of distributions for three sample size parameters are shown in Figure 1.7c. From the Kruskal-Wallis test, the hypothesis that the samples came from the same population, based on median grain size, was rejected for caves

relative to unconfined wells, sinkholes, and streams. The parameters representing grain sorting and skewness did not differentiate between any of the groups.

Concentrations of total petroleum hydrocarbon concentrations (TPH) are shown in Table 1.1. Chromatograms for two representative samples are shown in Figure 1.10. The highest TPH concentrations were found in cave and surface sediments; sediments from wells and springs had relatively low TPH.

Sample	site type	TPH (mg/kg)
Blowing Sink Black	cave	61.75
Blowing Sink Red	cave	75.73
Maple Ledge	cave	25.94
Whirlpool 3	cave	47.40
Kirschberg	formation rock	0.13
Marbridge Sink	sinkhole	25.74
Nairn Sink	sinkhole	29.55
Backdoor Spring	spring	1.37
Barton Lodge Sp E	spring	10.94
Brodie Oak Spring	spring	9.99
TxDoT 1	stream	31.26
Thames 1	well	12.56
Unisys	well	11.99

Table 1.1. Total petroleum hydrocarbon (TPH) concentrations for selected samples.

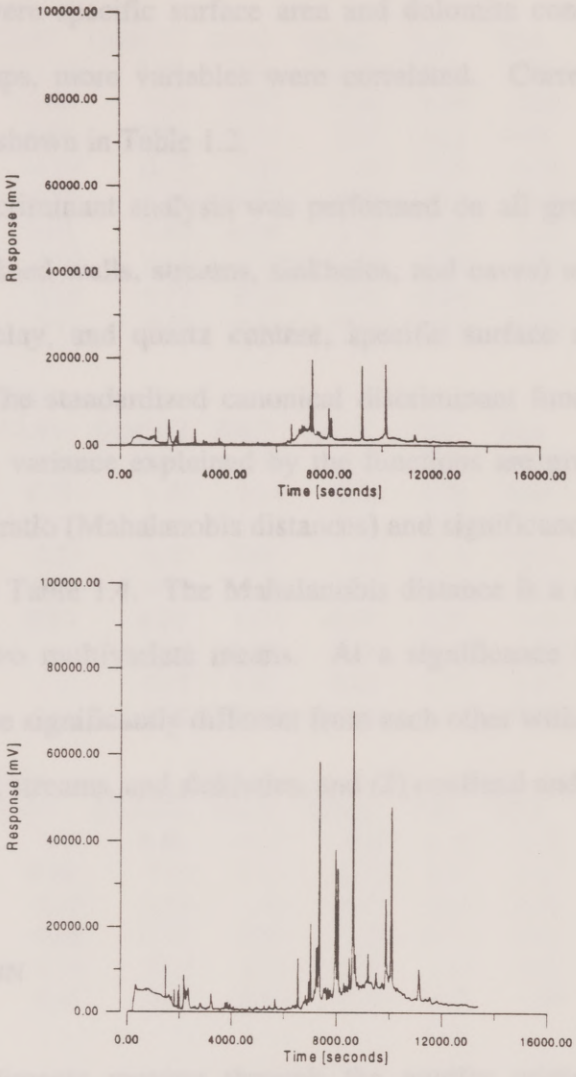

Figure 1.10. Gas chromatograms for TPH analysis.

On the top is shown Thames 1, a well, and on the bottom Whirlpool Cave.

A number of the parameters were significantly correlated, based on an alpha of 0.01. Based on all the samples grouped together, a positive correlation exists between clay and quartz content (r = 0.64), and clay content and specific

surface area (r = 0.88). Grain-size and sorting were negatively correlated (r = -0.90), as were specific surface area and dolomite content (r = -0.46). Within single groups, more variables were correlated. Correlations within individual groups are shown in Table 1.2.

Discriminant analysis was performed on all groups (springs, unconfined wells, confined wells, streams, sinkholes, and caves) using variables for calcite, dolomite, clay, and quartz content, specific surface area, and organic carbon content. The standardized canonical discriminant function coefficients and the cumulative variance explained by the functions are given in Table 1.3, and the pairwise F ratio (Mahalanobis distances) and significance between pairs of groups is given in Table 1.4. The Mahalanobis distance is a measure of the separation between two multivariate means. At a significance level of 0.01, all sample groups were significantly different from each other with the following exceptions: (1) springs, streams, and sinkholes, and (2) confined and unconfined wells.

DISCUSSION

Sediments moving through the aquifer originate both at the surface (allochthonous) and from the subsurface (autochthonous). A conceptual model of the sediment compartments for the Barton Springs aquifer is shown in Figure

Springs

	CLAY	QUARTZ	CALC	DOLO	TOC	SSA	MZ	GSD	GSK
CLAY	1.00	***0.97***	***-0.99***	-0.59	0.29	***0.90***	0.79	0.68	0.17
QUARTZ	***-0.99***	1.00	***-0.97***	-0.65	0.39	0.83	0.69	0.78	0.07
CALC	***-0.99***	***-0.97***	1.00	0.51	-0.29	***-0.88***	-0.73	-0.74	-0.09
DOLO	-0.59	-0.65	0.51	1.00	-0.19	-0.58	-0.89	-0.45	-0.40
TOC	0.29	0.39	-0.29	-0.19	1.00	0.03	0.16	0.58	0.00
SSA	***0.90***	0.83	***-0.88***	-0.58	0.03	1.00	0.90	0.01	-0.75
MZ	0.79	0.69	-0.73	-0.89	0.16	0.90	1.00	0.01	-0.44
GSD	0.68	0.78	-0.74	-0.45	0.58	0.01	0.01	1.00	-0.17
GSK	0.17	0.07	-0.09	-0.40	0.00	-0.75	-0.44	-0.17	1.00

Unconfined Wells

	CLAY	QUARTZ	CALC	DOLO	TOC	SSA	MZ	GSD	GSK
CLAY	1.00	***0.93***	0.19	-0.54	0.24	***0.86***	.	.	.
QUARTZ	***0.93***	1.00	0.14	-0.50	0.24	***0.81***	0.20	-0.19	0.46
CALC	0.19	0.14	1.00	***-0.93***	0.07	0.64	***-0.99***	***1.00***	-0.93
DOLO	-0.54	-0.50	***-0.93***	1.00	-0.15	***-0.87***	***0.97***	***-0.98***	0.86
TOC	0.24	0.24	0.07	-0.15	1.00	0.21	-0.20	0.19	-0.27
SSA	***0.86***	***0.81***	0.64	***-0.87***	0.21	1.00	-0.36	0.37	-0.38
MZ	.	0.20	***-0.99***	***0.97***	-0.20	-0.36	1.00	***-1.00***	***0.93***
GSD	.	-0.19	***1.00***	***-0.98***	0.19	0.37	***-1.00***	1.00	***-0.93***
GSK	.	0.46	-0.93	0.86	-0.27	-0.38	***0.93***	***-0.93***	1.00

Confined Wells

	CLAY	QUARTZ	CALC	DOLO	TOC	SSA	MZ	GSD	GSK
CLAY	1.00	***0.96***	-0.17	-0.68	0.16	0.47	.	.	.
QUARTZ	***0.96***	1.00	-0.07	-0.73	0.14	0.47	.	.	.
CALC	-0.17	-0.07	1.00	-0.61	0.24	0.68	.	.	.
DOLO	-0.68	-0.73	-0.61	1.00	-0.27	-0.96	.	.	.
TOC	0.16	0.14	0.24	-0.27	1.00	0.93	.	.	.
SSA	0.47	0.47	0.68	-0.96	0.93	1.00	.	.	.
MZ	.	.	.	.	.	.	1.00	.	.
GSD	.	.	.	.	.	.	.	1.00	.
GSK	.	.	.	.	.	.	.	.	1.00

Table 1.2. Correlation coefficients for sediment characteristics grouped by site type.

Those pairs for which there is an underlying significant linear correlation ($p<\alpha=0.01$) are italicized and in bold-face.

Sinkholes

	CLAY	QUARTZ	CALC	DOLO	TOC	SSA	MZ	GSD	GSK
CLAY	1.00	0.22	-0.45	0.53	0.21	0.79	***0.95***	0.25	0.10
QUARTZ	0.22	1.00	***-0.93***	-0.35	0.47	0.09	0.23	0.48	-0.14
CALC	-0.45	***-0.93***	1.00	0.06	-0.29	-0.51	-0.45	-0.40	-0.12
DOLO	0.53	-0.35	0.06	1.00	-0.11	0.77	0.51	-0.25	0.60
TOC	0.21	0.47	-0.29	-0.11	1.00	-0.07	0.14	0.32	-0.55
SSA	0.79	0.09	-0.51	0.77	-0.07	1.00	0.60	-0.36	0.27
MZ	***0.95***	0.23	-0.45	0.51	0.14	0.60	1.00	0.49	0.22
GSD	0.25	0.48	-0.40	-0.25	0.32	-0.36	0.49	1.00	0.06
GSK	0.10	-0.14	-0.12	0.60	-0.55	0.27	0.22	0.06	1.00

Streams

	CLAY	QUARTZ	CALC	DOLO	TOC	SSA	MZ	GSD	GSK
CLAY	1.00	0.37	-0.57	-0.50	0.48	***0.95***	0.17	0.87	-0.18
QUARTZ	0.37	1.00	***-0.87***	-0.39	-0.08	0.82	0.30	***0.98***	-0.14
CALC	-0.57	***-0.87***	1.00	0.10	-0.15	-0.74	-0.56	-0.73	0.37
DOLO	-0.50	-0.39	0.10	1.00	-0.08	-0.51	0.42	-0.57	-0.27
TOC	0.48	-0.08	-0.15	-0.08	1.00	0.48	-0.07	0.11	-0.33
SSA	***0.95***	0.82	-0.74	-0.51	0.48	1.00	0.03	0.81	0.22
MZ	0.17	0.30	-0.56	0.42	-0.07	0.03	1.00	0.37	-0.62
GSD	0.87	***0.98***	-0.73	-0.57	0.11	0.81	0.37	1.00	-0.27
GSK	-0.18	-0.14	0.37	-0.27	-0.33	0.22	-0.62	-0.27	1.00

Caves

	CLAY	QUARTZ	CALC	DOLO	TOC	SSA	MZ	GSD	GSK
CLAY	1.00	0.28	-0.37	-0.66	-0.19	***0.98***	0.61	0.45	-0.34
QUARTZ	0.28	1.00	-0.15	-0.53	0.37	0.32	0.23	0.23	0.15
CALC	-0.37	-0.15	1.00	-0.34	-0.20	-0.37	-0.58	-0.43	-0.49
DOLO	-0.66	-0.53	-0.34	1.00	0.16	-0.67	-0.19	-0.15	0.58
TOC	-0.19	0.37	-0.20	0.16	1.00	-0.24	-0.11	0.21	0.61
SSA	***0.98***	0.32	-0.37	-0.67	-0.24	1.00	0.71	0.36	-0.32
MZ	0.61	0.23	-0.58	-0.19	-0.11	0.71	1.00	0.22	0.11
GSD	0.45	0.23	-0.43	-0.15	0.21	0.36	0.22	1.00	0.11
GSK	-0.34	0.15	-0.49	0.58	0.61	-0.32	0.11	0.11	1.00

Table 1.2 continued.

Standardized Canonical Discriminant Function Coefficients

	FUNC 1	FUNC 2	FUNC 3	FUNC 4	FUNC 5
QUARTZ	0.70	0.48	-0.08	-0.05	-1.07
DOLO	1.12	-0.18	-0.26	0.71	0.09
CLAY	-1.35	0.71	-1.53	0.39	0.84
SURFACE	1.80	-0.15	1.63	0.12	0.17
TOC	-0.52	-0.22	0.50	0.81	0.06

Eigenvalues and Percent Variance Explained by Each Function

FCN	EIGENVALUE	VARIANCE	CUM PCT VARIANCE
1 *	3.99	73.84	73.84
2 *	0.96	17.83	91.66
3 *	0.29	5.31	96.98
4 *	0.16	2.95	99.93
5 *	0.00	0.07	100.00

Table 1.3. Results of discriminant function analysis.

Sample groups can be differentiated between using a linear combination of five descriptive variables (1) quartz, 2) dolomite, and 3) clay content by percent, 4) specific surface area, and 5) organic carbon content). Standardized canonical discriminant function coefficients for each of the variables, and eigenvalues and percent variance explained by each function are shown here. Over 90% of the variance between sample groups is explained by the first two functions.

GROUP	springs	unconfined wells	sinkholes	streams	caves
unconfined wells	8.69 0.00				
sinkholes	1.92 0.12	12.65 0.00			
streams	0.66 0.65	11.01 0.00	0.64 0.67		
caves	9.31 0.00	5.96 0.00	13.90 0.00	13.12 0.00	
confined wells	7.00 0.00	2.00 0.10	10.07 0.00	9.30 0.00	4.27 0.00

Table 1.4. Between-groups significance from discriminant function analysis.

F statistics and significances between pairs of groups after 5 variables were entered into the discriminant function analysis. The F statistic is listed above the significance in each case. The hypothesis that samples from the two different groups come from the same population is rejected for significance values $p<\alpha=0.05$.

1.11. Surface sediments enter the aquifer through sinkholes and fissures in creekbeds, some of which emerge from small, localized springs. Autochthonous sediments, the byproduct of subsurface chemical weathering, are eroded and carried through the aquifer system; they are found in caves and wells. Sediments issuing from Barton Springs, the main spring for the entire aquifer, have both an autochthonous and allochthonous source. Allochthonous sediments may act as vectors for contaminants: they have the potential to sorb contaminants and

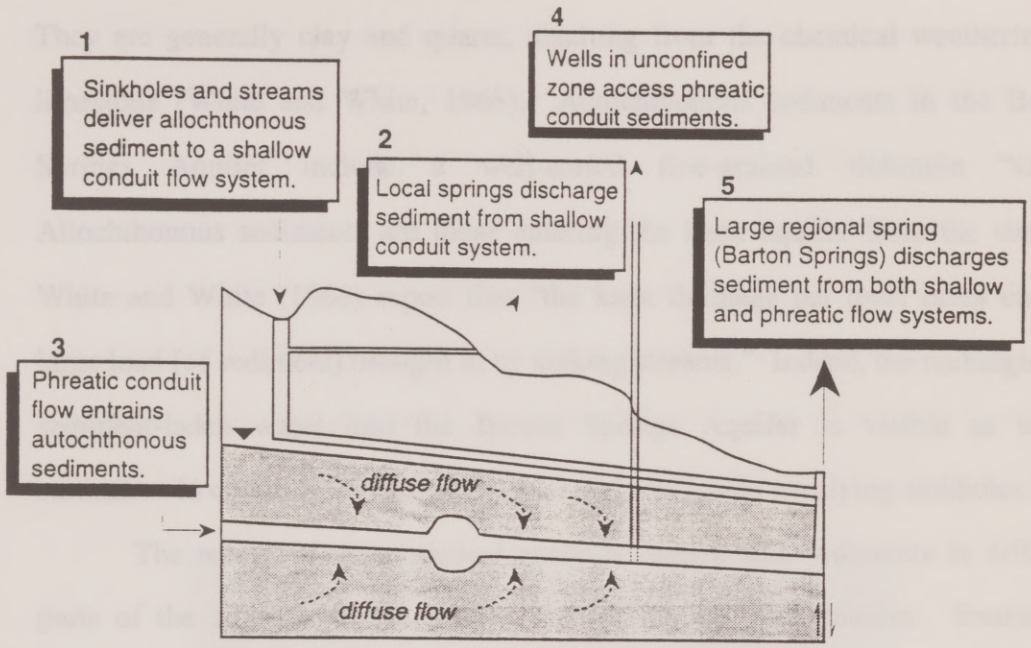

Figure 1.11. Conceptual diagram of sediment compartments and flow systems in the Barton Springs Aquifer.

Not to scale.

transport them through the aquifer. Some autochthonous sediments have physical characteristics which render them capable of sorbing and transporting dissolved organic carbon and contaminants brought in from the surface. Other autochthonous sediments have little potential to sorb contaminants. These differences are detailed in the following section.

Allochthonous vs. Autochthonous Sediments

Autochthonous sediments are those originating within a karst aquifer. They are generally clay and quartz, resulting from the chemical weathering of limestone (White and White, 1968). Autochthonous sediments in the Barton Springs Aquifer include a well-sorted fine-grained dolomite "sand". Allochthonous sediments are those entering the karst aquifer from the surface. White and White (1968) report that "the karst drainage net must often carry a large load [of sediment] brought in by sinking streams." Indeed, the recharging of sediment-laden water into the Barton Springs Aquifer is visible as turbid stormflow in creeks is sucked into vortices of whirlpools overlying sinkholes.

The results of the statistical analyses suggest that sediments in different parts of the aquifer may indeed originate from different sources. Examining differences between sample types based on individual characteristics (Kruskal-Wallis test) and overall differences between groups based on grouped characteristics (discriminant analysis), the sediments fall into three discrete groups: (1) wells; 2) caves; and 3) springs, streams, and sinkholes. Assessment of the different sediment characteristics analyzed, as detailed below, provides clues to the origin of these sediments and an explanation of why they differ.

The dolomite sand is the only mineralogical component that is unambiguously autochthonous. It is found soley in the subsurface sediment samples (wells and caves) and springs, with one exception. The sediments are made up of both single and intergrown dolomite crystals, ranging in size from 10 to 60 microns in diameter. Many of the crystals are of either the limpid euhedral

or the hollow box form described by Folk and Siedlecka (1974) and Folk and Land (1975), as shown in an example from the study site (Figure 1.12). The morphology of these grains is different than that of the pulverulite found locally in road cuts by Rose (1972), which he describes as rounded, "football shaped" grains. Folk and Siedlecka (1974) suggest that this crystal form is one indicator of a schizo-haline diagenetic environment (i.e., one which alternates between hyper-saline and freshwater conditions), thus providing both the high Mg/Ca ratio and slow crystallization kinetics necessary for precise Ca-Mg ordering. The limpid dolomite crystals thus formed, because of their well-ordered crystalline structure, are more resistant to dissolution than both ordinary dolomite and calcite

Figure 1.12. Scanning electron microscope photomicrograph of a "hollow box" dolomite grain from a well in the unconfined zone.

This grain morphology, along with euhedral "limpid" grains, is characteristic of a schizo-haline environment. This type of extremely well-ordered dolomite is highly resistant to dissolution (Folk and Siedlecka, 1974).

(Folk and Land, 1975). The dolomite sediments are morphologically similar to dolomite found in portions of the Kirschberg Member of the Edwards, which are exposed north of the aquifer region. These units conform to the description of "massive dolomite" given by Fisher and Rodda (1969): fine- to coarse-grain size (10-150 μm), loosely-knit fabric of euhedral crystals, moderate to high porosity, well-developed rhombs, and thickness of individual dolomite units greater than 0.6 m. Given that the Kirschberg Member is found only in the subsurface within the aquifer region, and that none of the surface sediments (with one exception, discussed later) contain more than 10% dolomite, I conclude that the dolomite sediments in these wells are autochthonous.

Sediment samples from wells in the recharge zone (unconfined well samples) are composed almost exclusively of this dolomite sand. Hauwert and Vickers (1994) noted high rates of sedimentation in many of these wells. Several of these wells are located along a known trough in the potentiometric surface, thought to signify a fault-controlled flow conduit (Hauwert, 1995). This suggests that the chemically-resistant dolomite rhombs are freed by the chemical dissolution of the surrounding calcite matrix; high-velocity groundwater flow through conduits subsequently entrains and transports the dolomite rhombs. Only three of eleven samples from the recharge zone contained more than 10% other mineral constituents.

Some cave samples and a few of the confined zone well samples contain the autochthonous dolomite. Cave mineralogy falls into two distinct categories: those sediments which contain no dolomite, and those which contain no calcite

(Fig. 1.5a). Accessible cave passages in the Edwards, which are generally narrow and linear, are thought to be ancient flow conduits; those which pass through the Kirschberg dolomite have the opportunity to entrain and transport the dolomite crystals. Only two of the confined well samples contained significant amounts of dolomite, and these two are located on Bear Creek, in a region where fluctuations of the water table can cause the wells to be under water table (unconfined) conditions when the aquifer level is low (Fig. 1.3) (Hauwert, personal communication). Veni (1988), in a survey of over 200 Texas caves, found that conduit flow in unconfined aquifers was rapid compared to flow in confined aquifers, and that in unconfined aquifers sediment load did not exceed stream competence, whereas in confined aquifers, sediment load commonly exceeded stream competence. This suggests that in portions of the unconfined section of the aquifer, conduit flow is sufficient to transport the dolomite sand, whereas in the confined section only clay is transported.

Only one of the surface samples contained dolomite sand. This sample was collected from the streambed of Onion Creek just downstream of a quarry, where it had formed a distinctive creamy white layer at the bottom of a shallow pool. Several meters upstream was noticeable evidence of runoff from the quarry eroding the steep creek bank. It is probable that some of the sediment in this section of Onion Creek is a product of the quarrying activities, and that the dolomite crystals in this sample actually originate within the rock units being quarried.

The other minerals found in the subsurface samples—quartz, calcite, and clay—are also found in many of the surface samples in similar proportions. Quartz and clay are the detrital remnants of chemical weathering; because chemical weathering occurs both at the surface and in the subsurface, the remnants can be expected to be found in both autochthonous and allochthonous sediments. Sediments collected in streambeds and sinkholes may contain a low proportion of clay minerals, not because clay minerals are not allochthonous, but because they are present as the smallest particles and will therefore tend to remain in suspension and either enter the aquifer with recharge or be carried out to the Colorado River. Calcite, in contrast, is the mineral which dissolves during chemical weathering. In general, calcite is present only in very low amounts in the cave and well samples, in amounts significantly lower than those found in the surface samples (Figs. 1.7a and 1.8a). This suggests that the presence of large amounts of calcite is an indicator of recent allochthonous sediment.

The mineralogy of two of the five confined well samples is similar to that of the Del Rio Clay: they contain clay, quartz, and calcite. It is possible that the Del Rio Clay, which is the confining unit overlying the aquifer, enters the subsurface flow system by filtering down into the aquifer units at the Del Rio Clay-aquifer interface. This ongoing process may be increasing: the owner of one of the confined wells reports to have seen an increase in the suspended sediment coming from his 20-year old well over the past 3-5 years; the situation has reached the point where he has installed both a holding tank and filters between the well and his house (Bettis, personal communication) so that his clothes,

according to him, will come out of the washing machine cleaner than when they went in. The cause of the increase is not immediately apparent.

The mineralogy of spring sediments is evidence of the continued transport of allochthonous sediments through the aquifer. The small springs, each of which drains a shallow, localized system (Slade et al., 1986), have mineralogies consisting of clay, quartz, and calcite, indistinguishable from the mineralogies of stream and sinkhole sediments (Figs. 1.5b and 1.8a) and dissimilar to those found in both caves and wells. One unconfined well sediment sample had sediment of a mineralogy similar to that of the surface and spring samples: 25% clay, 21% quartz, 42% calcite, 13% dolomite. The well is located a few meters from Little Bear Creek. As 85% of the recharge to the aquifer enters through fissures in the beds of six creeks, including Little Bear, it is likely that this well is intercepting one of these recharge fissures, and that the sediments in this sample originate from surface recharge.

Organic carbon is another indicator of allochthonous contribution to the aquifer. Organic carbon originates outside of the aquifer, produced as plant matter decays, and is incorporated into the soil profile. It is also a product of domestic waste, and can enter the aquifer through leaking sewer lines or poorly functioning septic systems. It may leach into the interstitial water or be leached out by rain water as dissolved organic carbon, which then may sorb to mineral particles, especially clays, and iron and aluminum oxides (Thurman, 1985). Although some dissolved organic carbon enters the aquifer with recharge and then sorbs to autochthonous sediments, a far larger amount will enter sorbed to

allochthonous sediments. Unconfined well and cave sediments contain the smallest proportion of organic carbon (Figs. 1.7c and 1.9), significantly different from the amount contained in surface sediments (Fig. 1.8b). Surface sediment samples from streams and sinkholes contained the most organic carbon. Organic carbon in small springs was intermediate, reinforcing the hypothesis that allochthonous sediments are carried through the aquifer to emerge at springs. Interestingly, two of the three confined wells from which a large enough sample was collected to make possible an organic carbon analysis contained almost as much organic carbon as the surface samples. This suggests that the clay which they transport may have an allochthonous origin. Cave sediments present an interesting case, in that they are generally agreed to contain a mix of autochthonous sediment (remnants of chemical weathering) and allochthonous sediment that has been washing into the system since the onset of karstification. The low organic carbon content of some of the cave sediments suggests that the sediment they contain, while possibly allochthonous, is not recently deposited—that it is paleo-fill. Three of the eleven cave samples, however, contained more than 0.4% organic carbon by weight, indicating that parts of the cave system are indeed receiving contemporary allochthonous input. Russell (1996) notes that at Blowing Sink Cave (in the Barton Springs Aquifer), fine black clay and organic debris from the surface, which has been overgrazed, is transported into the aquifer by floodwater.

Potassium and plagioclase feldspar are also indicative of allochthonous sediment. The three sample sites containing a significant amount of these two

constituents are all surface sites: two sinkholes and a streambed, containing 9%, 33%, and 13% total feldspar, respectively. The sinkholes both drain residential developments and the streambed drains a water quality pond behind a large commercial development. It is likely that the origin of the feldspar minerals is imported sand and gravel, for example from fill used in landscaping. Nine other samples contained trace (1-3%) amounts of total feldspar: one sinkhole, one streambed, one confined well, and six cave samples. This supports the hypothesis that the caves are receiving contemporary allochthonous input.

Size distribution proved to be an ineffective method for distinguishing between sediment sources in this environment. Buller and McManus (1972) found that comparing arithmetic measures of grain-size deviation and skewness produced linear trends with slopes reflecting depositional environment, decreasing in the sequence: aeolian—fluviatile—beach—"quiet water". The method of Buller and McManus involves plotting the median diameter in millimeters against grainsize deviation (S_A,) and S_A against sample skewness (Sk_a), where S_A and Sk_a are computed the same way as Graphic Standard Deviation (σ_G) and Graphic Skewness (Sk_G,) respectively, except that the parameters are computed using millimetres rather than phi size. A "best-fit" curve is drawn by hand through the points. This method was tried on the sediment samples collected for this study (Fig. 1.13). The points from each different type of source do show a distinct linear trend, but gradients do not differ enough to enable conclusive differentiation between any of the groups except the sediments from the unconfined wells, which show little variation in either median diameter or sorting.

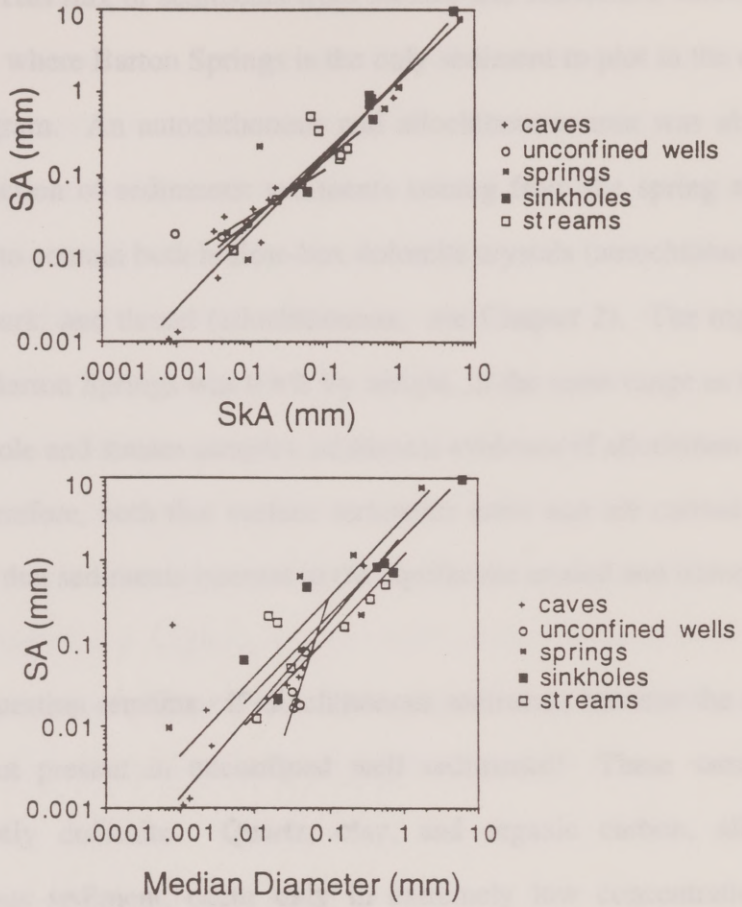

Figure 1.13. Comparison of arithmetic sample skewness (SkA) and median diameter to grainsize deviation (SA).

"Best fit" linear trend drawn by hand.

This conclusion agrees with what has already been surmised: namely, that the sediments from the unconfined wells come from a single, homogeneous source: schizo-haline dolomite in the Kirschberg.

the deeper conduit system may access the phreatic cavernous region in the Dolomitic/Kirschberg Member (Figure 1.3). Evidence in favor of this theory is that Airman's Cave, less than 3.5 km from Barton Springs, is located in the Leached/Collapsed Members. This cave, of which over 3 km of passages have been mapped, is normally dry, but in 1991 and 1992, a particularly wet period, the cave was an active flow system (Hauwert, 1995). If the unconfined wells are accessing the deeper, phreatic system, then they could be expected to contain dolomite sand mobilized from the Kirschberg. The second explanation is that allochthonous sediments are moving through the conduits intersected by the unconfined wells, but that clay does not collect in the wells. As high velocity storm flow slows, the large particles are deposited, while fine-grained clay remains in suspension. Organic carbon content, well-correlated with clay content, would also be expected to be low. This explanation does not, however, explain the absence of quartz, a large size particle, in these samples.

Contaminant Transport Potential

Contamination of the Barton Springs Aquifer is not purely hypothetical; although in general water quality is considered good, contamination from both point and non-point sources is a concern. Catastrophic events in the area have occurred: oil pipelines crossing the aquifer have ruptured, and spills reported to the Texas Water Commission from 1986 to 1992 included gasoline and diesel fuels, pesticides, ammonia, sodium hydroxide, hydrochloric acid, trichloroethane, and perchloroethene (U.S. Fish and Wildlife, 1994). Several contaminants have

recently been reported in aquifer samples, including petroleum hydrocarbons, pesticides, arsenic, and lead in wells and springs (Hauwert and Vickers, 1994), low levels of tretrachlorethylene in Barton Springs (Slade, 1991), and high levels of polycyclic aromatic hydrocarbons (PAHs) in sediments in Barton Creek and Barton Springs pool (City of Austin, 1994). Some samples of aquifer sediments analyzed in this study for total petroeum hydrocarbons (TPH) show that man's activities are beginning to affect aquifer sediments (Table 1.4). What role do mobile sediments in the subsurface play in the transport of these contaminants, as well as those that will be introduced into the aquifer in the future?

All but four sediment samples analyzed in this study have an organic carbon content (f_{oc}) greater than 0.1%, the threshold value at which partitioning of neutral organics compounds into organic carbon dominates sorption. Thus the effects of adsorption of neutral organics to polar mineral surfaces are unlikely to be significant in the Barton Springs aquifer. Surface samples have the highest organic carbon content, and thus have a high potential to bring sorbed nonpolar organic contaminants into the aquifer via recharging waters. Contaminants of concern in this category include petroleum hydrocarbons, PAHs, and perchloroethene. That these contaminants have the potential to travel through the aquifer and emerge from springs in the sorbed state is evidenced by moderately high spring f_{oc} values, which range from 0.22 to 1.1%. Interestingly, Allen-King et al. (1996) found that at low concentrations, organic-carbon correlation equations significantly underpredicted sorption of perchloroethene, and that the

importance of sediment-mediated transport of perchloroethene (and other chlorinated solvents) may thus be even greater than predicted.

In the samples collected, specific surface area (SSA) was highly correlated with clay content as expected. The highest SSA was found in cave sediments, followed by confined wells. This suggests that organic bases may sorb onto clays in caves. While those clays remain in place, they act to retard the transport of the contaminant. The presence of high surface area sediments in some of the confined well samples, however, indicates that this class of contaminants could be transported through the aquifer concentrated on mobile clay particles.

Elevated levels of lead and arsenic have been found in analyses of springs and wells in the Barton Springs Aquifer (Hauwert and Vickers, 1994). Concentrations of total lead significantly exceeded those of dissolved lead in most of the wells, demonstrating the importance of sorption in the transport of this metal. Freedman et al. (1994) undertook a study of metal-mineral surfaces interactions in a groundwater environment. They found that the distribution coefficient of lead between minerals and groundwater varied from about 30 to over 200, and that sorption increased as quartz < calcite < kaolinite. This suggests that minerals in all compartments of the aquifer have the potential to sorb and transport lead, from the dolomite crystals in the unconfined wells to the clays and quartz in the surface and springs sediments. Sorption of arsenic, in contrast, is correlated to Fe- and Al-oxide content. Oxide content was not analyzed in this study, but the distinctive red color of many of the cave clays was determined to be

Barton Springs discharges a mix of both allochthonous and autochthonous sediments. This mix of sediments from surface and subsurface sources is seen in Figure 1.5a, where Barton Springs is the only sediment to plot in the center of the ternary diagram. An autochthonous and allochthonous mix was also found by visual inspection of sediments: sediments issuing from the spring after a storm were found to contain both hollow-box dolomite crystals (autochthonous) and bits of calcite, bark, and thread (allochthonous; see Chapter 2). The organic carbon content of Barton Springs was 0.8% by weight, in the same range as that of many of the sinkhole and stream samples, additional evidence of allochthonous input. It appears, therefore, both that surface sediments enter and are carried through the aquifer and that sediments internal to the aquifer are eroded and transported out of the aquifer.

A question remains: if allochthonous sediments traverse the aquifer, why are they not present in unconfined well sediments? These samples contain predominantly dolomite. Quartz, clay, and organic carbon, all present in allochthonous sediment, occur only in extremely low concentrations in these samples. There are two possible explanations. The first is that two different types of flow systems are present in the aquifer: a shallow, perched conduit system that directly transports stormwater recharge from the surface to springs (including Barton Springs), and a more extensive, deep, phreatic conduit system that is fed by diffuse flow and is accessed by wells in the unconfined zone (Figure 12). The shallow system may recharge through the cavernous zones in the Leached/Collapsed Member which overlies the Regional Dense Member, while

due to goethite (FeO·OH). Arsenic might be expected to sorb to cave clays, but in most environments to be fairly mobile.

In summary, surface sediments have the potential to introduce different classes of contaminants into the aquifer: nonpolar organic contaminants and lead will be concentrated on these sediments due to the high organic carbon content, and ionizable organic contaminants will sorb to surface sediment clays. These sediments traverse the aquifer and emerge at springs. There are two different types of autochthonous sediments with contrasting properties and affinities for contaminants. Clays in caves and in confined zone wells may sorb ionizable organic contaminants and lead because of their large specific surface area; low surface-area dolomites have a low potential to sorb any contaminants, with the possible exception of lead. If contaminants enter the aquifer in a dissolved form, they may sorb to immobile cave clays, retarding their transport, but may later be remobilized when the cave sediments are re-entrained. Conversely, sorption to mobile clays found in wells in the confined zone will concentrate and enhance their transport.

Implications

The transport of contaminants through a karst aquifer is closely tied to that of the mobile sediments which move through it. Contaminants are likely to enter the aquifer sorbed to mobile surface sediments present in recharge water, because of their concentration on organic carbon contained in those sediments or on clay

surfaces. An increase in sediment concentrations entering the aquifer thus will have an impact on the total amount of contaminants entering the aquifer.

The Austin, Texas area is representative of many regions in the country where suburban development has begun to sprawl onto a sensitive watershed. As the watershed urbanizes, the sediment load entering the Barton Springs Aquifer will continue to increase. Impervious cover, exemplified by rooftops, roadways, and parking lots, is an indicator variable for increased urbanization (Arnold and Gibbons, 1996). Increases in impervious cover alter surface hydrology, decreasing infiltration and increasing the amount and velocity of runoff to surface streams during rain events, as shown in Table 1.5. The net result is to increase stormflow and decrease baseflow. As a result, turbidity in creeks increases for two reasons: 1) the increased velocity of runoff has a greater erosional power,

	Impervious Cover %			
	0%	10-20%	35-50%	75-100%
runoff	10	20	30	55
evapo-transporation	40	38	35	30
shallow infiltration	25	21	20	10
deep infiltration	25	21	15	5

Table 1.5. Changes in the hydrologic cycle associated with urbanization.

In general, an increase in impervious cover results in an increase in runoff and a decrease in evapotransporation and infiltration (Arnold and Gibbons, 1996).

causing runoff entering creeks to carry a greater sediment load; and 2) the volume of runoff causes increased stream power in creeks for a given rainfall intensity, increasing streambank erosion. Most of the recharge entering the Barton Springs Aquifer infiltrates through fissures in major creekbeds, therefore an increase in turbidity of surface streams will correspond to an increase in the load of surface sediment in aquifer recharge. This study shows that at least some portion of these allochthonous sediments move through the aquifer to emerge at springs.

Changes in surface hydrology caused by increased impervious cover may also affect erosional processes in the subsurface. Of the rainfall that falls on the recharge zone proper, approximately 60% of that enters the aquifer through direct recharge features such as sinkholes. (This number is computed based on 15% of total recharge occurring through direct infiltration (Slade et al., 1986), all of which must occur on the recharge zone; the total area from which precipitation contributes to recharge is 917 km^2 (contributing zone plus recharge zone), 15% of which is 137 km^2, representing 59% of the recharge zone.) With urbanization, small sinkholes and other recharge features are filled in or paved over. As a result, for a given rainfall intensity, 1) those features still exposed receive more runoff than previously; and 2) head in the creeks will be higher, increasing recharge over previous levels. Each of these factors increases the velocity of conduit flow. In the areas where the conduits pass through the dolomite units, increased flow velocity will result in increased subsurface erosion and conduit diameter. Enlarging the conduit diameter will have two positive feedback effects: it will allow increased penetration of fresh water for additional calcite matrix

dissolution, and will allow earlier onset of turbulence and accompanying entrainment of more sediment. Additionally, higher velocity groundwater will better entrain clays, which, due to their cohesiveness, require a higher velocity than larger, more spherical particles to bring into suspension.

Modeling contaminant transport in any environment requires knowledge of all the phases in which the contaminant is present. In groundwater, these are usually assumed to be a mobile aqueous phase, an immobile solid phase (the aquifer matrix), and sometimes a colloidal phase. This study demonstrates that in modeling contaminant transport in karst aquifers, a mobile sediment phase should also be included, as it would be in a model of contaminant transport in a surface system. The parameters necessary to describe this aspect of contaminant transport include sediment density, sediment grain-size range, and characteristics determining the contaminant distribution coefficient, i.e., organic carbon content, specific surface area, and mineralogy (Onishi, 1981; Wu and Gschwend, 1988). The results of this study illustrate that in a karst aquifer, these parameters are not uniform throughout the aquifer. In the Barton Springs Aquifer, autochthonous and allochthonous sediments differ greatly in all these characteristics, and even autochthonous sediments exhibit wide variability, ranging from dolomite crystals (10-60 μm, low organic carbon content, low specific surface area) to clays (< 10 μm, intermediate organic carbon content, high specific surface area). Although these values are specific to the Barton Springs Aquifer, other karst aquifers may exhibit similar variability. Clearly, for construction of a model which accurately

predicts contaminant fate and transport in karst, field values for these parameters must be obtained.

CONCLUSION

The Barton Springs Aquifer, a karst aquifer in Central Texas, transports both allochthonous and autochthonous through the karst system to emerge at springs. Sediments from creekbeds and sinkholes are indistinguishable by mineralogy, organic carbon content, specific surface area, or size distribution. They consist of calcite, quartz, and clay, and have a fairly high organic carbon content (arithmetic mean of 1.28% organic carbon by weight). Sediments from small, localized springs have similar characteristics. These allochthonous sediments enter the aquifer by recharging water through sinkholes and fissures in creekbeds. In contrast, sediments found in wells from the unconfined zone of the aquifer consist largely of well-sorted, silt-sized dolomite grains with a low organic carbon content (arithmetic mean of 0.25%) and low specific surface area. These originate from geologic units within the aquifer. Sediments from caves mostly consist of clay, quartz, and dolomite, and also have a low organic carbon content (average of 0.31%). Based on mineralogy, organic carbon content, and specific surface area, three groups of sediments are statistically distinguishable: 1) stream, sinkhole, and small springs sediments; 2) confined and unconfined well sediments; and 3) cave sediments. Sediment issuing from Barton Springs, which discharges 96% of spring flow from the aquifer, has a mineralogy and organic carbon content which reflects a mix of both allochthonous and

autochthonous sources and indicates that both types of sediment are moving through the karst system. Differences in sediment characteristics at the surface, in the subsurface, and from Barton Springs suggest that there may be two different conduit systems feeding Barton Springs: a shallow, perched system which is directly fed by stormwater, and a deeper, phreatic system which is fed by diffuse flow.

Both allochthonous and autochthonous sediments have the capacity to sorb contaminants, either through sorption to associated organic carbon or through direct adsorption to mineral surfaces. Some contaminants have already been detected in the aquifer, including petroleum hydrocarbons, chlorinated solvents, pesticides, and trace metals. It is likely that these contaminants will be concentrated onto mobile sediment moving through the aquifer.

Changes in landuse, from rural/ranchland to urban/suburban, are accompanied by changes in the surface hydrology. Increases in impervious cover decrease infiltration and increase runoff to creeks. As a result, for the same rainfall duration and intensity, runoff and creek flow have a higher velocity and increased erosional power; the sediment load carried by the creeks is higher, as is that in the recharging water. Thus landuse practices which increase erosion, either of the land surface or of streambanks, will increase the amount of allochthonous sediments moving through the aquifer and any contaminants or organic carbon they have sorbed.

The field values obtained for subsurface sediment characteristics demonstrate that sediments in a karst aquifer are by no means uniform. They

exhibit marked variation in size distribution, mineralogy, and potential to sorb and transport sediment. A model which attempts to predict contaminant fate and transport in a karst system should not only include a mobile sediment phase, but also have adequate information concerning the characteristics of the different types of sediment mobile in the subsurface.

Chapter 2. Muddy Waters: Temporal Changes in Characteristics of Sediment Discharging from a Karst Spring

INTRODUCTION

Karst aquifers provide a vital portion of the world's potable water, supplying drinking water to an estimated 25% of the global population (Ford and Williams, 1989); approximately 20% of the United States is underlain by karst aquifers (Mull et al., 1988). These aquifers, while highly productive, are more susceptible to pollution than those in any other type of geologic media. This is because karst aquifers are characterized by: 1) thin soils, which act as poor filtering agents and allow rapid infiltration; 2) lack of granular texture, which inhibits mechanical filtration as a self-purification mechanism; and 3) short residence times, which reduce the time possible for biological purification processes (White, 1988).

Sediment plays an important role in determining water quality. Sediment itself is considered a contaminant: among other detrimental effects, it degrades species habitat, smothers biota, changes the ambient temperature characteristics of flow systems, and impairs the esthetic appearance of spring and river water. Mobile sediment may also act as a vector for the transport of nutrients and contaminants, particularly poorly soluble compounds such as metals, pesticides, and hydrocarbons (e.g., McCarty et al., 1981; Smith et al., 1988; Schwarzenbach, et al., 1993).

There is abundant anecdotal evidence that sediment is mobile in karst aquifers. Karst aquifers are characterized by flow through solutional conduits, centimeters to meters in diameter. Conduit flow can be turbulent, particularly in response to storms (White, 1988), and therefore can entrain and transport sediments as bedload and suspended load (White and White, 1968). White (1988) suggests that rapid facies changes in cave sediments are evidence of subsurface stream flow "subject to large annual fluctuations," and states that "transport [of sediment] in caves is highly episodic ...." Inside aquifers, sediment decreases aquifer permeability, fills in wells, and causes pumps to seize (Hauwert and Vickers, 1994). Sediments and associated contaminants, originating at the surface, can move rapidly through the aquifer to exit at a spring or well (Mull et al., 1988; Thrailkill, 1989).

While many researchers have investigated variations in karst spring chemistry at seasonal and short-term scales, no studies were found that analyzed variations in sediment geochemistry. Karst spring chemistry has largely been used to infer internal architecture and evaluate karst system response to recharge events. Karst systems were initially classified as either conduit or diffuse, based on seasonal and short-term variations in spring chemistry (Shuster and White, 1971; Jacobson and Langmuir, 1974. Conduit-flow systems were characterized by high variability in hardness, a high degree of undersaturation, and dilution of total dissolved solids (TDS) in response to rainfall, whereas diffuse-flow systems had a fairly constant hardness, were on the average near saturation, and showed an increase in TDS in response to rain. It has since been recognized that karst

systems lie along a continuum of which these two classifications are endmembers. While the majority of the storage occurs in narrow fissures in the matrix (the diffuse-flow part of the system), most of the transport occurs in enlarged conduits (Atkinson et al., 1973). Atkinson also defines two types of recharge: *quickflow*, comprised of stream sink water and infiltration from closed depressions, and *baseflow*, comprised of slow infiltration from areas other than closed depressions; the conduits derive some of their flow from the quickflow and some from the draining of the matrix. Karst systems often respond to precipitation with an early increase in hardness followed by a more or less rapid decrease; the peaks have been interpreted as the arrival of high Ca, Mg pre-storm water that has been displaced from conduits by storm water, and the broad minimum following as the maximum dilution of groundwater by storm water recharge (Hess and White, 1988; Dreiss, 1989).

Ryan and Meiman (1996) were among the first to focus their investigation on temporal variations in nonpoint source pollutants in spring flow—fecal coliform bacteria and suspended sediment—and their relation to landuse. By sampling at 2- to 3-hour intervals, they were able to detect concentrations of both pollutants more than two orders of magnitude higher than background levels for short periods of time, and they point out that the peak concentrations of pollutants did not coincide with peak discharge. Additionally, through dye traces, they established that the nonpoint-source pollutants originated from the agricultural portion of the watershed rather than the forested portion. This is the only study to

consider the suspended sediment carried by springs, but is restricted to a description of change in concentration of total suspended solids.

This chapter describes in detail the temporal changes in characteristics of the suspended load in spring discharge in response to two storm events, and relates them to sediment source, aquifer hydraulics, and potential for contaminant transport. In addition, it analyzes temporal changes in concentrations of all major ions in spring water collected at hourly sampling intervals following the two storms.

This project was undertaken at Barton Springs, Austin, Texas. Barton Springs, the fourth largest spring in Texas (Brune, 1981), is located within sight of downtown Austin's high-rises. Barton Springs water quality is important for a number of reasons. First, the major set of spring orifices feeds a 225 m-long swimming pool enjoyed by over 340,000 people per year. Barton Springs Pool is considered by many to be Austin's "crown jewel", a significant contribution to Austin's quality of life, and an important tourist attraction. Second, Barton Springs contributes to Austin's municipal water supply. Water from Barton Springs discharges to Barton Creek which feeds into the Colorado River approximately 0.6 km upstream from the Green Water Treatment Plant, one of three plants that treats and delivers the municipal water supply for the City of Austin. Depending on releases from upstream dams and Barton Springs discharge, the contribution of Barton Springs to flow in this section of the Colorado River varies from less than 1 percent to more than 90 percent (Slade et al., 1986). Third, Barton Springs is home to the Barton Springs Salamander

(*Eurycea sosorum*), which was proposed for listing as an endangered species by the U.S. Fish and Wildlife Service in 1994 (US Fish and Wildlife Service, 1994). In 1996 the Service withdrew the proposal, an action that, as of March 1997, was still under litigation. The Barton Springs Salamander lives only in Barton Springs and is extremely vulnerable to changes in water quality (US Fish and Wildlife Service, 1994).

This study focuses on temporal changes in sediment issuing from the springs. Suspended sediment was collected at the springs at hourly intervals following two rain events: one at the end of a period of normal rainfall, and one at the end of a six-month period of little rain. Temporal changes in the concentration, composition, and size distribution of the sediment in response to the storm pulse were investigated, as well as temporal changes in the water chemistry.

Study Area: Hydrogeologic Setting

Barton Springs is fed by the Barton Springs segment of the Edwards Aquifer, located in Central Texas (Fig. 2.1), and referred to herein as the Barton Springs Aquifer. Ninety-six percent of flow in this system discharges at Barton Springs, with the remaining 4% discharging at small, intermittent springs. The Barton Springs Aquifer is composed of lower Cretaceous limestones and dolomites which dip gently to the east, and is characterized by both lateral and vertical porosity which developed at different periods in its history. The aquifer extends across 391 km^2 southwest of Austin, Texas; surface water flow is generally from west to east, while the predominant direction of groundwater flow

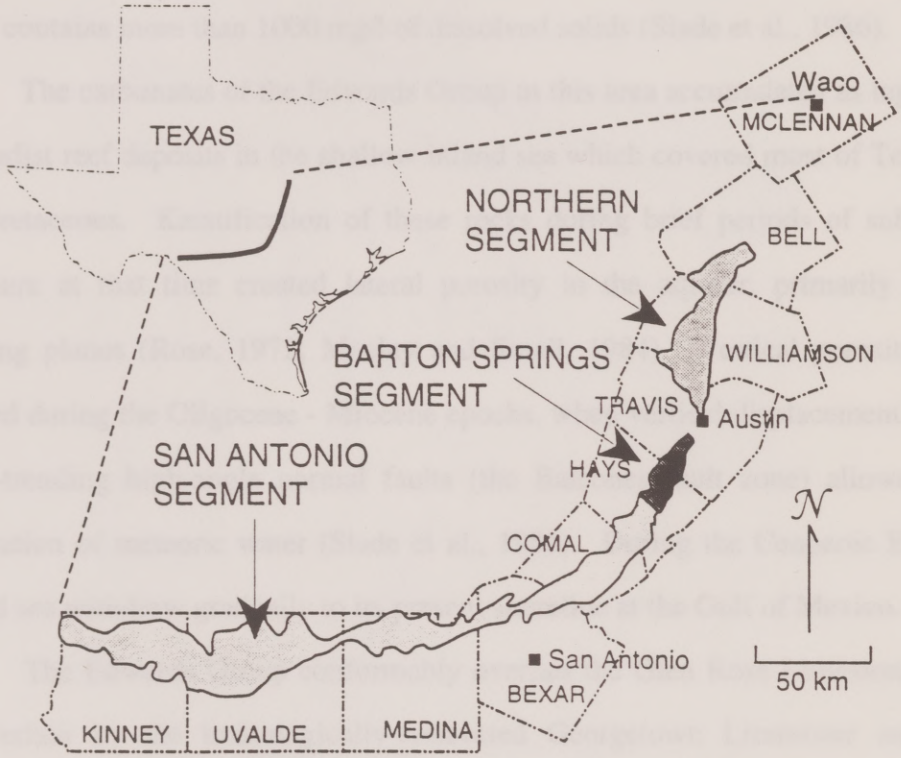

Figure 2.1. The three segments of the Edwards Aquifer, Texas.

The three segments are: the San Antonio segment, the Barton Springs segment, and the Northern segment. Barton Springs is located at the northern tip of the Barton Springs segment. Adapted from Senger (1983).

is NNE (Fig. 2.2), following the trend of the Balcones Fault Zone. The Barton Springs Aquifer is bounded to the north by the Colorado River, to the west by the fault-controlled interruption of the Edwards limestone, to the south by a groundwater divide, and to the east by the "bad-water line" beyond which the water contains more than 1000 mg/l of dissolved solids (Slade et al., 1986).

The carbonates of the Edwards Group in this area accumulated as lagoonal and rudist reef deposits in the shallow inland sea which covered most of Texas in the Cretaceous. Karstification of these rocks during brief periods of subaerial exposure at that time created lateral porosity in the aquifer, primarily along bedding planes (Rose, 1972; Maclay and Small, 1984). Vertical porosity was created during the Oligocene - Miocene epochs, when vertical displacement along NNE-trending high-angle normal faults (the Balcones fault zone) allowed the infiltration of meteoric water (Slade et al., 1986). During the Cenozoic Era the inland sea withdrew gradually to its present shoreline at the Gulf of Mexico.

The Edwards Group conformably overlies the Glen Rose Limestone, and is overlain by the hydrologically-connected Georgetown Limestone and the relatively impermeable Del Rio Clay (Fig. 2.3). Displacement along the Balcones fault zone and subsequent erosion resulted in juxtaposition of the outcrop of the older Glen Rose Formation with that of the younger Edwards; this contact forms the western boundary of the Barton Springs Aquifer. The downwarping of the shelf toward the Gulf of Mexico results in the younging of exposed sediments to the east.

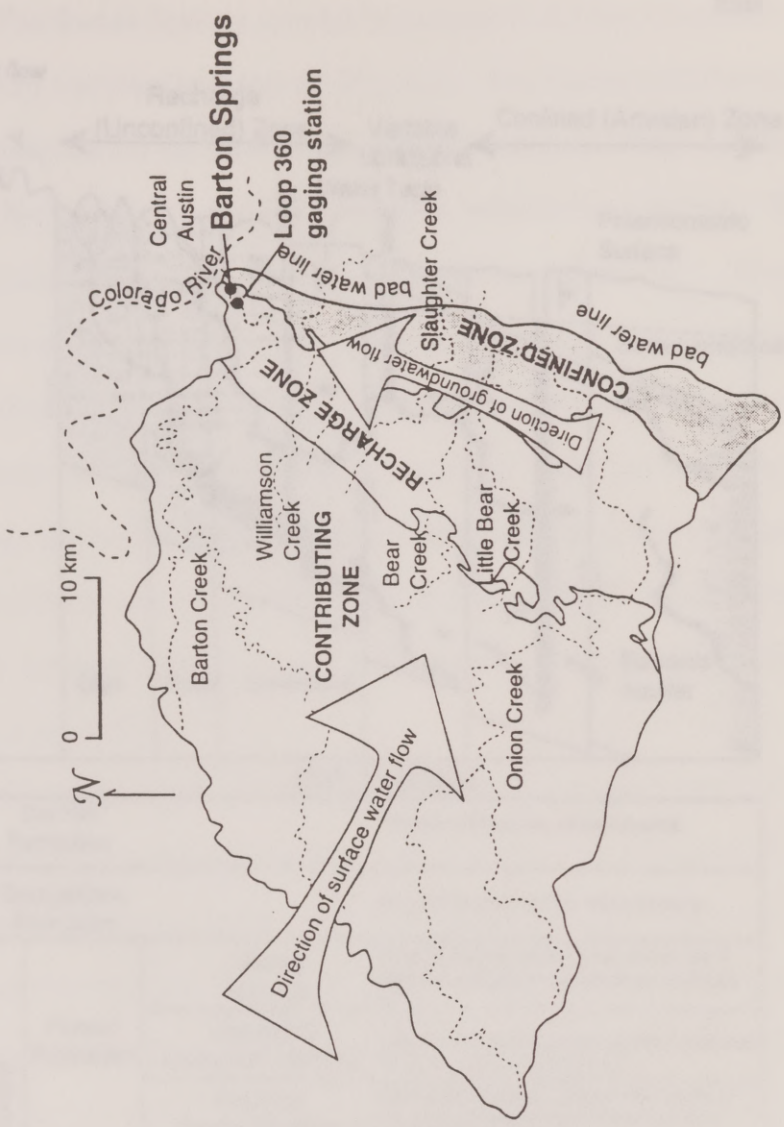

Figure 2.2. The zones of the Barton Springs Aquifer and watershed.

Surface water flows to the east across the Contributing Zone in creeks. When it crosses onto the Recharge Zone it infiltrates through fissures in the exposed Edwards Limestone into the aquifer; groundwater flows NNE toward Barton Springs. The Confined Zone is the portion in which the Edwards is overlain by the Del Rio Clay.

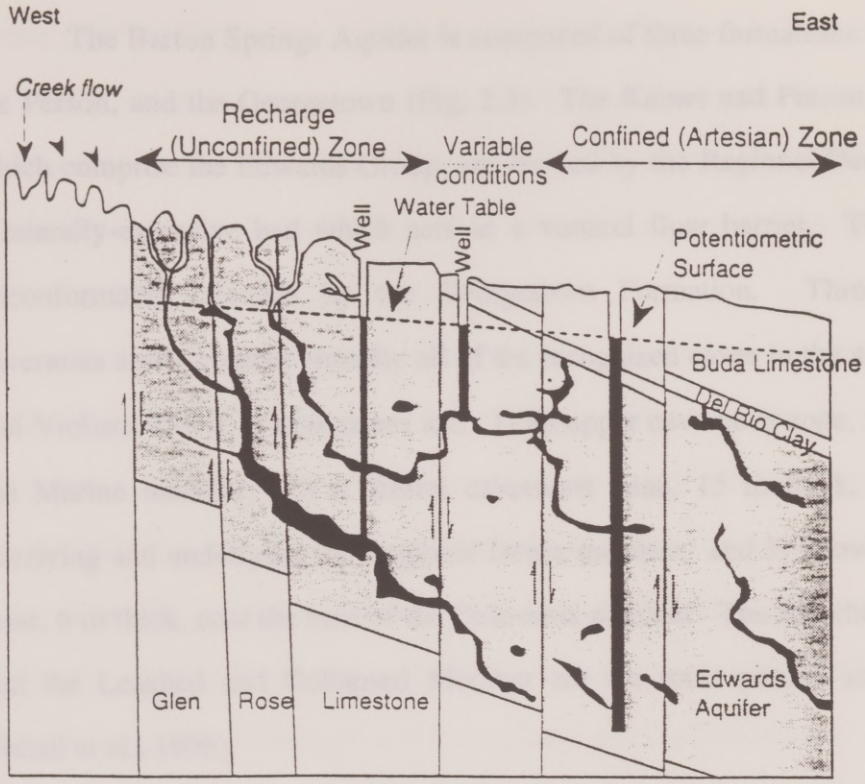

Barton Springs Aquifer	Del Rio Formation		Principal confining bed above Edwards.
	Georgetown Formation		Dense limestone; very low matrix porosity.
	Edwards Group	Person Formation	Marine Member	Reefal limestone; laterally extensive zones of significant porosity and permeability; karstified unit.
			Leached & Collapsed Member	Tidal and supratidal deposits; laterally extensive zones of honeycombed porosity.
			Regional Dense Member	Deep water limestone; negligible permeability and porosity; laterally extensive bed acts as vertical flow barrier.
		Kainer Formation	Grainstone Member	Shallow lagoonal sediments; cavernous, honeycombed layer occurs near the middle; interparticle porosity locally significant.
			Dolomitic & Kirschberg Members	Supratidal at top; tidal to subtidal below; very porous and permeable zones formed by boxwork porosity.
			Basal Nodular Member	Hard, dense, clayey limestone; negligible porosity and permeability.

Figure 2.3. Schematic cross-section of the Barton Springs Aquifer and the hydrogeologic stratigraphy of the members.

Cross-section adapted from Slade et al. (1986) and hydrostratigraphy from Maclay and Small (1976) and Rose (1972).

The Barton Springs Aquifer is composed of three formations: the Kainer, the Person, and the Georgetown (Fig. 2.3). The Kainer and Person Formations, which comprise the Edwards Group, are divided by the Regional Dense Member, a laterally-extensive bed which acts as a vertical flow barrier. The Person is unconformably overlain by the Georgetown Formation. Three horizontal cavernous zones contain virtually all of the recognized caves in the area (Hauwert and Vickers, 1994). These zones are: 1) an upper cavernous zone, 3 m thick, in the Marine member; 2) a central cavernous zone, 15 m thick, in the units overlying and underlying the Regional Dense member; and 3) a lower cavernous zone, 6 m thick, near the base of the Dolomitic member. The Kirschberg Member and the Leached and Collapsed Member are the most porous and permeable (Small et al., 1996).

The Barton Springs Aquifer and its watershed are divided into three areas: the contributing zone, the recharge zone, and the artesian zone (Fig. 2.2). The contributing zone, which covers 684 km^2, is that portion of the watershed which is underlain by the Glen Rose Limestone; surface flow from this area ultimately recharges the aquifer. The outcrop of the Edwards and Georgetown Limestones defines the 233 km^2 recharge zone. The artesian zone (or confined zone) is the eastern part of the aquifer, covering 158 km^2, where the Edwards and Georgetown limestones are confined by the relatively impermeable Del Rio clay. Seasonal fluctuations in the water table cause a narrow strip of this portion adjacent to the recharge zone to be under water table conditions at some times (Fig. 2.3). Most surface water flows east across the contributing zone contained in one of six main

creeks (Barton, Williamson, Slaughter, Little Bear, Bear, and Onion). Once these creeks cross onto the recharge zone, they recharge the aquifer through sinkholes and fractures in the creekbeds. Slade et al. (1986) estimate that 85% of recharge occurs through these creekbeds. The direction of groundwater flow is NNE, following the trend of the Balcones fault zone.

Barton Springs water is, in general, a calcium-magnesium bicarbonate water (Senger, 1983; Slade et al., 1986). When aquifer levels are low, concentrations of primarily sodium and chloride and to a lesser extent sulfate and magnesium increase. Slade et al. (1986) attribute this to encroachment of the bad water zone. As conditions in the aquifer change from high-discharge to drought conditions, the greatest water-level fluctuations are seen in the confined (eastern) part of the aquifer. Changes in the potentiometric surface indicate that although the general direction of groundwater flow is to the east then north, during periods of low flow some water from east of the bad water line may ultimately discharge at Barton Springs (Fig. 2.4).

Barton Springs consists of three major sets of hydrologically-connected springs: Eliza Springs (also known as Concession Springs and the Polio Pit), Old Mill Springs (also known as Sunken Gardens and Walsh Spring), and, the largest of the trio, Parthenia Springs (also known as Main Springs) (Fig. 2.5). In 1910 a dam was built just downstream of Parthenia springs, creating Barton Springs Pool (Slade et al., 1986). Barton Creek above Barton Springs pool is routed around the pool by a bypass structure. Only under extreme conditions does creekflow

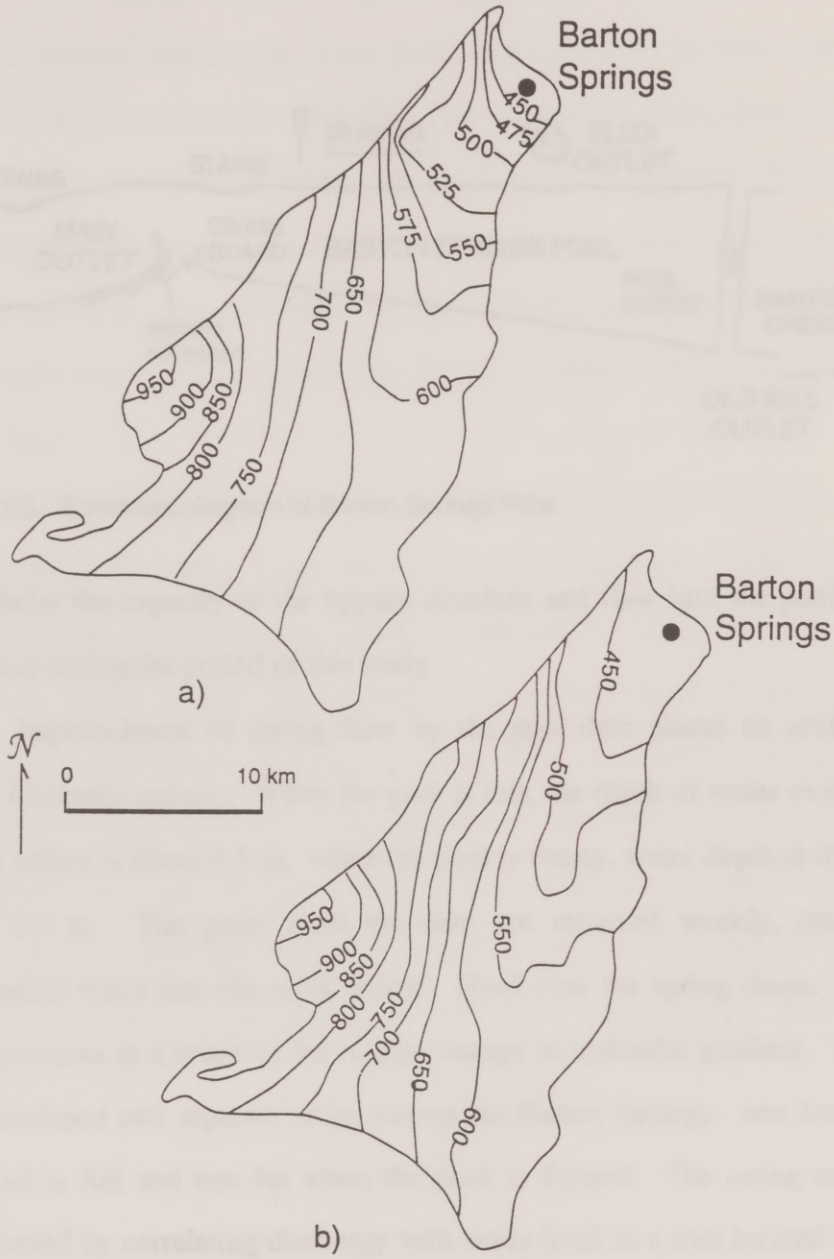

Figure 2.4. Potentiometric surface of the Barton Springs Aquifer under contrasting aquifer conditions.

Figure 2.4a represents the potentiometric surface when aquifer level is high, and 2.4b when aquifer level is low. Adapted from Slade (1986).

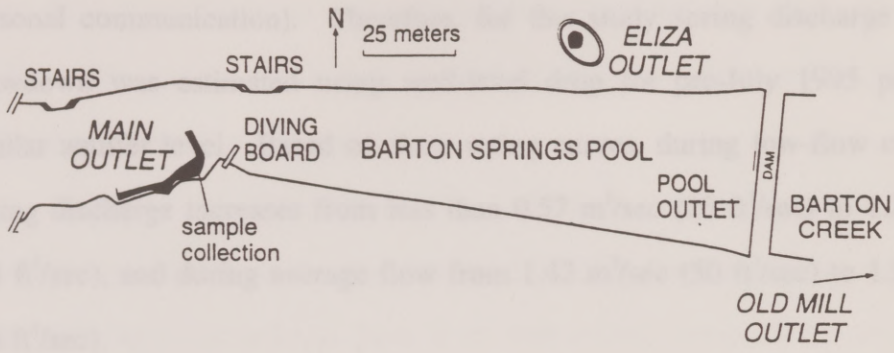

Figure 2.5. Schematic diagram of Barton Springs Pool.

overwhelm the capacity of the bypass structure and flow into the pool; this did not occur during the period of this study.

Impoundment of spring flow by the pool dam places an artificial head above Parthenia springs. When the pool is full, the depth of water over the main spring orifice is about 4.5 m; when the pool is empty, water depth at that point is about 3.2 m. The gates from the dam are removed weekly, releasing the impounded water into the creek below. Head over the spring drops, and spring flow increases as a result of the sudden change in hydraulic gradient. The USGS has developed two separate rating curves for Barton Springs: one for use when the pool is full and one for when the pool is drained. The rating curves were constructed by correlating discharge with water level in a well located 61 m from Parthenia Springs. Use of these rating curves is discussed in detail by Senger (1983) and Slade et al. (1986). Up until July 1995 the average drop in well level caused by draining of the pool was 1.22 m. After July 1995, the average drop was

0.23 m. This change was caused by the addition of a mechanical stop in the well bore to prevent the sensor from becoming entangled in tree roots (Dorsey, personal communication). Therefore, for this study spring discharge for pool drawdown was estimated using well-level drop for pre-July 1995 periods of similar aquifer level. Based on these rating curves, during low-flow conditions spring discharge increases from less than 0.57 m^3/sec (20 ft^3/sec) to 1.25 m^3/sec (44 ft^3/sec), and during average flow from 1.42 m^3/sec (50 ft^3/sec) to 1.93 m^3/sec (68 ft^3/sec).

Data collected by the City of Austin show an increase in specific conductance of spring water following pool drawdown. The City collects measurements of temperature, specific conductance, pH, depth, and turbidity in the main orifice of the pool springs at 15-minute intervals with a Hydrolab DataSonde 3 automatic data logger. The increase in conductance caused by pool drawdown ranges from 5% under high-flow conditions to 12% under low-flow conditions; the maximum increase occurs 12 hours after the pool is drained, and the initial conditions are recovered 12 to 13 hours after the gates are replaced and the pool has filled (refilling the pool takes from one to several hours, depending on spring flow).

METHODS

Sample Collection

Samples for both sediment and water analyses were collected from an orifice of Barton Springs located to the south of and approximately 2 meters

higher than the main orifice (Fig. 2.5). The crevice in the limestone from which the water issues is wide enough to allow sample collection, and the force of the spring flow is sufficient to prevent backflow from the pool from entering the crevice. This sample site is used by both the City of Austin and the USGS for analyses of Barton Springs water.

Sediment and water samples were collected at hourly intervals following two high-intensity storm events. Shortly following these storm events the dam gates were removed and the pool level was drawn down. To determine the changes in water chemistry and turbidity that might be caused by the drawdown as opposed to the rain event, water samples were collected at hourly intervals following pool drawdown at a time when there had been no recent rainfall.

The first event ("Storm 1") occurred on October 31-November 1, 1995. From 4:00-6:00 pm on October 31st 27.9 mm of rain fell. At 5:30 pm that afternoon water in the pool was still very clear, with good visibility to the bottom, a depth of approximately 4 meters. The pool gates were lowered at 10 pm. The following morning, November 1st, 57.1 mm of rain fell from 1:00-6:00 am, with most of it falling from 1:00-2:00 am and 5:00-6:00 am. At 8:00 am water in the pool was noticeably turbid, and the bottom was no longer visible. At 5:00 am the pool gates were reinstalled and the pool level allowed to rise; the gates were again removed at 10:00 am and not reinstalled until 5:30 a.m. November 2nd.

The second event sampled was on May 30th, 1996, when 44 mm of rain fell between 3:00-4:00 am, daylight savings time ("Storm 2"). Between these two storms, the only precipitation greater than 10 mm occurred on April 5 when 24

mm of rain fell. Storm 2 thus represents the first significant rainfall following six months of drought. The day prior to this rainfall event water in the pool was clear; by 7:00 am that morning pool water had become cloudy. The pool was drawn down at 9:15 a.m. May 30th and allowed to fill again at 7:00 p.m. the same day.

On July 18-19, 1996, samples were collected hourly from the spring beginning fifteen minutes before drawdown at 8:00 p.m. ("drawdown"). There had been no rainfall the three weeks previous except for 1.0 mm of rain on July 10th. The pool gates were reinstalled at 5:00 am July 19th, then removed again at 10 pm the same day.

Turbidity, pH, conductivity, and dissolved oxygen were measured in situ using a Horiba Model U-10. Samples for sediment and water chemistry analyses were collected in 20-liter polyethylene containers (two per sample) by submerging the container in the springflow issuing from the crevice; care was taken to insure that only spring flow, rather than pool water, was collected. Aloquots for alkalinity, anion, cation, and particle size distribution analyses were removed after transport to the laboratory. (During the drawdown event, water samples for cation, anion, and alkalinity analysis were filtered onsite and stored on ice.) Aloquots for alkalinity, anion, and cation analysis were filtered to 0.22 μm, and cation samples were acidified with concentrated nitric acid to a pH of 3. Alkalinity analyses were performed immediately after separation of the aloquot; anion and cation samples were kept refrigerated until analysis. One-liter samples were removed for measurement of total suspended solids.

The particulate fraction in the remaining sample (approximately 38.5 liters) was concentrated by in-line centrifugation. The sample was pumped at a steady rate of 120 ml/min through a Servall in-line system rotating at 6000 rpm. Residence time was 3.3 minutes, corresponding to collection of the > 0.3-μm fraction. A composite sediment sample from the main orifice of Barton Springs was also collected, so that enough sample could be obtained to performed an organic carbon analysis. One day prior to Storm 2, bundles of cotton fibers were placed inside a kicknet and secured inside the orifice. After the storm event, the cotton bundles were removed and the sediments rinsed out. The sediment obtained was passed through a 63-μm sieve to remove any cotton fiber and concentrated by in-line centrifugation; the <63 μm fraction was viewed under a binocular microscope to verify the absence of fibers.

Analyses

Changes in total suspended solids concentration (TSS), particle size distribution, and whole rock mineralogy were determined for suspended sediment collected approximately hourly after each of the two storm events. Clay mineralogy and organic carbon content were determined for the composite sample. Alkalinity, cation, and anion concentrations were determined for water samples collected after the two storm and drawdown events. All analyses were performed at the University of Texas at Austin Department of Geological Sciences, with the exception of the particle size distribution analyses, which were

performed at the Environmental and Water Resources Engineering area of the Department of Civil Engineering, University of Texas at Austin.

Total suspended solids were determined by weight difference after vacuum filtration. One-liter samples were passed through 0.22 μm 47-mm diameter filters (MSI MicronSep) and allowed to dry for 48 hours. The filters were weighed before and after filtration. The average difference in weight of three filters through which distilled deionized water had been passed was subtracted from the computed sample weight. The filters were then examined under a binocular microscope.

Whole-rock mineralogy was analyzed by X-ray diffraction (XRD). Samples were ground to a powder and back-loaded into sample holders. The sample for clay analysis was prepared by ultrasonically disaggregating the sample, removing the <1 μm fraction by centrifugation, and orienting the sample by the Millipore filtration technique, as described by Lynch (1994). Whole-rock XRD spectra were collected on a Siemens D-500 diffractometer, using a 0.02° 2θ step and a 2-second time count. The data were interpreted as described in Lynch (1994).

Particle size distributions were determined by the Coulter Counter system (Coulter Multizer, Couleter Electronics), which measures the number and size of particles suspended in an electrolyte solution. In brief, an electric current is held constant between two electrodes in the solution, one on either side of a small aperture. The suspension is pulled through this small opening, and as each particle passes through the aperture, the change in resistance induces a voltage

pulse which is proportional to the particle volume. A range of aperture sizes is used to measure number concentration over a range of particle sizes. Fifteen, 100, and 280 μm apertures in a 4%, 2%, and 2% NaCl solutions, respectively, were used for Storm 1. Thirty, 100, and 280 μm apertures with a 2% NaCl solutions were used for Storm 2.

Total organic carbon content for the composite sample was determined by dissolution of the carbonate minerals with nitric acid, elution of the non-purgeable fraction of the organic carbon, and analysis of both the non-purgeable organic carbon (NPOC) and soil organic carbon (SOC). Analyses were performed on a Dohrmann DC-180 carbon analyzer by UV-promoted wet-oxidation and infrared detection of the evolved CO_2 for the NPOC, and high-temperature vaporization and subsequent oxidation of CO_2 by a continuous O_2 flow followed by infrared detection for the SOC. Total organic carbon (TOC) was computed as the sum of the NPOC and the SOC.

Alkalinity was measured using a Metrohm 702 SM Titrino auto-titrator and reported as concentration of bicarbonate ion. Concentrations of anions were determined by single-column ion chromatography (Waters Ion Chromatograph) by EPA method A-1000. Each sample was passed through a Waters Sep-Pak cartridge, and analyzed using a 150 x 4.6 mm IC-Pak A HC column and borate/gluconate eluent. Cation concentrations were determined on a JY inductively-coupled atomic emission plasma spectrometer. Cation and ion imbalance was less than 5% for all samples except one sample from Storm 2 which was therefore discarded.

RESULTS

Precipitation and Discharge

Discharge for both storms, computed based on the rating curves developed the USGS and discussed earlier, are shown in Figure 2.6. Draining of the pool after both storms increased spring discharge dramatically. It is impossible to ascertain when and at what volume discharge would have peaked had the pool not been drained; however, based on the spring hydrographs (Fig. 2.6), for Storm 2 it appears that the maximum discharge would have between 12 and 24 hours after rainfall began, and it is probable that the same is true for Storm 1.

Particulates

Total suspended solids (TSS), in milligrams per liter, and whole rock mineralogy, in percent by weight, are shown in Figure 2.7. Parameters are plotted versus time after rainfall. For this and subsequent graphs, the time datum for Storm 1 was chosen to be the rainfall which occurred in the early morning hours of November 1st, as it greatly exceeded the rainfall of the previous afternoon. Total suspended solids began increasing about 8-9 hours after rainfall

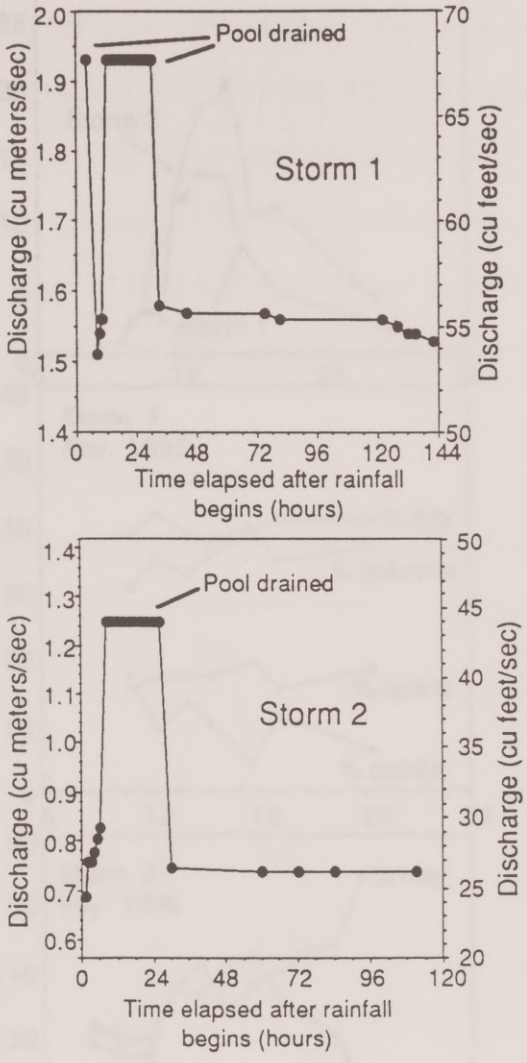

Figure 2.6. Discharge from Barton Springs for Storm 1 (November, 1995) and Storm 2 (May-June, 1996).

Discharge increases dramatically when the pool is drained. Discharge determination is based on well-levels in a nearby well and rating curves developed by the USGS.

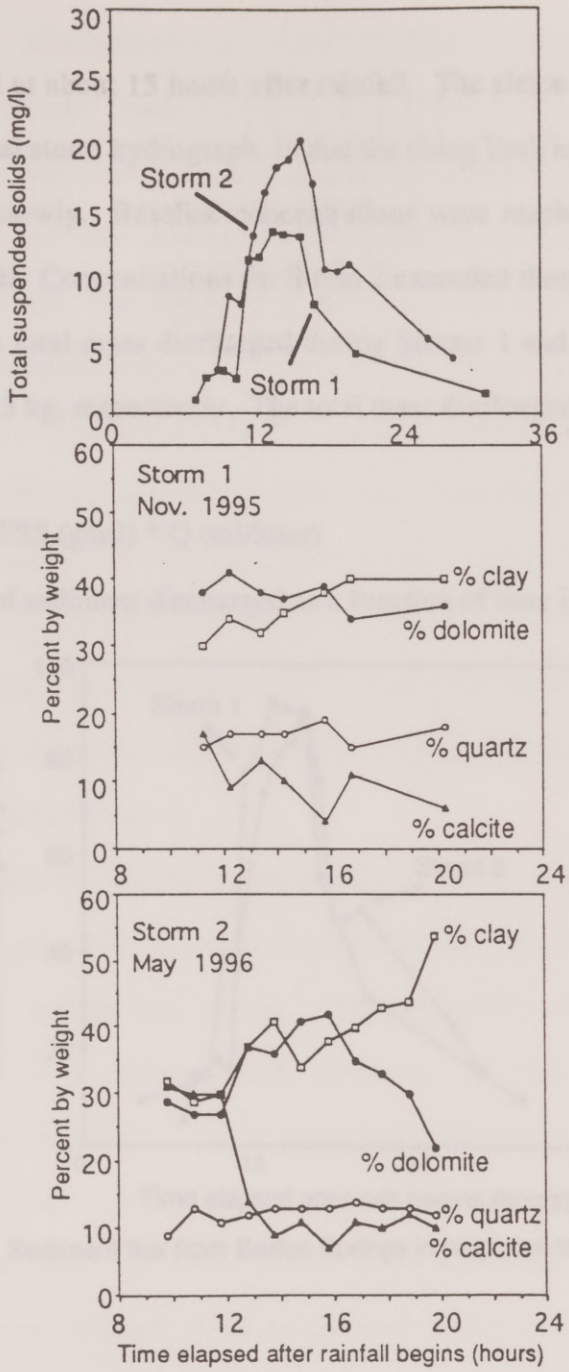

Figure 2.7. Changes in total suspended solids and mineralogy in response to storm events.

Shown here are: total suspended solids in response to both storms, mineralogy for Storm 1, and mineralogy for Storm 2.

and peaked at about 15 hours after rainfall. The shape of the curves looks much like a typical storm hydrograph, in that the rising limb is steep and the falling limb tapers off slowly. Baseline concentrations were reached at more than 30 hours after rainfall. Concentrations for Storm 2 exceeded those for Storm 1.

The total mass discharged during Storms 1 and 2 was approximately 805 kg and 1013 kg, respectively. The total mass discharged was calculated as

$$\sum \text{TSS (g/ml)} * \text{Q (ml/hour)} \qquad (2.1)$$

The mass of sediment discharged as a function of time is shown in Figure 2.8.

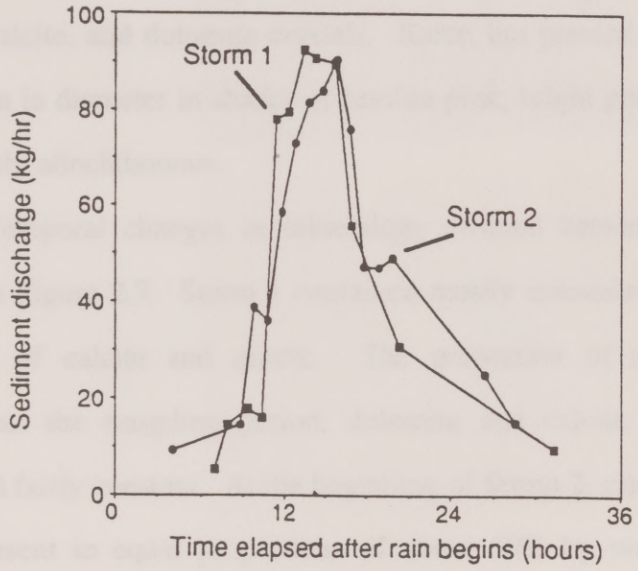

Figure 2.8. Sediment flux from Barton Springs in response to Storms 1 and 2.

After filtration of particles for measurement of TSS, the color of the filters ranged from nearly white for the first sample to a rich tan at peak TSS. Inspection

and organic, allochthonous and autochthonous material. Most striking was the number of colored fibers collected on virtually all of the filters. Fiber length ranged from hundreds of microns to one millimeter or more, and colors included white, black, red, blue, pink, green, and purple in a variety of shades. Some fibers were coated with what appeared to be organic matter and others were ensnared in clumps of inorganic particles (Fig 2.9a). The organic matter contained was a dark brown-black. The amount of the organic material appeared to increase with increasing TSS and is probably what gave the filters their tan color. Individual pieces of organic matter ranged from a few microns to 50 microns in diameter (Fig. 2.9b,c). Recognizable inorganic particles retained by the filter included quartz, calcite, and dolomite crystals. Rarer, but present, were colored particles 10-20 μm in diameter in shades of fuschia-pink, bright green, and turquoise blue, most likely allochthonous.

Temporal changes in mineralogy differed between the two storms, as shown in Figure 2.7. Storm 1 contained mostly dolomite and clay, with smaller amounts of calcite and quartz. The proportion of clay content increased throughout the sampling period, dolomite and calcite decreased, and quartz remained fairly constant. At the beginning of Storm 2, clay, dolomite, and calcite were present in equal proportions of about 30% by weight, while the quartz content was 10%. At about twelve hours after rainfall, the calcite proportion dropped to that of quartz, while proportions of clay and dolomite began to

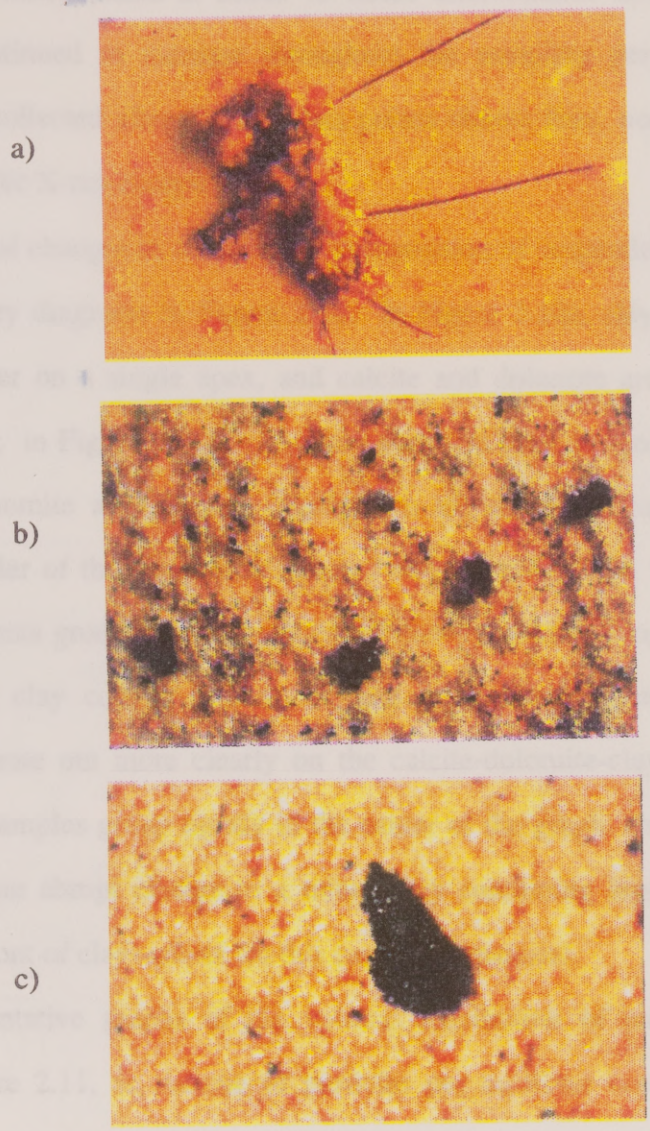

Figure 2.9. Particulates discharged from Barton Springs after a storm.

(a) Particulate discharged from Barton Springs after Storm 1. Field of view is 1.7 mm. The particle appears to be purple thread ensnared in a clump of mineral grains and organic matter. (b) and (c) Organic matter (dark particles) discharged from Barton Springs after Storm 2. Field of view is 0.75 mm and 1.7 mm, respectively.

increase. Dolomite peaked at about 15 hours after rainfall and then dropped, while clay continued to increase throughout the sampling period. Although samples were collected after the last data points shown here, not enough solids were retrieved for X-ray analysis.

Temporal changes in mineralogic composition of suspended sediments are shown in ternary diagrams in Figure 2.10. In Figure 2.10a, clay and quartz are grouped together on a single apex, and calcite and dolomite are each assigned their own apex; in Figure 2.10b, clay and quartz are each assigned an apex, and calcite and dolomite are grouped together on the third as "carbonate." The chronologic order of the samples is denoted with numbers. On both graphs the Storm 1 sediments group tightly together but show a gradual progression toward an increase in clay content and a decrease in carbonate content. Storm 2 sediments separate out more clearly on the calcite-dolomite-clay+quartz graph: the first three samples group tightly in the center of the graph, and the following samples show an abrupt change to a mineralogy containing less calcite and an increasing amount of clay+quartz (in this case clay) material.

Representative graphs of the volume distribution of particle sizes are shown in Figure 2.11, as volume of particles per milliliter versus log particle diameter. The volume of particles was computed by assuming a spherical shape and multiplying the number distribution by the volume of a sphere. Each value on the ordinate was normalized by dividing it by the logarithmic interval of particle size (log dp) associated with each size, in this case a constant value of 0.012. The division was performed so that the same suspension measured by a different

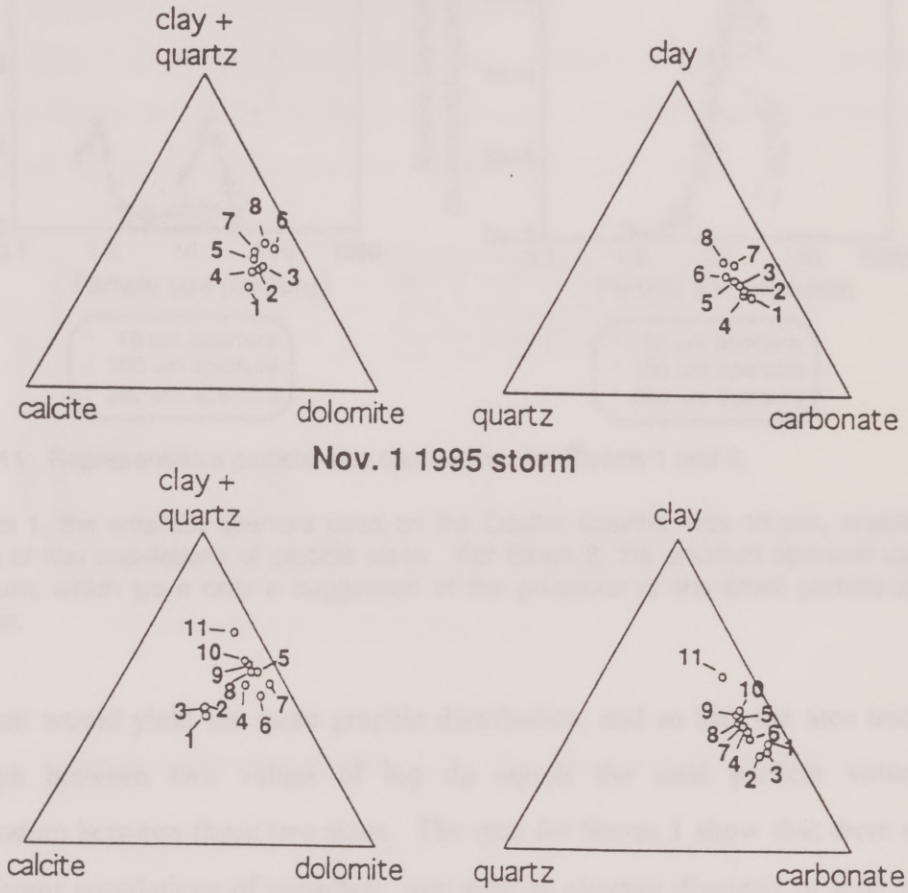

Figure 2.10. Changes in the mineralogic composition of sediments discharging from Barton Springs in response to Storms 1and 2.

Numbers represent the chronological order of samples. In figure (b) the carbonate apex represents dolomite + calcite.

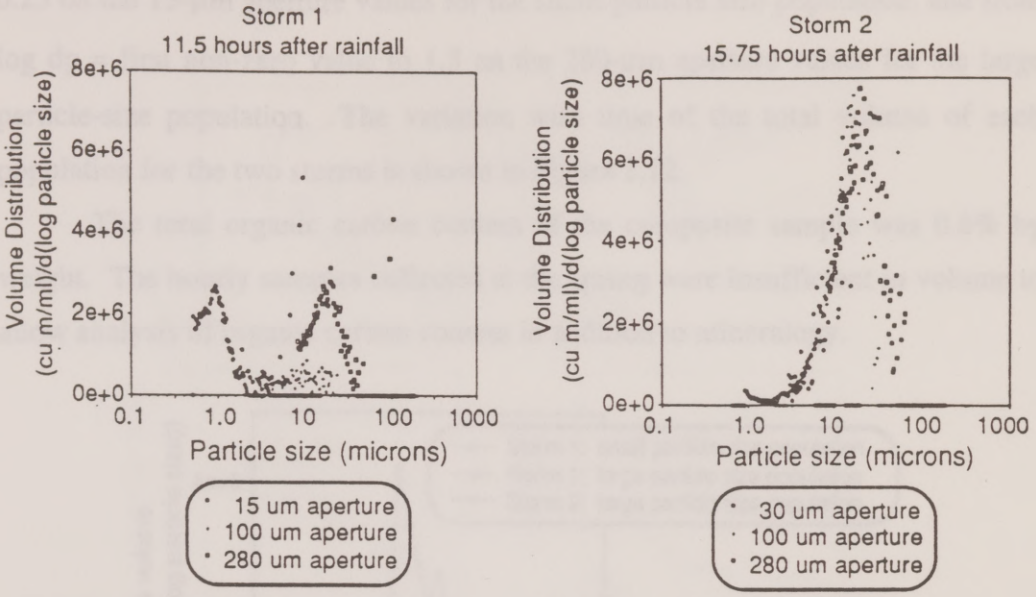

Figure 2.11. Representative particle-size distributions for Storms 1 and 2.

For Storm 1, the smallest aperture used on the Coulter Counter was 15 μm, enabling detection of two populations of particle sizes. For Storm 2, the smallest aperture used was 30 μm, which gave only a suggestion of the presence of the small particle-size population.

instrument would yield the same graphic distribution, and so that the area under the graph between two values of log dp equals the total particle volume concentration between those two sizes. The data for Storm 1 show that there are two different populations of particles: one with an average diameter of 0.65 μm and one with an average diameter of 13 μm. Unfortunately, the smallest Coulter counter aperture used for Storm 2 was 30 μm, in contrast to the 15-μm aperture used for Storm 1. The 30-μm aperture was not sufficiently small to capture the smaller particle-size population; there is a strong suggestion that the population exists in these samples but it is impossible to determine what the distribution looks like. The total volume of each population for each sample was calculated by integrating under the population curve from log dp = first non-zero value to

0.25 on the 15-μm aperture values for the small-particle size population, and from log dp = first non-zero value to 1.5 on the 280-μm aperture values for the large particle-size population. The variation with time of the total volume of each population for the two storms is shown in Figure 2.12.

The total organic carbon content of the composite sample was 0.8% by weight. The hourly samples collected at the spring were insufficient in volume to allow analysis of organic carbon content in addition to mineralogy.

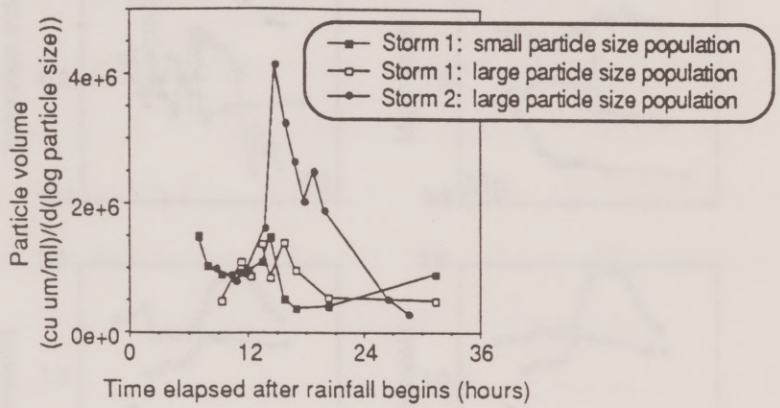

Figure 2.12. Changes in volume of particles of both small- and large-size populations in response to rainfall.

Particle volume is expressed as cubic microns per milliliter divided by the log of the particle-size increment. The area under the curve thus represents total volume.

Aqueous Chemistry

The results of the water chemistry analyses for Storm 1, Storm 2, and drawdown are shown in Figure 2.13. Both storms are displayed in terms of time

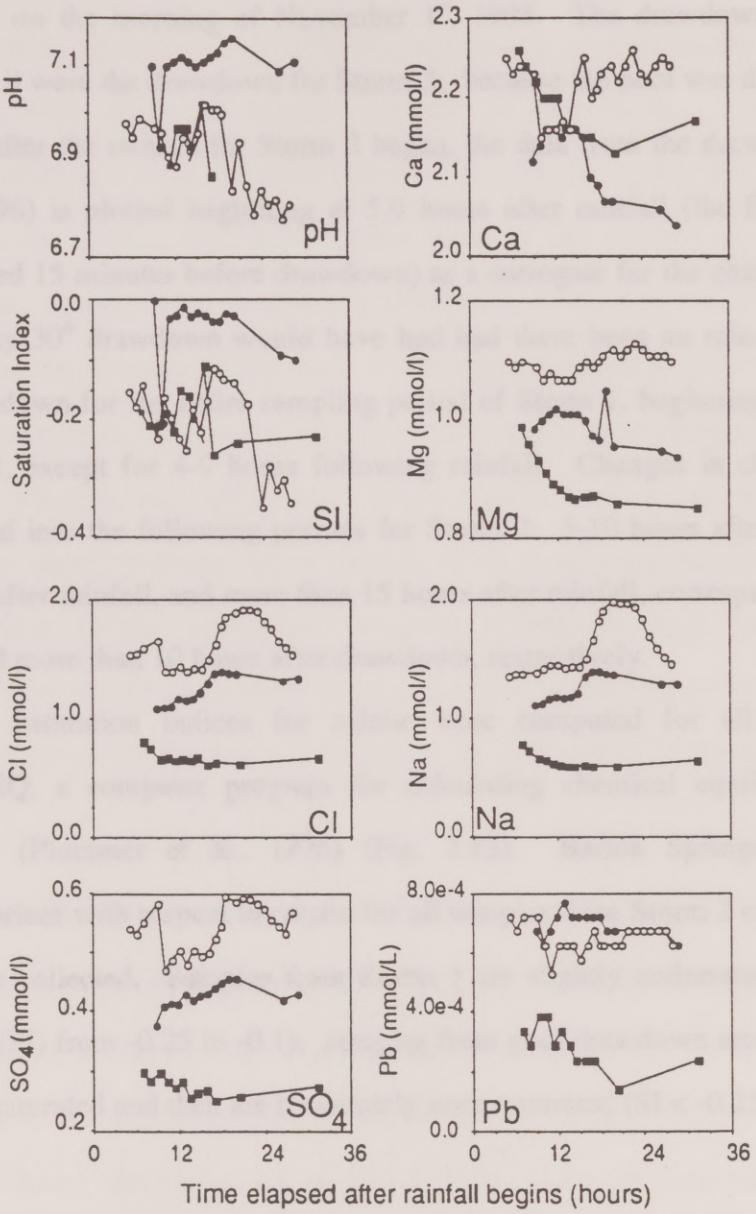

Figure 2.13. Changes in aqueous chemistry in response to rainfall and pool draining.

Samples from Storm 1 are represented by squares, from Storm 2 by closed circles, and from pool draining (drawdown) by open circles.

elapsed after rainfall. Here again the time datum chosen for Storm 1 was the rainfall on the morning of November 1st, 1995. The drawdown is graphed as though it were the drawdown for Storm 2; because the pool was drawn down 5.25 hours after the rainfall for Storm 2 began, the data from the drawdown (July 18-19, 1996) is plotted beginning at 5.0 hours after rainfall (the first sample was collected 15 minutes before drawdown) as a surrogate for the chemical effect that the May 30th drawdown would have had had there been no rain. The pool was drawn down for the entire sampling period of Storm 1, beginning 3 hours before rainfall, except for 4-9 hours following rainfall. Changes in chemistry can be grouped into the following periods for Storm 2: 5-10 hours after rainfall, 10-15 hours after rainfall, and more than 15 hours after rainfall, corresponding to 0-5, 5-10, and more than 10 hours after drawdown, respectively.

Saturation indices for calcite were computed for all samples using WATEQ, a computer program for calculating chemical equilibria of natural waters (Plummer et al., 1976) (Fig. 2.13). Barton Springs water was in equilibrium with respect to calcite for all samples from Storm 2 except the second sample collected. Samples from Storm 1 are slightly undersaturated (saturation index (SI) from -0.25 to -0.1); samples from pool drawdown are initially slightly undersaturated and then are moderately undersaturated (SI < -0.25).

Discussion

Storm events transport up to a metric ton of allochthonous and autochthonous sediment through the aquifer after a storm event, most of which is

discharged from the aquifer within the first 24 hours following rainfall. Mineralogic composition of the sediments is a function of both source and particle size; similar behavior of two different populations of particle sizes indicates that clay particles enter the aquifer already in suspension. Changes in the concentration of suspended solids through time reflects hydrologic response to the storm at the surface and in the distal parts of the aquifer rather than spring discharge. Spring water chemistry is affected by antecedent conditions, the storm itself, and the draining of the pool. Low aquifer levels and pool drawdown both cause intrusion of "bad water" into spring discharge, increasing concentrations of sodium, chloride, and sulfate ion. When aquifer level is low, this "bad water" signature largely swamps out the diluting effect on spring chemistry of rain water. In addition, when antecedent moisture conditions have been very dry, precipitation causes concentrations of some ions to increase rather than decrease, probably caused by flushing of water from the diffuse part of the aquifer.

Suspended Solids

Both allochthonous and autochthonous sediments discharge from Barton Springs after a storm event. The presence of colored fibers on filters was visible evidence of anthropogenic particulates (Fig. 2.9). Organic matter was also visible on the filters; the composite sample collected from the main orifice of Barton Springs had a total organic carbon content of 0.8%. In Chapter 1 it was suggested that organic carbon is an indicator of allochthonous sediments, as sediments in

creek beds and sinkholes contained a higher percentage by weight of organic matter, from 0.5 to 4%, than sediments in caves and wells.

The mineralogic composition of the sediments also suggests both allochthonous and autochthonous origin. The calcite content of samples collected after Storm 1 decreases as the storm response progresses, while the clay content increases. In the samples from Storm 2, change in the mineralogic signature as the storm response progresses is even more pronounced. The first samples collected after Storm 2 have equal proportions of clay, calcite, and dolomite, placing them in the center of the ternary diagram (Fig. 2.10a). As the storm progressed, the mineralogic composition moves toward the dolomite-clastic axis, and then toward the clastic apex as clay content increases. In Chapter 1 it was shown that allochthonous sediments grouped along the calcite-clastic axis of a ternary diagram, whereas autochthonous sediments grouped along the clastic-dolomite axis. It appears, then, that the sediment samples have a mineralogic signature that is initially mixed allochthonous-autochthonous, which becomes more autochthonous approximately 12 hours after rainfall. This supports the "two flow system" hypothesis proposed in Chapter 1: that Barton Springs is fed by both a shallow vadose flow system, and a deeper phreatic flow system (Figure 1.11). The mineralogic results suggest that the shallow system responds more quickly to surface recharge, conveying calcite-rich sediments to Barton Springs, which is then diluted by input from the deeper, phreatic system.

The mineralogic composition of Barton Springs sediments becomes increasingly clay-rich as the response time to both storms progresses. This may

be an indicator of sediment source: sediments from caves, in particular, contain a high proportion of clay. Alternatively, the low proportion of clay in the surface sediments and the increase in the proportion of clay in the springs as time elapsed after rainfall increases may be imposed by the hydraulics of sediment entrainment and transport. Clay mineral particles tend to be smaller, more cohesive, and have a greater drag coefficient than other mineral particles because of their platey habit (White, 1988). They require a greater erosional force to entrain than larger particles but once in suspension remain suspended at lower flow velocities than larger particles (Fig. 2.14). Thus sediments collected in streambeds and sinkholes

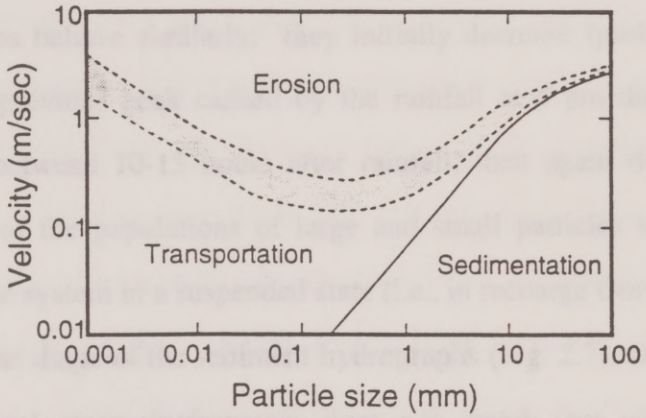

Figure 2.14. Depiction of conditions of sediment deposition and transport.

The shaded band is the experimentally-determined Hjulstrom's curve, which represents the velocity required as a function of particle size to bring particles into suspension. The straight solid line is the Shields curve, which describes conditions necessary to keep material in transport once they have been entrained. Adapted from White (1988).

may contain only small amounts of clay minerals, not because clay minerals are not allochthonous, but because they remain in suspension in surface water flow and either enter the aquifer with recharge or are carried to the Colorado River rather than being deposited in the creekbed. Similarly, the increasing proportion of clay minerals at the end of the sampling periods following the storms may be

caused by decreasing flow velocities in which larger particles are deposited while small particles continue stay in suspension.

The question of the origin of the clay can be clarified by examination of the grain-size distributions, which suggest that the clay entered the aquifer in suspension rather than being eroded internally. As discussed above, small particles require a greater flow velocity to be entrained than large particles (Fig. 2.14). If clay particles are being eroded from within the aquifer, we would expect the increase in volume of small particles to lag behind that of large particles. From Figure 2.12, however, it appears that both the small and large grainsize populations behave similarly: they initially decrease (probably evidence of the end of a previous peak caused by the rainfall at 4 pm the previous day), then increase between 10-15 hours after rainfall, then again decrease. The similar behavior of the populations of large and small particles suggests that the clay entered the system in a suspended state (i.e., in recharge from the surface).

The shape of the sediment hydrographs (Fig. 2.7), although similar to that of a typical storm hydrograph, does not match that of the Barton Springs discharge hydrograph. The Barton Springs hydrograph is unlike that of a typical spring hydrograph because of the change in discharge artificially caused by lowering the pool (Fig. 2.6). After Storm 1, discharge at Barton Springs remained at a constant high from midnight October 31st until midday November 2nd except for a few hours the morning of October 31st, yet TSS rises and falls over a ten hour period from 11:00 am to 9:00 pm November 1st. Following Storm 2, the pool was lowered and discharge doubled from mid-day May 30th through the morning of

May 31st with no interruptions, yet TSS rose and fell between 1:00 and 11:00 pm on May 30th. Furthermore, during the drawdown event monitored in mid-July 1996, the increase in spring discharge caused by lowering the pool had no effect on the turbidity, which remained constant. The changes in the concentration of particles thus cannot be directly attributed to changes in discharge at the springs; it must therefore be caused either by changes in flow conditions at the surface or in the more distal parts of the aquifer unaffected by a change in head at the spring. The shape of the sediment hydrograph at Barton Springs is more similar to the storm hydrograph of Barton Creek, measured at a gaging station upstream from Barton Springs (Loop 360, Figure 2.2) and shown in Figure 2.15, than it is to the spring hydrograph. The peak in sediment concentration at the springs lags that of flow at Barton Creek by about 12 hours. This suggests that the suspended sediment discharging from the springs was brought in by recharging storm water. This hypothesis is supported by the abundance of colored fibers in the samples, whose possible origins include discarded blankets and clothing in creekbeds, discharge of domestic wastewater from package treatment plants, and spray-irrigated wastewater.

The bulk of the sediment discharge from the spring occurred within 24 hours of rainfall. By sampling at hourly intervals the sediment hydrograph was well-described; sampling at twelve hour or longer intervals, the length of many typical sampling regimes, would have been insufficient to characterize or possibly even detect the sediment discharge.

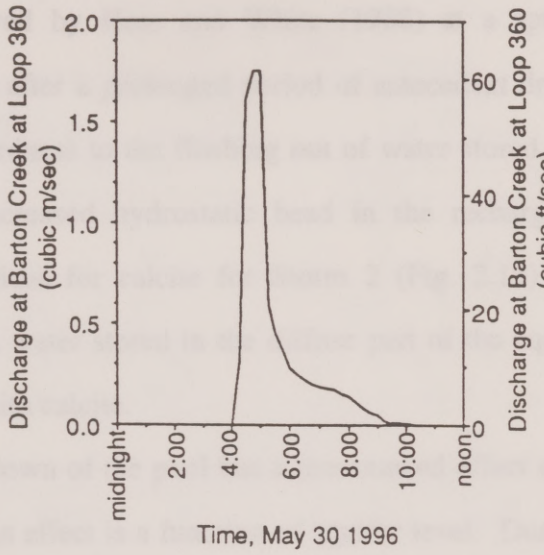

Figure 2.15. Creek discharge at Barton Creek and Loop 360 for Storm 2.

Data collected by USGS.

Aqueous Chemistry

Antecedent moisture conditions affect the response in spring chemistry to the two storms. Storm 1 occurred during a period of normal rainfall, whereas Storm 2 occurred after a six-month drought. After Storm 1, concentrations of major ions decreased as recharge diluted the aquifer (Fig. 2.13). This is the expected response to precipitation in a conduit-flow karst aquifer during normal

flow conditions (Hess and White, 1988; Dreiss, 1989). In contrast, after Storm 2, concentrations of both calcium and magnesium increased. This is similar to the effects observed by Hess and White (1988) at a spring in Mammoth Cave National Park after a prolonged period of antecedent dryness; they attribute the increase in hardness to the flushing out of water stored in the diffuse part of the aquifer by increased hydrostatic head in the recharge area. The calculated saturation indices for calcite for Storm 2 (Fig. 2.13) are consistent with this hypothesis, as water stored in the diffuse part of the aquifer is expected to be in equilibrium with calcite.

Drawdown of the pool has a pronounced effect on spring chemistry. The strength of this effect is a function of aquifer level. During normal aquifer levels (spring discharge 1.4 m^3/sec), draining the pool causes an increase in specific conductance of about 5%, whereas at low-flow conditions (spring discharge < 0.6 m^3/sec), the increase in specific conductance is about 12%. The pool was drained during all or part of the periods following both Storms 1 and 2, however, it had a greater effect after Storm 2 because the aquifer was under low-flow conditions.

Lowering the head over the springs by draining the pool has three sequential effects: 1) the concentration of most ions decreases as the spring water is diluted ; 2) concentrations of sodium, chloride, and sulfate increase, as seen in Figure 2.13 and 2.16; 3) the spring water chemistry returns to its original composition. This process, and the degree to which it affected spring chemistry following the two storms, is shown in Figure 2.16, in which samples from the three events are plotted in a manner similar to that done by Senger (1983), which

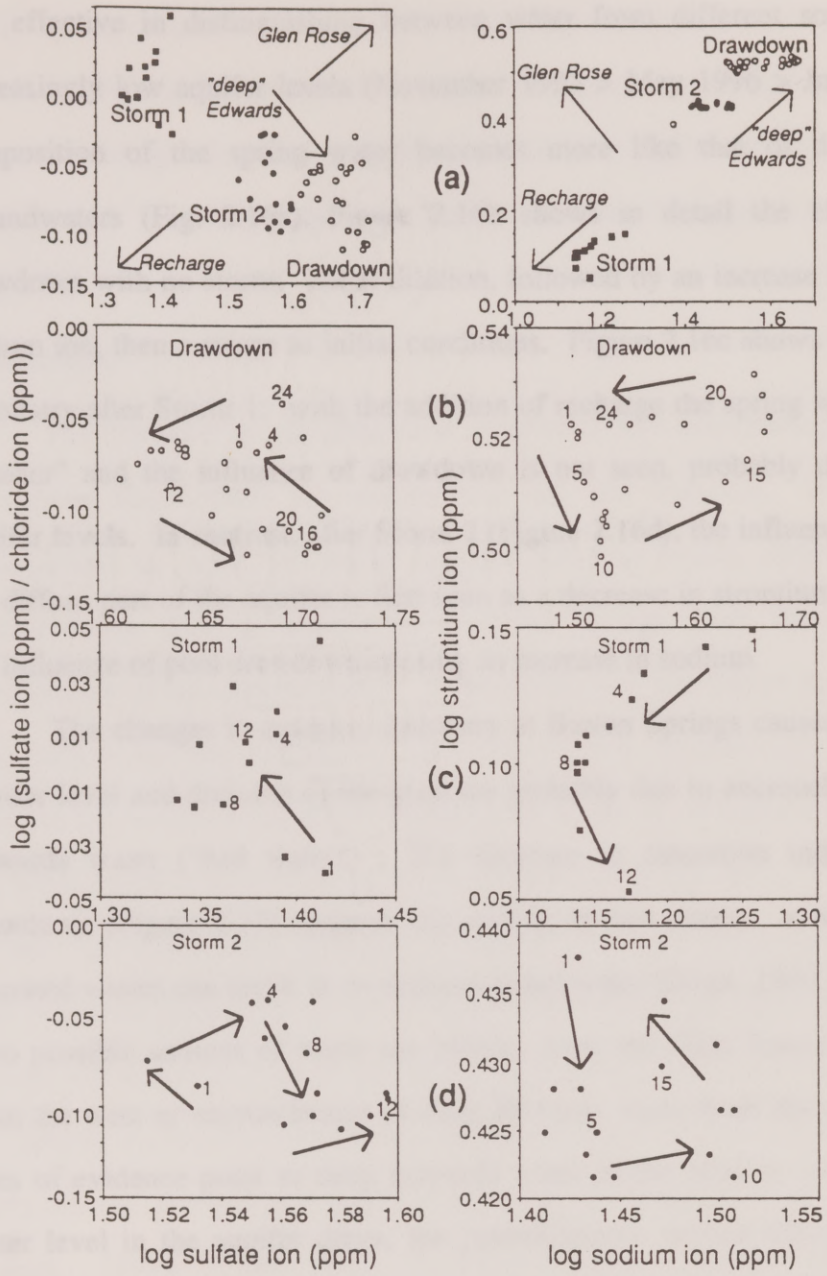

Figure 2.16. Variations in the relation between sulfate and chloride concentration and strontium and sodium concentration.

a) Storm 1, Storm 2, and pool drawdown. b) Drawdown in detail. c) Storm 1 in detail. d) Storm 2 in detail. Numbers represent chronological order of samples; arrows represent direction of chemical change. Source water chemistry from Senger (1983).

was effective in distinguishing between water from different sources. With increasingly low aquifer levels (November 1995 > May 1996 > July 1996), the composition of the spring water becomes more like that of deep Edwards groundwaters (Fig. 2.16a). Figure 2.16b shows in detail the effect of pool drawdown with no storm: initial dilution, followed by an increase in sulfate and sodium ion, then a return to initial conditions. Figure 2.16c shows the change in chemistry after Storm 1: with the addition of recharge the spring water becomes "fresher" and the influence of drawdown is not seen, probably due to normal aquifer levels. In contrast, after Storm 2 (Figure 2.16d), the influence of flushing the diffuse part of the aquifer is first seen as a decrease in strontium, followed by the influence of pool drawdown causing an increase in sodium.

The changes in aqueous chemistry at Barton Springs caused by both low aquifer level and draining of the pool are probably due to encroachment of deep Edwards water ("bad water"). The decrease in saturation index after pool drawdown (Figure 2.13) suggests the mixing of two waters: a mixture of two saturated waters can result in an undersaturated water (Bögli, 1980; White, 1988). Two possible sources of water are leakage from the Glen Rose from below or from the west or encroachment of deep Edwards water from the east. Multiple lines of evidence point to deep Edwards water as the mixing water: 1) as the water level in the aquifer drops, the potentiometric surface changes (Fig. 2.4), curving inward toward Barton Springs from the southeast; 2) the sulfate/chloride ion ratio of Barton Springs water decreases as aquifer level drops or the pool is drained—deep Edwards water has a lower sulfate/chloride ion ratio than "normal"

Barton Springs water while that of the Glen Rose is higher; 3) the concentration of sodium in the spring water increases both in response to dropping aquifer level and pool draining—deep Edwards groundwater has a higher sodium concentration than "normal" Barton Springs water, and that of Glen Rose groundwater is lower (Fig. 2.16).

Implications

The transport of allochthonous suspended sediment through the aquifer has critical implications for contaminant fate and transport. Poorly soluble contaminants, in particular neutral organics and trace metals, sorb to particles at concentrations tens to thousands of times greater than their equilibrium concentration in the aqueous phase. Contamination of the Barton Springs Aquifer from both point and non-point sources is not just hypothetical. Catastrophic events in the area have occurred: oil pipelines crossing the aquifer have ruptured, and spills reported to the Texas Water Commission from 1986 to 1992 included gasoline and diesel fuels, pesticides, ammonia, sodium hydroxide, hydrochloric acid, trichloroethane, and perchloroethene (US Fish and Wildlife Service, 1994). Several contaminants have been reported in well and spring samples: a study by the Barton Springs/Edwards Aquifer Conservation District found petroleum hydrocarbons, pesticides, arsenic, and lead in wells and springs (Hauwert and Vickers, 1994); the U.S. Geological Survey found low levels of tretrachlorethylene in Barton Springs on eleven occasions (Slade, 1991); the City of Austin found high levels of polycyclic aromatic hydrocarbons (PAHs) in sediments in Barton Creek and Barton Springs pool on two occasions (City of

Austin, 1994). Mobile sediment in the aquifer may play an important role in the fate and transport of contaminants such as these.

The degree to which concentration of hydrophobic organic contaminants on solid particles occurs is a function of both organic carbon content and mineralogy of the sediments. The composite sample collected at Barton Springs had an organic carbon content of 0.8%, significantly exceeding the threshold of 0.1% at which partitioning of non-polar organic compounds into organic matter is the dominant sorption process (Schwarzenbach et al., 1993). Particle size and organic carbon content are often inversely correlated (Smith et al., 1988). Therefore the small particle-size population (i.e., the clay) moving through the aquifer has the capacity to carry the greatest concentration of neutral organic contaminants. Because these particles originate at the surface where most contaminant spills occur, they are important potential vectors for contaminant transport.

Mobile sediment can also concentrate and transport trace metals. Lead is of particular concern in the Barton Springs Aquifer, as elevated levels of lead have been detected in wells and springs (Hauwert and Vickers, 1994). Hauwert found that concentrations of total lead significantly exceeded those of dissolved lead in most of the wells, evidence of the importance of sorption in the transport of this metal. Sorption of lead in soils is correlated with organic carbon and clay content (Singh and Sekhon, 1977; Adb-Elfattah and Wada, 1981), and increases strongly on both materials with increasing pH (Griffin and Shimp, 1976). Lead can also participate in surface exchange reactions on carbonates, as it readily

forms fairly insoluble carbonate complexes (log dissolution coefficient of -13.1) (Stumm and Morgan, 1981). Therefore not only the clay but also the calcite and dolomite particles have the potential to sorb and transport lead. Relatively high concentrations of lead (exceeding drinking water standards) were detected in water samples from Barton Springs (Fig. 2.13). Lead concentrations decreased after Storm 1, but increased in response to Storm 2. This may have been caused by the difference in antecedent moisture conditions: lead concentrating in the soil horizon during the dry period preceding Storm 2 would have then been flushed into the aquifer—mobile particulates may have been responsible at least in part for this transport.

As urbanization of the watershed continues the amount of sediment being transported through the aquifer will increase. Suspended clay particles in surface water enter the aquifer as recharge, therefore as the concentration of suspended sediment in recharging creeks increases so will the concentration moving through the aquifer. TSS in surface waterways in directly correlated with percentage impervious cover, an indicator variable for urbanization (Arnold and Gibbons, 1996). Increases in impervious cover—for example rooftops, roadways, and parking lots—alter surface hydrology, decreasing infiltration and increasing the amount and velocity of runoff to surface streams during rain events (Table 1.5). The net result is an increase in stormflow and a decrease in baseflow. Turbidity in creeks increases for two reasons: first, the increased velocity of surface runoff has a greater erosional power, causing runoff entering creeks to carry a greater sediment load; and second, the increased volume of surface runoff causes

increased stream power in creeks for a given rainfall intensity, increasing streambank erosion. Because most of the recharge entering the Barton Springs Aquifer infiltrates through fissures in major creekbeds, an increase in turbidity of surface water will cause an increase in the amount of surface sediment in aquifer recharge. This study shows that at least some portion of these allochthonous sediments move through the aquifer to emerge at Barton Springs.

CONCLUSIONS

This study is the first to examine characteristics of sediment discharging from a karst spring. On the order of a metric ton of sediment discharged from Barton Springs, the fourth largest spring in Texas, following each of two storms. Most of this sediment was discharged from the spring within 24 hours following rainfall; a sample interval less intensive than every few hours would have been insufficient to describe the peak. The suspended sediment was comprised of two discrete populations of particle sizes; the similar behavior of both populations with time implies that the smaller size fraction is entering the aquifer suspended in recharging surface water. Changes in the mineralogic character of discharging sediments over time supports the hypothesis that Barton Springs is fed by two types of flow systems: a shallow, rapid-response conduit system accessed only during rainfall, and a deeper, phreatic, diffuse-fed conduit system. The concentration of sediment in spring discharge will increase with continued urbanization of the aquifer, because of the increased erosional power of stormflow resulting from increased impervious cover. The high organic carbon and clay

content of the sediments give them the capacity to transport both hydrophobic organic contaminants and trace metals.

Springflow is impounded in a pool, adding more than a meter of head over the spring under normal aquifer conditions. Draining of the pool lowers the head and affects both discharge volume and chemistry. The effect is more pronounced when aquifer level is low. The pool was drained either during or just following each of the storm events, but the increase in discharge had no effect on suspended sediment concentration, implying that sediment concentration is affected either by changes in volume of surface water flow or recharge into the more distal parts of the aquifer rather than flow through the aquifer in the area close to Barton Springs.

General climatic conditions, draining of the pool, and recharge from storms affects spring chemistry. This study investigated changes in spring chemistry in response to both storm events and draining of the pool through intensive sampling. As the aquifer changes from normal-flow to low-flow conditions, concentrations of sodium, chloride, and sulfate in spring water increase, and the overall chemistry becomes more like that of deep Edwards water in the bad water zone. Draining of the pool has the same effect on a more dramatic scale: concentrations of major ions first decrease as conduit water is drained, then concentrations of sodium, chloride, and sulfate increase as water from the bad water zone is drawn in. After the first storm, which occurred during a period of normal rainfall, concentrations of major ions decreased, caused by the dilution of aquifer water by rain water. In contrast, the second storm occurred

after a prolonged period of little rain, and in response concentrations of calcium and magnesium increased. The response of spring chemistry to the draining of the pool may be an indication of the effect on spring chemistry if aquifer levels continued to drop in response to increased pumping or drought conditions.

Chapter 3. Lanthanide clay: A New Sediment Tracer for Use in Karst Terranes

INTRODUCTION

Sediment and sediment surfaces are a fundamental control on the transport and fate of organic contaminants. In porous-media aquifers, sediments retard contaminant transport because of sorption and partitioning to the immobile solid-phase surfaces. In fractured or karst aquifers, in contrast, a wide range of sediments are mobile (Gale, 1984; Thrailkill, 1989; White and White, 1968), and suspended solids may thus act as vectors for contaminant transport (Ford and Williams, 1989), particularly for poorly soluble hydrophobic organic compounds (e.g., McCarty et al., 1981; Onishi, 1981; Schwarzenbach et al., 1993). In complex karstic systems, settling of contaminated sediment may even result in temporary storage of contaminants that may later re-mobilize during a storm event. The movement of sediment, therefore, is intimately connected with the movement of contaminants in a conduit-flow aquifer.

While water flow in karst aquifers can be characterized with readily-available solution tracers, little is known about the source and movement of sediment. Although anecdotal evidence of sediment discharging at springs is common, with grainsize ranging from clay to boulders, sediment source, subsurface residence time, and transport distance have not been characterized (White, 1988). Existing sediment tracers are limited in their detectability and flexibility. Consequently, karst sediment transport dynamics remain largely a

mystery. This chapter describes the development and testing of a new tracer technology that uses a lanthanide-element labeled clay to characterize sediment transport in a karst aquifer.

A variety of particle tracers have been attempted in the last thirty years (Table 3.1). Early efforts to track particle movements used sand labeled with radionuclides (Sayre and Hubbell, 1965) or coated with fluorescent paint (Ingle, 1966; Kennedy andKouba, 1970; Rathbun et al., 1971). Other deliberate tracers include plastic particles (Carey, 1989; Wheatcroft, 1991), luminophores (Gerino, 1990; Mahaut and Graf, 1987), glass beads (Wheatcroft, 1992), lycopodium spores (Atkinson et al., 1973), baker's yeast (Wood and Ehrlich, 1978), sediment labeled with noble metals (Olmez et al., 1994; Wheatcroft et al., 1994), rare earth element oxides (Krezoski, 1989), and carboxylate-modified polystyrene latex microspheres (Reimus et al., 1996). These particle tracers have been used to study fluvial transport of sand- and gravel-sized particles (Kennedy and Kouba, 1970; Sayre and Hubbell, 1965), beach erosion (Ingle, 1966), bioturbation (Carey, 1989; Gerino, 1990; Wheatcroft, 1991; Wheatcroft, 1992; Wheatcroft et al., 1994), transport of microbes through sand and gravel aquifers (Wood and Ehrlich, 1978), and colloid transport in fractured rock (Reimus et al., 1996).

Each of these tracer approaches has provided some information on sediment movement, but their usefulness in karst aquifers is limited by poor detectability, inappropriate physical characteristics, or requirement of complex procedures or expensive analytical instruments. Colored lycopodium spores are the only particulate tracers to have been used in karst aquifers (e.g., Aley and

Sediment Tracers

particle type	detection method	detection sensitivity	size	specific gravity	advantages	disadvantages
sand labeled with Ir-192 (Sayre and Hubbell, 1965)	scintillation detector	N/A	0.1-1.2 mm	2.65	radioactivity measured continuously w/o removing samples from stream	environmental implications
fluorescent sand (Kennedy and Koubs, 1970) (Ingle, 1966) (Rathbun et al., 1971)	manual counting	100ng/g	0.15-1.3 mm	2.65	inexpensive different colors available	limited to sand-size paint flakes off manual counting is labor intensive
lycopodium spores (Atkinson et al., 1973)	manual counting	N/A	30 um	~ 1?	6 colors available	single size only low density
baker's yeast (Wood and Ehrlich, 1978)	colonies are grown then manually counted	N/A	2-3 um	~ 1 ?	appropriate size	low specific gravity only 1 signature available
fluorescent plastic (Carey, 1989)	filter fluorometer	N/A	3-6 um	1.4	different colors available appropriate size	low specific gravity
lanthanide oxides (Krezoski, 1989)	neutron activation analysis	N/A	N/A	8.35	sensitive, automated detection	high specific gravity detection expense no control over size
luminophores (Gerino, 1990)	manual counting	N/A	10-200 um	N/A		manual counting is labor intensive
plastic microtaggants (Wheatcroft, 1991)	manual counting	N/A	50-180 um	1.4	inexpensive	one color only manual counting is labor intensive large size
glass beads (Wheatcroft, 1992)	manual counting	N/A	8-420 um	2.4	inexpensive several size ranges correct density	manual counting is labor intensive
gold/silver doping (Olmez and Pink, 1994) (Wheatcroft et al., 1994)	INAA	0.1-1 ng/g	38-125 um	same as sediment	mimics natural sediment automated, sensitive detection	limited to 2 tracers INAA costs $9/sample if done out of house cannot use on carbonate sediments
carboxylate-modified polystyrene latex (Reimus, 1996)	flow cytometry	N/A	0.3-1 um	~1 ?		has not been field tested low density flow cytometry not readily available

Fletcher, 1976; Atkinson et al., 1973; Drew and Smith, 1969). They may be dyed up to five different colors to avoid cross-interference, are non-toxic, and pose no health threat (Davis et al., 1985). They present limitations, however, in their utility for tracing sediment through karst aquifers. First, lycopodium spores are difficult to use: coloring the spores is laborious, there is a high potential for contamination of samples, and detection is performed manually under a microscope following filtration and centrifugation (Davis et al., 1985). Second, being composed of cellulose, their specific gravity is close to that of water, and they therefore will have a tendency to remain in suspension, better mimicking the behavior of water than that of sediment.

Lanthanide tracers have shown great promise as environmental tracers of aerosols, chemical wastes, and herbicide dispersal (Loveland, 1989), because of their low cost, non-toxicity, and sensitive detection. Lanthanide oxides mixed with natural fine-grained sediments were used by Krezoski (1989) to measure sediment reworking and transport in the Great Lakes. Lanthanide oxides, however, have a specific gravity several times greater than that of natural sediment, so that while they may be serviceable in evaluating bioturbation, they would be less useful in studies of transport of suspended sediment.

The lanthanide-labeled clay tracer was developed to characterize sediment transport in karst. The clay tracer is in all respects representative of sediment that moves through a karst aquifer, and the use of different lanthanide elements results in multiple tracer signatures for simultaneous deployment. The tracer is easy to prepare and detect, and is reasonably sensitive. This chapter describes the

methodology for using this tracer, and the results of three field trials in surface and ground waters.

MATERIALS AND METHODS

An ideal sediment tracer should meet several minimal criteria. First, it should have a low detection limit so that it can be used in small quantities and be sensitively identified. Second, it should be available with several differentiable signatures to avoid cross-interference of tracers. Third, it should be inexpensive to produce, detect, and quantify, preferably by standard in-house analytical methods. Fourth, it should be environmentally benign. Finally, it should have physical characteristics such as density, size, and morphology similar to the sediment which it is intended to mimic.

For this tracer technology, lanthanide cations are intercalated into montmorillonite clay, replacing the original interlayer cation. After collection of the sediment sample, the interlamellar lanthanide is removed from the clay lattice by complexation and quantified by high performance liquid chromatography (HPLC). The tracer is detectable at very low concentrations, can be synthesized with a number of different signatures, is physically similar to ambient sediment, and is environmentally non-hazardous.

Preparation of the Lanthanide Montmorillonite

Wyoming montmorillonite (SWy-2, University of Missouri-Columbia Source Clay Minerals Repository) was homoionized to the lanthanide form following the method of Bruque et al. (1980). Physical characteristics of the montmorillonite are given in Table 3.2. Montmorillonite clay (40 g) was first

dispersed in one liter of water, sonicated for five minutes, then shaken overnight on a wrist shaker. All water used throughout the process was Type III reagent water. Organic matter was oxidized using hot 10% hydrogen peroxide (Paecht-Horowitz and Eirich, 1988), and the 0.1 to 1.1 μm fraction (e.s.d.) was isolated by centrifugation. The organic-free fine fraction was then homoionized to the sodium form by washing twice in 2 N NaCl-0.1 N HCl solution, twice in a 2 N NaCl solution, and then repeatedly in water until the specific conductivity was less than 10 μs. The volume was adjusted with water to make a 1% clay solution by weight, and the clay suspension homoionized to the H-form using Dowex 50-WX-8 resin in the hydrogen form (0.6 ml resin/gram clay) (Aldrich and Buchanan, 1958).

SiO_2	62.9	CaO	1.80
Al_2O_3	19.3	Na_2O	1.54
TiO_2	0.16	K_2O	0.56
Fe_2O_3	3.85	P_2O_5	0.06
FeO	0.12	ign. loss	5.10
MnO	0.01	CO_2	1.33
MgO	2.80		

specific surface area (m^2/gm)	340
C.E.C. (mequiv./100 g)	119

Table 3.2. Physical characteristics of the montmorillonite, Swy-2, used in the tracer experiments.

The H-montmorillonite was then homoionized to the desired lanthanide form by saturating it with the chloride form of the lanthanide element, here either cerium chloride (Sigma), neodymium chloride (Aldrich), or lanthanum chloride (Sigma). A 2-symmetry solution of the lanthanide salt (where one symmetry addition, S, is equal to the cation exchange capacity (CEC) of the montmorillonite, ~1.2 mEq/g) was added to the clay and shaken for 20 minutes. The clay was isolated by centrifugation, then resuspended in an 8 S solution, agitated, and isolated by centrifugation. The lanthanide montmorillonite was then repeatedly washed with water and centrifuged until the supernatant had a specific conductance of < 10 μs. Before deployment, the clay tracer was equilibrated with water from the sampling site for 24 hours, and the supernatant examined at regular intervals for dissolved lanthanide. If the tracer was found to be stable in the target solution matrix, the clay solution was then centrifuged, the supernatant removed, and the clay resuspended in the sampling site water to 1% by weight and shaken on a wrist shaker for 30 minutes until dispersed.

Lanthanide ions were stripped from the clay for analysis using 300 millimolar (mM) hydroxyisobutyric acid (HIBA) (Aldrich), 10 mM sodium octanesulfonate (Kodak) at pH 3.8. This was the same solution later used as the HPLC mobile phase. One μl of the 1% by weight clay suspension was diluted 1:1000 with HIBA in a 1.5 ml eppendorf tube, vortexed for 15 seconds, then rotated overnight at 8 rpm. The tubes were centrifuged for 5 minutes at 14,000 rpm, and 300 μl of the supernatant removed for analysis.

Laboratory Batch Tests

The stability of the lanthanide clay was examined in the laboratory using batch suspensions of Ce-montmorillonite in distilled water, seawater, and solutions covering a range of ionic strength, pH, and calcium concentration (Table 3.3). Fifteen µl of the 1% clay suspension was diluted to a total volume of 1000 µl with the desired solution in a 1.5 ml eppendorf. The samples were vortexed for 15 seconds and rotated at 8 rpm. The amount of clay used was determined by computing the quantity required to allow detection of a release of as little as 0.4% of the CEC. For comparison, 1 µl of the 1% by weight clay solution was also diluted to 1000 µl in HIBA. Each sample was run in triplicate. After 48 hours, 500 µl was removed, centrifuged at 14,000 rpm for 5 minutes, and 300 µl of the supernatant removed for analysis. After a total of 7 days, the remaining 500 µl was centrifuged and the supernatant removed for analysis.

pH
5.5
6.5
7.5

$CaCl_2$ (pH = 6.5)
0.5 mM
1.0 mM
5.0 mM

I (pH = 6.5)
0.01587 (1 mM $NaNO_3$)
0.02621 (10 mM $NaNO_3$)
0.121 (100 mM $NaNO_3$)

Table 3.3. Chemistry of the solutions used to test stability of the lanthanide-clay in batch experiments.

All solutions were buffered to the desired pH with sodium phosphate salts. Ionic strength was held constant in the pH and $CaCl_2$ solutions at I-0.026 with the addition of $NaNO_3$.

Lanthanide Detection and Quantification

Lanthanides in the supernatant HIBA solution were separated by isocratic HPLC using 0.8 mls/min of 300 millimolar HIBA, 10 mM sodium octanesulfonate at pH 3.8 on a Waters Resolve C_{18} column. Detection of the separated lanthanides was by absorbance at 658 nm after post-column complexation by arsenazo III (Millipore Corporation, 1989). Multi-point calibration curves were constructed using NBS traceable lanthanide standards (Aldrich) (Figure 3.1). Method detection limits for the three lanthanides using a 200 µl injection size are ~10 µg/l. Background sediments, extracted using the above procedure, did not interfere with the target lanthanides.

This method was developed to rapidly analyze only the five lightest lanthanide elements with good detectability. Depending on the background lanthanide content, however, these elements may not be compatible, requiring the use of heavier lanthanides. The alternate method, using a gradient elution, can detect all of the lanthanide elements in a single run, with detection limits of 5-50 µg/l (Millipore Corporation, 1989). The gradient method is much slower, however, because of the equilibration time between gradient runs.

Field Tracer Tests

One surface and two subsurface field tracer tests were completed and evaluated. For the surface water experiment neodymium-labeled montmorillonite was tested in Waller Creek, a small urban creek in Austin, Texas (Figure 3.2). A stretch of approximately 65 m was chosen through which the water flowed without pooling, with samples stations established at 15 m and 61 m downstream

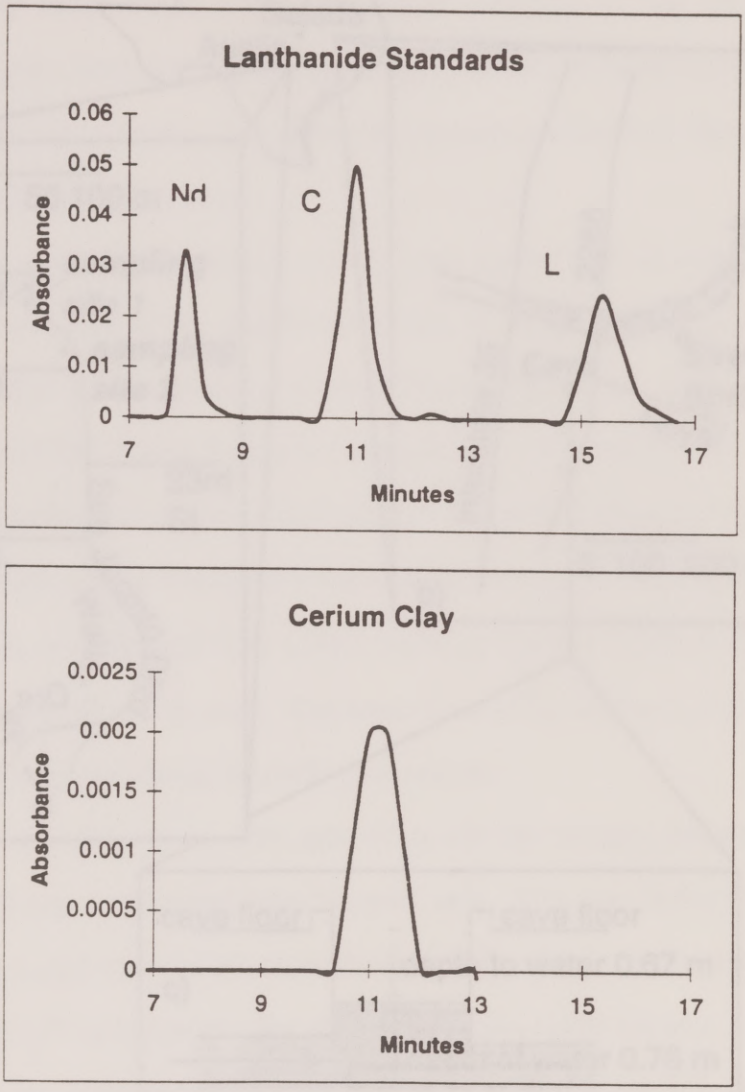

Figure 3.1. HPLC response peaks.

On the top is shown a standard solution of the rare earth elements lanthanum, cerium, and neodymium; below is the response of an injection of cerium eluted from 0.5 µg Ce-clay.

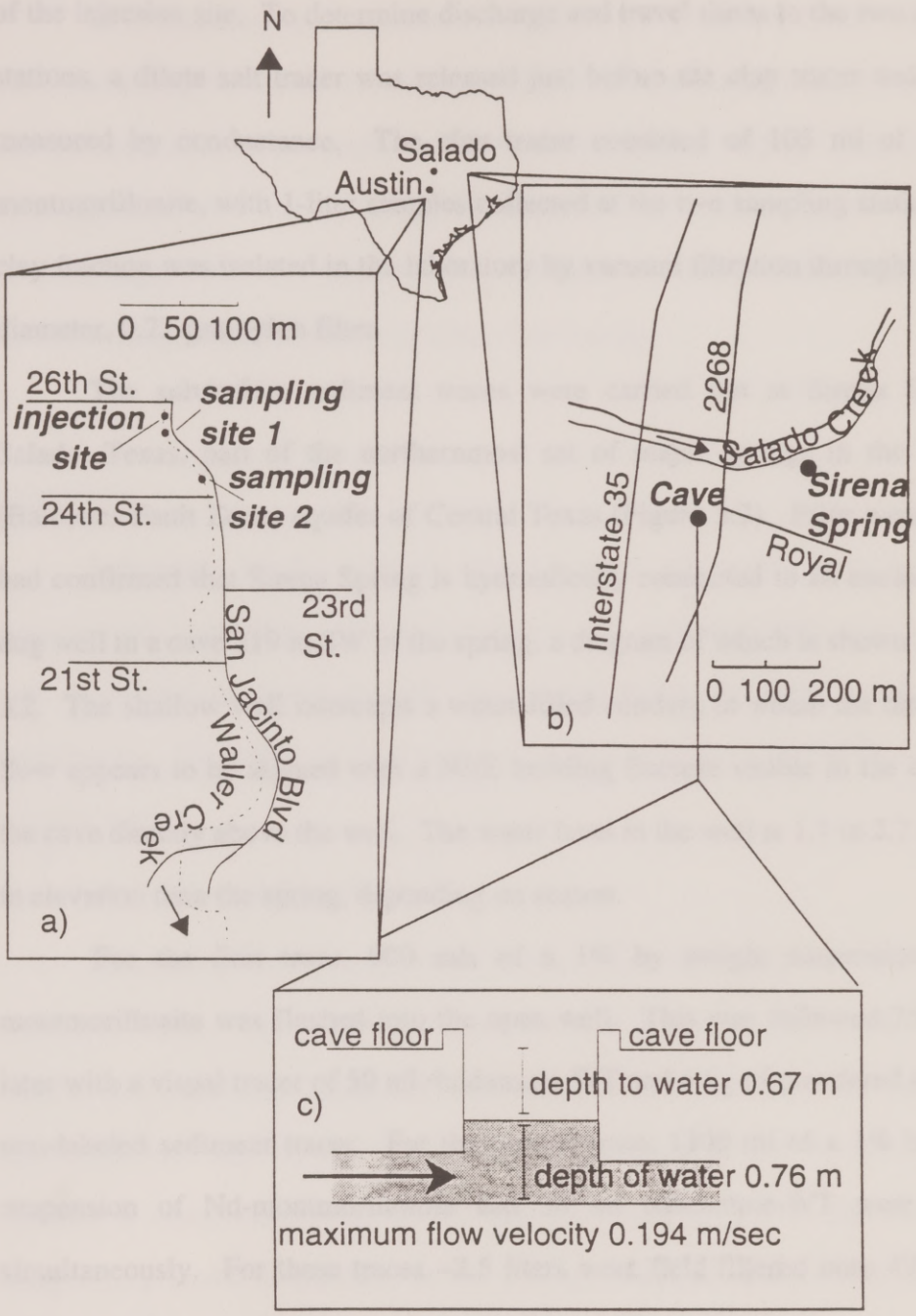

Figure 3.2. Locations of surface water and groundwater traces.

Also shown is a schematic diagram of the well inside the cave in Salado, Texas.

of the injection site. To determine discharge and travel times to the two sampling stations, a dilute salt tracer was released just before the clay tracer and dilution measured by conductance. The clay tracer consisted of 105 ml of 1% Nd-montmorillonite, with 1-liter samples collected at the two sampling stations. The clay fraction was isolated in the laboratory by vacuum filtration through a 25-mm diameter, 0.22-μm nylon filter.

The subsurface sediment traces were carried out at Sirena Spring in Salado, Texas, part of the northernmost set of major springs in the Edwards (Balcones Fault Zone) aquifer of Central Texas (Figure 3.2). Prior water tracing had confirmed that Sirena Spring is hydraulically connected to an uncased hand-dug well in a cave 219 m SW of the spring, a diagram of which is shown in Figure 3.2. The shallow well intercepts a water-filled conduit, in which the direction of flow appears to be aligned with a NEE trending fracture visible in the ceiling of the cave directly above the well. The water level in the well is 1.7 to 2.7 m higher in elevation than the spring, depending on season.

For the first trace, 900 mls of a 1% by weight suspension of Ce-montmorillonite was flushed into the open well. This was followed 75 minutes later with a visual tracer of 50 ml rhodamine-WT and 6 kg of powdered silica as a non-labeled sediment tracer. For the second trace, 1100 ml of a 1% by weight suspension of Nd-montmorillonite and 30 ml rhodamine-WT were injected simultaneously. For these traces ~2.5 liters were field-filtered onto 47mm 0.22 μm nylon filter membranes using a peristaltic pump.

After filtration, loaded filters were placed in 1.5 ml acid-washed eppendorf tubes containing 0.5 ml of 300 HIBA, 10 mM sodium octanesulfonate at pH 3.8, and the eppendorf tubes turned on a rotater overnight at 6 rpm. The tubes were then centrifuged at 14,000 rpm for 10 minutes to isolate the stripped clay, and 300 µl of the supernatant was pipetted off for analysis by HPLC. The optical solution tracers were quantified directly by filter fluorometry.

RESULTS

Laboratory results indicated that the tracer was stable under a range of natural-water conditions. The travel time of the sediment tracer was similar to that of a solution tracer in both the surface water and groundwater tracing experiments. The detection limit was similar to that of rhodamine WT, a common solution tracer.

Tracer stability and detection

Laboratory batch experiments confirm that the lanthanide-clay tracer is extremely stable. The lanthanides were found to be tightly held within the clay matrix; no detectable lanthanide was released from all but two of the twenty-seven solutions after up to 7 days. One of the three 48-hour seawater samples released a concentration of 0.5926 mg Ce/l solution (3.95 mg Ce/g clay), representing 11.6% of the CEC of the montmorillonite; however, the remaining two samples of that triplicate set and all three of the 7-day samples showed no release of cerium. It is likely that the cerium detected in the one sample was the results of the inadvertent injection of a small amount of the clay itself into the

HPLC, where the cerium was immediately released upon mixing with the HIBA mobile phase. All of the 48-hour deionized distilled water samples and two of the three 7-day samples released an average of 0.1485 +/- 0.05 (SE) mg Ce/l solution (0.99 mg Ce/g clay), representing 2.9% of the CEC of the montmorillonite. The experiment was repeated for the distilled water samples, being careful not to disturb the clay after centrifugation; only one of the three 48-hour and one of the three 7-day samples released any cerium. This may have been due to poor flocculation of the clay in distilled water, resulting in a small amount being brought back into suspension during the removal of the supernatant during the first experiment. The stability of the tracer was further confirmed by HPLC analysis of supernatant from a one-year old 1% neodymium-montmorillonite suspension, in which no neodymium was detected.

Method efficiency was determined in the laboratory using a 1% suspension of a lanthanide montmorillonite. The clay suspension was diluted 1:1000 with HIBA to release lanthanide ions and filtered, with HPLC detection on a 200 µl injection of the supernatant. The supernatant solution from the La-montmorillonite contained 0.432 mg/L of lanthanum ion, corresponding to 0.929 mEq La/g clay, or 124% of the CEC. The Nd-montmorillonite extract contained 0.292 mg/L neodinium ion, corresponding to 0.6071 mEq Nd/g clay, or 82% of the CEC. The extract from the Ce-montmorillonite used in the batch experiment contained 0.351 mg/L cerium ion, corresponding to 0.666 mEq Ce/g clay, or 89% of the CEC.

The final method efficiency and maximum dilution is a function of the quantity of the suspended solid concentration, the volume of water filtered, the volume of extract and the extraction efficiency, and the injection size. Assuming a two liter water sample, 0.5 ml HIBA for the extraction, and a 200 µl injection size, the lanthanide-montmorillonite is reliably detected at a concentration of 0.1 µg La-montmorillonite/l sample or 0.2 µg Nd-montmorillonite/l sample. This corresponds to a dilution of 10^8 of a one liter injection of 1% clay suspension. This dilution factor can be improved by filtering a larger volume of solution, or by injecting a larger volume on the HPLC.

Surface Water Sediment Tracing

Preliminary analysis of the natural suspended and bedload sediment at Waller Creek, the site of the surface water field test, showed no detectable lanthanide elements or interfering species. Breakthrough curves for the sediment tracer (Nd-montmorillonite) and conservative water tracer (NaCl) are shown in Figure 3.3. Based on dilution of the conservative NaCl tracer, the computed discharge of the creek was 6.3 l/sec (0.225 ft^3/sec) ± 0.34 l/sec (SE). Using this discharge and integrating over the sampling interval, 224.3 mg of Nd-montmorillonite was transported past the sampling site 15 m downstream of the injection point. This represents 21.4% of the total injected. Sixty-five meters downstream from the injection point, 34.4 mg of Nd-montmorillonite traversed the second sampling site, corresponding to 3.3% of the total injected. Thus 78.6% of the sediment tracer settled out of suspension in the first 15 m of the creek, and an additional 18.5% settled out in the 50 m between the two sample sites. The

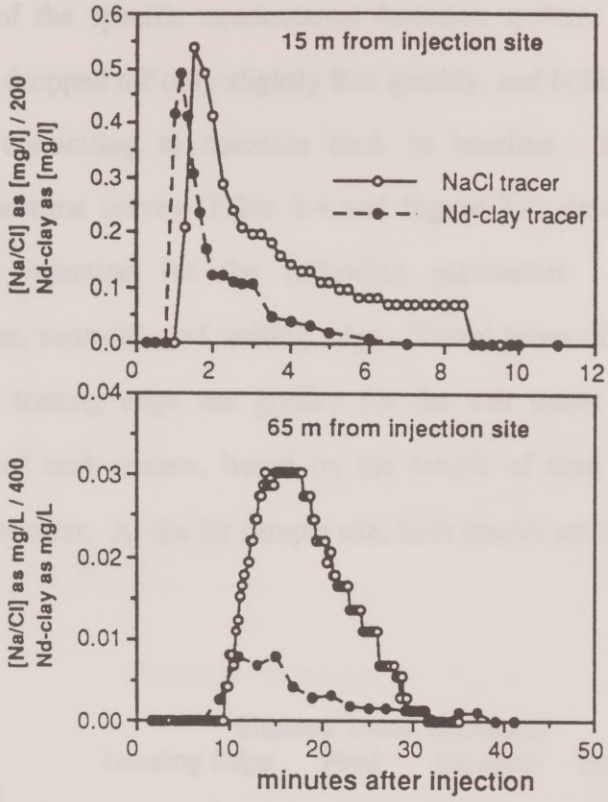

Figure 3.3. Concentration-time curves for the water and particle tracers in Waller Creek, Austin, Texas.

A NaCl solution was used as a water tracer and Nd-clay for the particle tracer

peak concentration of 0.492 mg/l of Nd-clay was collected 1.17 minutes after injection at the near sample site, therefore the clay was diluted by a factor of $2x10^4$ after 15 m of transport. At the far sample site, the peak concentration of 0.00795 mg/l of Nd-clay was collected 15 minutes after injection, a dilution of a factor of 1.26×10^6 after 65 m of transport.

The shape of both the particle and water tracer breakthrough curves is similar (Figure 3.3). The sudden drop-off in NaCl concentration at 9 minutes is

an artifact of the specific conductance detection system. Both tracers peaked quickly and dropped off only slightly less quickly, and both show a slight leveling off before continuing to decrease back to baseline. Characteristics of the concentration-time curves (Table 3.4 and Figure 3.4) describe the elapsed time after tracer injection for the following parameters: leading edge, peak concentration, centroid, and trailing edge. Travel times of all parameters except that of the trailing edge are greater for the salt tracer than the clay tracer. Dispersion of both tracers, based on the length of time required to return to baseline, is similar. At the far sample site, both tracers arrived at approximately

	Elapsed Times (minutes)			
	Leading Edge	*Peak*	*Centroid*	*Trailing Edge*
Station 1				
NaCl	1.25	1.50	2.37	8.75
La-clay	1.00	1.00	1.55	11.00
Station 2				
NaCl	9.50	16.25	22.00	31.50
La-clay	9.00	15.00	15.50	37.00
	Travel Times (minutes)			
	Leading Edge	*Peak*	*Centroid*	*Trailing Edge*
NaCl	8.25	14.75	19.63	22.75
La-clay	8.00	14.00	13.95	26.00

Table 3.4. Travel-time data for water and particle tracers in Waller Creek, Austin, Texas.

Elapsed time represents the time for the tracer characteristic to arrive at the sampling station. Travel time represents the time for the tracer characteristic to travel from one station to the next.

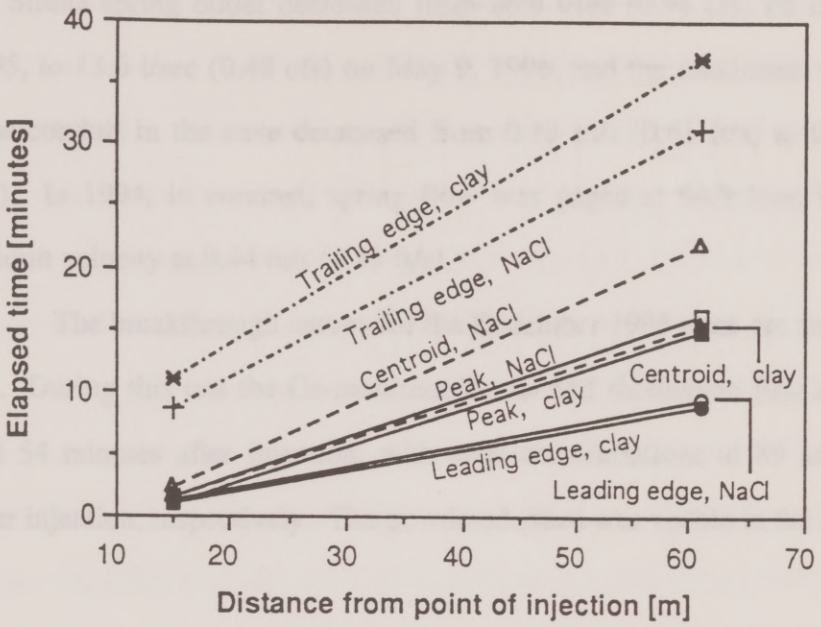

Figure 3.4. Travel-time curves for the water and particle tracers in Waller Creek, Austin, Texas.

the same time, and it appears that the peak in particle tracer concentration preceded the peak in the water tracer concentration, although it is difficult to compare the peaks given the slight drop in concentration of the particle tracer at 13 minutes. Arrival time of the water tracer centroid, however, exceeds that for the particle tracer by 40%.

Subsurface Sediment Tracing

Subsurface sediment and water traces were performed in early December 1995 and early May 1996. During this period central Texas was experiencing a drought which began in in the autumn of 1995. From November 1, 1995, to May

31, 1996, no significant rainfall occurred. Consequently, the gaged discharge at the Sirena spring outlet decreased from 26.6 l/sec (0.94 cfs) on December 12th, 1995, to 13.6 l/sec (0.48 cfs) on May 9, 1996, and the maximum velocity in the flow conduit in the cave decreased from 0.18 m/s (0.61 ft/s) to 0.14 m/s (0.45 ft/s). In 1994, in contrast, spring flow was gaged at 94.9 l/sec (3.35 cfs) and conduit velocity at 0.44 m/s (1.45 ft/s).

The breakthrough curves for the December 1995 trace are shown in Figure 3.5. During this test the Ce-montmorillonite and rhodamine first appeared at 43 and 54 minutes after injection, with peak concentrations at 89 and 94 minutes after injection, respectively. The powdered silica was visible in the centrifuge

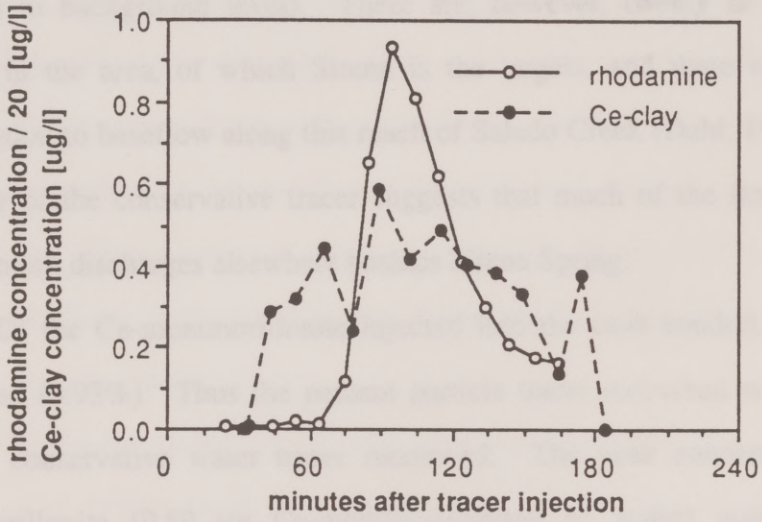

Figure 3.5. Breakthrough curves for groundwater tracing test.

Both conservative water tracer (rhodamine WT) and particle tracer (Ce-montmorillonite) are shown.

tubes from samples collected 164 and 174 minutes after its injection, corresponding to 216 and 226 minutes after injection of the Ce-clay. While the natural suspended sediment contained no detectable lanthanide elements, the powdered silica, when eluted in HIBA and analyzed by HPLC, produced a broad peak which interfered with the detection of cerium. During the May test the rhodamine first appeared 101 minutes after injection and peaked 131 minutes after injection. The sediment tracer was not detected.

During the December trace approximately 2.5% of the rhodamine injected was recovered, based on a spring discharge of 26.6 l/sec (0.94 cfs) and integration under the breakthrough curve. This may have been caused by premature ending of the sampling (i.e., the level of fluorescence in the spring water had not fully returned to background level). There are, however, twenty or more flowing springs in the area, of which Sirena is the largest, and there is a significant contribution to baseflow along this reach of Salado Creek (Dahl, 1990). The low recovery of the conservative tracer suggests that much of the flow through the cave conduit discharges elsewhere besides Sirena Spring.

Of the Ce-montmorillonite injected into the cave conduit, 83.5 mg was recovered (0.93%). Thus the percent particle tracer recovered was 37% of the percent conservative water tracer recovered. The peak concentration of Ce-montmorillonite (0.59 µg Ce-montmorillonite/l of water) was collected 89 minutes after injection of the particle tracer, and represents a dilution of 1.7×10^7.

DISCUSSION

The montmorillonite clay readily accepts the lanthanide ion into the clay matrix, from which it is efficiently complexed by HIBA. The lanthanide-montmorillonite fulfills the desired criteria for a serviceable particle tracer; it assisted in the determination of sediment travel time and inference of subsurface architecture. It should prove useful for tracing of sediment transport in karst terrane as well as in other environments.

Chemistry of Lanthanide-clays

The lanthanides comprise a group of elements, periodic numbers 57-71, which have very similar geochemical properties. They have two important chemical characteristics that allow them to be incorporated into the clay lattice: they are all trivalent at Earth surface conditions, and they have an ionic radius in eight-fold coordination ranging from 0.87 (Sc^{3+}) to 1.16 (La^{3+}), similar to that of Ca^{2+} and Na^{+}. They are present at low concentrations in basalts, granites, gneisses, shales, and silicate rocks, but their low abundance in carbonate rocks makes them an ideal tracer in karst aquifers.

The lanthanide ions are readily accepted into the montmorillonite lattice. Bruque et al. (1980) found that the replacement of H^{+} by Ln^{3+} was very rapid. They also found that the exchange process ceased after 80% of the CEC was reached when using up to a 12 S solution for saturation, but that by using an 18 S solution 100% CEC was reached. They attribute this to exchange of the lanthanide ion for Al^{3+} at the higher symmetry addition, and note that it can be

achieved at 7-10 S if the pH is kept near 5. At pH > 5 they found that lanthanide hydroxide precipitated and at a pH < 2 aluminization occurred. At an optimum pH of 4-5, 5 S was sufficient for saturation of the CEC, and they were able to induce up to 146% saturation of the CEC. At ambient temperatures (up to 300° C) the interlamellar lanthanide ions are hydrated and no crystalline phases are present (Muñoz-Páez et al., 1994).

The initial wash of the Ln-montmorillonite with water from the sampling site always resulted in the release of a small amount of lanthanide ion. However, after the initial washing, lanthanide ion was not removed by subsequent immersion in the sample site water, suggesting that there is a small percentage of the lanthanide that is mobile due to exchange with calcium in solution, but the stability constant favors the lanthanide elements. This suggests that, while most of the lanthanide ion is intercalated into the montmorillonite lattice, some of it also adsorbed to the outer surface of the clay. This surface-adsorbed lanthanide is then available for exchange with calcium, or complexation by carbonate ion in solution (Wood, 1990). Erel and Morgan (1991) express the ratio of the dissolved (i.e., forming complexes in solution) to adsorbed species as

$$\frac{[REE]_{diss}}{[REE]_{ads}} = \frac{[CO_3^{2-}] * (\beta^0_{1MCO_3} + \beta^0_{2MCO_3} * [CO_3^{2-}])}{(\beta^0_{1MOH}) * 10^b * \frac{[\text{surface sites}]}{[H^+]}} \qquad (3.1)$$

where $[REE]_{diss}$ and $[REE]_{ads}$ are the adsorbed and dissolved (including partitioning between carbonate-REE complexes in solution) concentrations of a particular

REE in moles/liter; $[CO_3^{2-}]$ is the concentration of carbonate in solution in moles/liter; $\beta^0_{1MCO3}$and β^0_{2MCO3} are the first and second equilibrium constants for the formation of REE-carbonate complexes in water; β^0_{1MOH} is the first hydroxide binding constant; and b is a constant relating the adsorption constant to the first hydroxide binding constant. Using values for $\beta^0_{1MCO3}$and β^0_{2MCO3} from Cantrell and Byrne (1987), for β^0_{1MOH} from Turner et al. (1981), b from Dzombak and Morel (1990), and typical values of $[CO_3^{2-}]$ and $[H^+]$ from karst spring systems ($10^{-5.41}$ and $10^{-7.2}$, respectively), the ($[REE]_{diss}/[REE]_{ads}$) for this experimental system is approximately 10^{-6}.

The extreme efficiency of hydroxyisobutyric acid (HIBA) in complexing lanthanide ions (Elchuk and Cassidy, 1979) is the key to the success of this sediment tracer. HIBA was used both to strip the lanthanides from the clay lattice and as the HPLC mobile phase. The HIBA complexed intercalated lanthanides representing more than 80% of the CEC of the montmorillonite, which resulted in a very low detection limit. As the HIBA can be added to the sampling filters on-site, the supernatant removed within twenty-four hours, and directly injected for analysis, the process is quick and simple. The direct complexation of the target elements into the HPLC eluent results in a clean chromatographic baseline, and no need for cleanup, matrix matching, or dilution.

Field Sediment Traces

The subsurface sediment trace offers some insight into both particle transport and subsurface conduit geometry in a karst aquifer. The measured downhole velocity in the cave conduit at Salado in December, 1995, was ~0.19

m/sec, suggesting a direct-line travel time of 19 minutes. The travel time for peak appearance of the rhodamine dye, however, was 89 minutes, making the linear velocity between the cave and the spring only 0.04 m/sec. In May, 1996, the measured downhole velocity had decreased to ~0.14 m/sec, the travel time for peak appearance of the rhodamine dye was 130 minutes, the suggested direct-line travel time 22.5 minutes, and the linear velocity between the cave and the spring 0.024 m/sec. This suggests that the conduit geometry changes significantly between the cave and the spring. Further evidence of a change in conduit geometry is the complete loss of the sediment tracer in the low-flow May conditions compared to the higher flow conditions in December.

One of many possibilities is that the conduit opens up into a larger cavity, causing a decrease in the groundwater velocity. One very simple geometry is shown in Figure 3.6, where flow velocity decreases when the water enters a wider

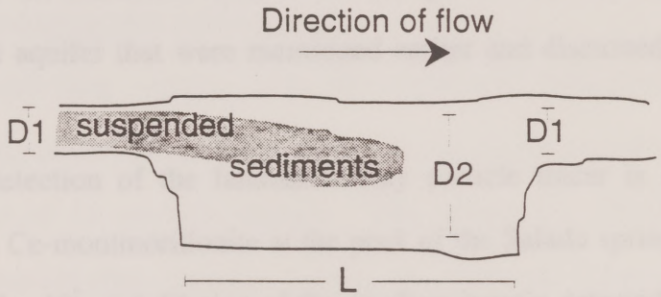

Figure 3.6. Hypothetical geometry of the Salado conduit system.

Here the diameter of the conduit through the well, D1, is 0.3 m; opening to a diameter, D2, of 1 m for a length (L) of 55-75 m would allow some portion of 1 μm-clay particles to travel through the system at the December, 1995 initial groundwater velocity of 0.19 m/sec, but to settle out at the May, 1996 initial groundwater velocity of 0.14 m/sec.

portion of the conduit. In December, 1995, the velocity was great enough that a portion of the tracer particles would have passed through such a configuration to emerge at the spring; however, in May, 1996, the groundwater velocity had decreased to the point that the tracer particles would have settled below the large conduit outlet. Such a change in conduit geometry would explain the lack of detection of the particle tracer during the May trace. In other words, sediment in karst is transported under some hydraulic regimes, and under others goes into storage.

Lanthanide-Clays as Particle Tracers

Field tests in both surface and groundwater systems show that lanthanide-labeled clays are serviceable particle tracers. Tracer breakthrough curves (Figures 3.3 and 3.5) show reasonable agreement with those of a conservative water tracer both in terms of time of first appearance and peak concentration. Further, clay homoionized to the lanthanide form has all the qualities desired to trace sediment through a karst aquifer that were mentioned earlier and discussed in more detail below.

First, detection of the lanthanide-clay particle tracer is quite sensitive. Dilution of the Ce-montmorillonite at the peak of the Salado springs trace was on the order of 1.7×10^7, and dilution of the smallest sample detected (0.14 µg clay/l water) was 7.1×10^7. This was based on 3 liters of spring water per filter. In more turbid waters, the amount of La-montmorillonite collected may be limited by the amount of other sediment in suspension, with less volume passed through each filter. A 47 mm diameter, 0.22 µm filter can capture approximately 250 mg

of sediment before it clogs. Therefore in waters containing approximately 80 mg/l or more total suspended solids, it may be more useful to express the detection sensitivity in terms of mg La-montmorillonite/kg ambient suspended sediment.

The detection limit with the HPLC system used in this research, using isocratic flow and single pressure regulation of the post-column reagent, was approximately 1 ng lanthanide ion, or 100 ng La-montmorillonite/g ambient sediment (100 ppb). Assuming a 2-liter filter volume and 93% CEC removal, this corresponds to a minimum tracer concentration of 15 ng/l, approximately an order of magnitude less than that of the solution tracer Rhodamine WT. Cassidy (1988) reported detection of 0.1-0.5 ng lanthanide ion using gradient elution and two-stage regulation, an improvement of almost an order of magnitude sensitivity. Using a system such as he describes, detection of La-montmorillonites could be improved to 10-50 ng/g. This compares favorably with detection limits for other tracers, such as doping with noble metals.

Lanthanide-clay tracers can be produced with several different differentiable signatures. There are 14 different lanthanides plus lanthanum itself, making a total of 15 possible tracers. This allows the simultaneous use of different lanthanide-clay particle tracers at different locations within the watershed, or repeated injection of different lanthanide-clay tracers at the same location without worry of cross-interference with previous traces.

A major advantage of the lanthanide-clay tracer is its rapid and inexpensive detection by HPLC. Sample preparation is minimal, involving only

the treatment of nylon or membrane filters with HIBA and centrifugation. HPLC systems are easily automated, making detection quick, reproducible, and far less tedious than detection by manual counting, as is necessary for fluorescent sand, lycopodium spores, yeast, luminophores, plastic microtaggants, and glass beads. HPLC also requires less time than detection by neutron activation analysis (Loveland, 1989); results are obtainable within 24 hours of running the tracer test. Additionally, HPLC, unlike INAA or laser cytometry, is a standard laboratory procedure, and set-up of HPLC instrumentation, which has a wide range of uses, is comparatively inexpensive. The tracers themselves are cost-competitive with standard fluorescent water tracers (Loveland, 1989).

Lanthanide-clays have a distinct advantage over other, more exotic particles in that they are the same size and density as the sediment whose behavior they are designed to mimic. Sediment-associated contaminant transport is largely due to clay-sized particles, due to their high surface area-to-volume ratios and their likelihood of remaining in suspension. Therefore, a tracer in the 1-5 μm range is desirable. Although several of the synthetic particle tracers fall into this category, they have a lower specific gravity than clay, causing them to stay in suspension at lower fluid velocities. As the tracer is itself simply clay homoionized to a lanthanide form, it is well-suited to trace clay transport.

Finally, lanthanide-labeled clays have the benefit of being environmentally benign at the concentrations necessary for sediment tracing: 10 ng to 1 μg lanthanide ion per gram of ambient sediment. Rare earth elements are found in trace quantities in many soils and sediments, often far exceeding, in fact, the

concentration needed for tracing in a lanthanide-free environment: Goldstein and Jacobsen (1988) found that suspended sediments in rivers contained concentrations of 7.72-72.8 mg/kg La, 18.2-143 mg/kg Ce, and 12.6-52 Nd mg/kg, depending on the geology of the contributing basin. The drawback, of course, is that the use of La-clays tracers in rivers carrying sediments naturally high in lanthanide concentrations will be limited to the elements with low background levels. Overall, lanthanides have been found to be most abundant in granites and basalts, less abundant in shales, and least abundant in carbonates (Haskin et al., 1966). Jarvis et al. (1975) suggest that it is the insoluble residue in carbonates which affects the lanthanide content, and that carbonates in which quartz is the primary insoluble material will have a lower abundance of lanthanides than those in which clay is the primary insoluble material. In sediments, the lanthanide elements will tend to be located in the fine-grained fraction (i.e., those most likely to be in suspension) (Taylor and McLennan, 1988). Even in carbonate terrane, care should be taken to fully characterize and account for the background lanthanide concentration. No background lanthanide signature in suspended sediments was detected from either Waller Creek or Sirena Spring.

Implications

Particle tracing with La-clay may have a variety of uses in karst terranes. It could be used to determine the source of sediment in a system, to determine sediment residence times as a function of flow conditions, or to infer subsurface flow conduit geometry. The number of differentiable signatures available will

prove extremely useful in groundwater tracing as it allows several traces over both spatial and temporal domains without cross-interference. For example, tracers with different signatures can be introduced simultaneously at different points throughout the aquifer, or several different tracers can be introduced over time at one location, and their time of arrival distinguished between at a single point. Alternatively, clay particles in different size ranges can be given different signatures and their travel times compared.

Field results from sediment tracer tests will assist in parameter calibration for contaminant transport models. Transport models require estimation of, among other parameters, particle velocity, concentration, and source. Use of a particle tracer to obtain true field values for these parameters will allow evaluation of current models and construction of improved models.

Although La-clay is an ideal tracer for karst systems, it may prove useful in a variety of other environments as well. For example, it could also be used in conjunction with extant particle tracers to compare the transport behavior of different types (size, density) of particles. It would be interesting to compare, for example, the behavior of La-clay to that of synthetic microspheres, such as those used by Reimus et al. (1996), in fractured aquifers. Although the particles are in the same size range, La-clay is a mineral, while the carboxylate-modified polystyrene latex microspheres may behave more like organic colloids. In bioturbation studies, the redistribution of gold-doped particles in the silt- and sand size range could be compared to that of La-clay particles in the clay-size range.

CONCLUSIONS

La-clay is a particle tracer with characteristics desirable for tracing sediment through karst aquifers. Cost of production is similar to that of standard fluorescent water dyes and requires only standard laboratory equipment. Detection limits are extremely low. Sample analysis is straightforward and automated; using HPLC, results are available within 24 hours of the tracer test. The tracer can be made with up to 15 differentiable signatures, potentially eliminating cross-interference in the field over both time and space. Finally, the tracer presents no environmental hazards at the concentrations needed.

Lanthanide-clays may prove to be useful in the study of sediment transport in other environments in addition to karst. It could be used, for example, in research on bioturbation or transport in fractured aquifers. It may also be used in conjunction with particle tracers with contrasting characteristics to examine the differences in transport behavior exhibited by different types of naturally-occurring particles.

Appendix A. Barton Springs Aquifer Sample Descriptions

sample	type	sampler	sampling method
Maple Run 1	cave	A. Remington	Scooped from ledge in 2nd room of Maple Run Cave
Whirlpool 3	cave	A. Remington	Scooped from cave ledge
Blowing Hole Black	cave	A. Remington	Scooped from cave wall
Blowing Hole Red	cave	A. Remington	Scooped from cave wall
Whirlpool 1	cave	A. Remington	Scooped from cave floor
Whirlpool 4	cave	A. Remington	Scooped from cave floor
Whirlpool 2	cave	A. Remington	Scooped from cave floor
Maple Run Pool	cave	A. Remington	Scooped from pool in 3rd room of cave
Airmans	cave	N. Hauwert	Scooped from cave floor
Eileen's River	cave	B. Russell	Scooped from cave stream
Maple Run 2	cave	A. Remington	Scooped from ledge in last cave room
Castle Cave	cave	N. Hauwert	Scooped from cave passage wall
Bear Creek Park II	confined well	B. Mahler	Pumped from collection tank
Bear Creek 1	confined well	B. Mahler	Pumped from collection tank
Slaughter Creek Acres	confined well	B. Mahler	Pumped from collection tank
Onion Crk Mdws 2	confined well	B. Mahler	Pumped from collection tank
Village of San Leanna I	confined well	B. Mahler	Pumped from collection tank
J. Thomas	confined well	B. Mahler	Pumped directly from well
Del Rio Clay	Del Rio	B. Mahler	Scooped from exposure behinc Toys R Us
Leached Collapsed marl	Edwards rock	B. Mahler	Collected from roadway exposure, Loop 360
Regional Dense marl	Edwards rock	B. Mahler	Collected from roadway exposure, Loop 360
Basal Nodular	Edwards rock	N. Hauwert	Hammered from exposure
upper Dolomitic	Edwards rock	N. Hauwert	Hammered from exposure
Grainstone member	Edwards rock	N. Hauwert	Hammered from exposure
Rhythmic Beds Dolomitic	Edwards rock	N. Hauwert	Hammered from exposure
Leached Collapsed	Edwards rock	N. Hauwert	Hammered from exposure
Kirschberg Evaporite	Edwards Rock	B. Mahler	Gouged from exposure
Travis Country Sink	sinkhole	B. Mahler	Scooped from sinkhole
Nairn Sink	sinkhole	B. Mahler	Scooped from sinkhole
Barbara Falls Sink	sinkhole	B. Mahler	Scooped from sinkhole
Barton Lodge Sink	sinkhole	B. Mahler	Scooped from sinkhole
Barton Ropeswing	sinkhole	B. Mahler	Scooped from sinkhole

Marbridge	sinkhole	B. Mahler	Scooped from sinkhole
Shady Hollow	sinkhole	B. Mahler	Scooped from sinkhole
Barton Lodge W	spring	B. Mahler	Scooped from inside spring orifice
Barton Lodge Sp E	spring	B. Mahler	Scooped from inside spring orifice
Martine Springs	spring	N. Hauwert	Collected from spring cistern
Lost Creek Spring	spring	D. Johns	Collected at spring mouth
Backdoor Spring	spring	D. Johns	Collected at spring mouth
Brodie Sp (Toys)	spring	N. Hauwert	Collected at spring mouth
Onion Crk Centex	stream	B. Mahler	Scooped from streambed
TxDoT 1	stream	B. Mahler	Scooped from streambed above TxDoT regional water quality pond
Slaughter Creek 1826	stream	B. Mahler	Scooped from streambed
Onion Creek FM 150	stream	B. Mahler	Scooped from streambed
Gaines Creek	stream	B. Mahler	Scooped from streambed below TxDoT water quality pond 3
TxDoT 2	stream	B. Mahler	Scooped from streambed below TxDoT regional water quality pond
Bear Creek	stream	B. Mahler	Scooped from streambed at Friendship Baptist Church
Williamson Creek	stream	B. Mahler	Scooped from streambed above Old Bee Caves Rd
Outfall 2 "Best Buy"	stream	B. Mahler	Scooped from outlet below TxDoT water quality pond 2
Copper Hills	unconfined well	B. Mahler	Pumped from collection tank
58-57-6RB	unconfined well	B. Mahler	Pumped directly from well
Unisys well	unconfined well	B. Mahler	Collected from well bore w/corer
Thames I	unconfined well	B. Mahler	Collected from post-well filter
HE Brodie 3	unconfined well	N. Hauwert	Collected from well bore
Sunset Valley Tank	unconfined well	N. Hauwert	Scooped from collection tank
Little Bear @ Arbor Tr	unconfined well	B. Mahler	Collected from post-well filter
HE Brodie 2	unconfined well	N. Hauwert	Collected from well bore
Sunset Valley Tank 1	unconfined well	B. Mahler	Pumped from collection tank
Sunset Valley Tank 2	unconfined well	B. Mahler	Pumped from collection tank
BS storm composite	Barton Springs	R. Hansen	Collected on cotton fiber bundles

Appendix B. Geochemistry of Barton Springs Aquifer Samples

name	type	clay%	qtz%	ksp%	plag%	calc%	dolo%
Maple Run Ledge	cave	82	18	0	0	0	0
Whirlpool Cave 3	cave	20	23	2	1	9	44
Blowing Hole Black	cave	60	30	0	0	7	2
Blowing Hole Red	cave	61	37	0	0	1	0
Whirlpool 1	cave	12	8	0	0	4	77
Whirlpool 4	cave	19	19	2	0	3	58
Whirlpool 2	cave	21	9	1	0	3	66
Maple Run Pool	cave	13	15	0	0	71	0
Airmans	cave	37	15	1	0	46	0
Eileen's River	cave	46	40	2	1	8	2
Maple Run Btm Rm Ld	cave	38	40	2	1	19	0
Castle Cave	cave	83	13	0	0	4	0
Bear Creek Park II	confined well	0	1	0	0	29	70
Vill. of San Leanna I	confined well	21	19	1	0	46	14
J. Thomas	confined well	48	22	0	0	24	5
Bear Creek 1	confined well	0	1	0	0	8	91
Slaughter Creek Ac.	confined well	0	2	0	0	95	4
Onion Crk Mdws 2	confined well	50	23	0	0	20	6
Del Rio Clay	Del Rio	53	21	0	0	26	0
Regional Dense Marl	Edwards rock	13	4	0	0	83	0
Leached Coll. Marl	Edwards rock	18	2	0	0	80	0
Basal Nodular	Edwards rock	0	0	0	0	2	98
upper Dolomitic	Edwards rock	0	0	0	0	98	1
Grainstone member	Edwards rock	0	0	0	0	100	0
Rhythmic Beds Dolo.	Edwards rock	0	1	0	0	99	0
Leached Collapsed	Edwards rock	0	0	0	0	100	0
Kirschberg Evaporite	Edwards rock						100
Travis Country Sink	sinkhole	26	30	7	2	32	2
Nairn Sink	sinkhole	33	9	0	0	48	9
Barbara Falls Sink	sinkhole	20	6	0		70	4
Barton Lodge Sink	sinkhole	18	9	1	0	70	1
Barton Ropeswing	sinkhole	34	17	0	0	47	2
Marbridge	sinkhole	11	4	0	0	84	1
Shady Hollow	sinkhole	19	34	24	9	14	0
Barton Lodge W	spring	32	17	0	0	50	0
Barton Lodge Sp E	spring	20	11	0	0	68	0
Martine Springs	spring	10	7	0	0	83	0
Lost Creek Spring	spring	11	6	0	0	78	4
Backdoor Spring	spring	4	4	0	0	86	6

name (cont.)	I/S%	Ill%	Kaol%	TOC%	SSA
Maple Run Ledge	42	18	40	0.072	128.30
Whirlpool Cave 3	74	12	15	0.459	33.27
Blowing Hole Black	46	20	34	0.6185	79.79
Blowing Hole Red	26	32	42	0.289	90.51
Whirlpool 1	70	17	12	0.331	18.88
Whirlpool 4				0.4835	23.46
Whirlpool 2	63	16	20	0.086	35.71
Maple Run Pool				0.144	13.56
Airmans				0.275	65.83
Eileen's River				0.272	75.10
Maple Run Bottom Rm Ldg	30	25	44		64.94
Castle Cave	42	9	49	0.17	111.60
Bear Creek Park II				0.294	3.32
Village of San Leanna I	44	24	33	0.596	44.82
J. Thomas					
Bear Creek 1				0.099	1.62
Slaughter Creek Acres				0.666	75.88
Onion Crk Mdws 2					63.24
Del Rio Clay					
Regional Dense Marl					
Leached Collapsed Marl					
Basal Nodular					
upper Dolomitic					
Grainstone member					
Rhythmic Beds Dolomitic					
Leached Collapsed					
Kirschberg Evaporite					
Travis Country Sink	70	11	19	3.92	17.81
Nairn Sink	78	9	13	0.767	35.83
Barbara Falls Sink	64	21	15	0.823	17.15
Barton Lodge Sink	47	20	32	0.735	7.77
Barton Ropeswing				1.536	27.57
Marbridge	63	18	19	1.236	15.25
Shady Hollow	44	18	38	0.67	
Barton Lodge W	64	11	25	1.73	25.85
Barton Lodge Sp E	63	14	23	0.194	37.89
Martine Springs	72	9	19	0.354	13.76
Lost Creek Spring	60	21	18	1.103	5.90
Backdoor Spring				0.303	4.44

name (cont.)	Mz	GSD	GSk
Maple Run Ledge	10.23	1.50	-0.41
Whirlpool Cave 3	6.80	2.78	0.57
Blowing Hole Black	5.78	3.73	0.60
Blowing Hole Red	7.10	3.10	0.48
Whirlpool 1	4.85	1.66	0.23
Whirlpool 4	6.65	2.70	0.72
Whirlpool 2	6.60	3.30	0.64
Maple Run Pool	0.93	1.50	-0.87
Airmans	8.58	2.18	-0.01
Eileen's River	8.27	3.00	-0.27
Maple Run Bottom Rm Ldg			
Castle Cave	7.73	4.85	-0.79
Bear Creek Park II			
Village of San Leanna I			
J. Thomas			
Bear Creek 1			
Slaughter Creek Acres			
Onion Crk Mdws 2			
Del Rio Clay			
Regional Dense Marl			
Leached Collapsed Marl			
Basal Nodular			
upper Dolomitic			
Grainstone member			
Rhythmic Beds Dolomitic			
Leached Collapsed			
Kirschberg Evaporite			
Travis Country Sink	4.48	4.50	0.04
Nairn Sink	6.50	2.88	0.91
Barbara Falls Sink			
Barton Lodge Sink	3.37	4.83	0.56
Barton Ropeswing	6.83	3.68	-0.13
Marbridge	-2.57	1.85	0.03
Shady Hollow	2.27	3.72	0.49
Barton Lodge W	4.75	5.20	0.03
Barton Lodge Sp E	6.07	1.75	0.31
Martine Springs			
Lost Creek Spring	2.30	1.50	0.40
Backdoor Spring	-1.07	2.80	-0.14

name	type	clay%	qtz%	ksp%	plag%	calc%	dolo%
Brodie Sp (Toys)	spring	24	15	0	0	62	0
Onion Crk Centex	stream	5	2	0	0	63	30
TxDoT 1	stream	32	16	0	0	51	1
Slaughter Creek 1826	stream	23	7	0	0	68	1
Onion Creek FM 150	stream	7	2	0	0	90	1
Gaines Creek WQP3	stream	11	6	1	1	78	3
TxDoT 2	stream	24	16	0	0	55	3
Beer Creek & FBC	stream	32	13	1	0	52	1
Williamson at OBC	stream	31	11	1	0	55	3
Outfall 2 "Best Buy"	stream	16	38	9	4	33	0
Copper Hills	unconfined well	0	1	0	0	94	5
58-57-6RB	unconfined well	0	0	0	0	4	95
Unisys well	unconfined well	0	1	0	0	1	98
Thames I	unconfined well	0	1	0	0	35	64
HE Brodie 3	unconfined well	0	7	0	0	2	91
Sunset Valley Tank	unconfined well	0	0	0	0	1	98
Little Bear @ Arbor Tr	unconfined well	25	21	0	0	42	13
HE Brodie 2	unconfined well	3	4	0	0	3	91
Sunset Valley Tank 1	unconfined well	0	2	0	0	5	94
Sunset Valley Tank 2	unconfined well	5	3	0	0	6	86
BS storm composite	Barton Springs	28	13	0	0	27	32

name (cont.)	I/S%	Ill%	Kaol%	TOC%	SSA
Brodie Sp (Toys)	27	26	48	0.775	24.26
Onion Crk Centex				0.865	4.12
TxDoT 1	53	19	28	0.446	20.68
Slaughter Creek 1826	78	15	7	1.24	21.16
Onion Creek FM 150	48	31	22	0.9455	4.68
Gaines Creek WQP3	60	19	21	0.428	7.73
TxDoT 2	56	14	30	0.45	22.19
Beer Creek & FBC	81	10	9	2.108	29.96
Williamson at OBC	62	21	17	3.3	
Outfall 2 "Best Buy"	48	22	30	0.684	
Copper Hills				0.111	16.42
58-57-6RB				0.887	
Unisys well	54	13	33	0.263	1.38
Thames I				0.171	2.11
HE Brodie 3				0.115	1.88
Sunset Valley Tank				0.135	0.14
Little Bear @ Arbor Tr	66	12	22	0.2	31.59
HE Brodie 2				0.132	2.37
Sunset Valley Tank 1				0.034	2.25
Sunset Valley Tank 2				0.034	4.97
BS storm composite	33	27	41		

name (cont.)	Mz	GSD	GSk
Brodie Sp (Toys)	2.93	4.53	0.23
Onion Crk Centex	6.55	1.45	0.00
TxDoT 1	5.90	4.55	0.10
Slaughter Creek 1826			
Onion Creek FM 150	1.20	1.60	0.38
Gaines Creek WQP3	5.78	2.85	0.39
TxDoT 2	5.91	4.62	-0.03
Beer Creek & FBC	3.32	3.55	0.62
Williamson at OBC	6.03	3.88	-0.39
Outfall 2 "Best Buy"			
Copper Hills			
58-57-6RB			
Unisys well	4.33	1.76	-0.06
Thames I	0.76	1.05	0.84
HE Brodie 3	5.17	0.90	0.45
Sunset Valley Tank	4.93	0.85	0.24
Little Bear @ Arbor Tr			
HE Brodie 2			
Sunset Valley Tank 1	5.00	1.08	0.00
Sunset Valley Tank 2			
BS storm composite			

Appendix C. Geochemistry of Barton Springs Suspended Sediment Samples

Storm 1
11/1/95

Time	Clay %	Quartz %	Clastic %	Calcite %	Dolomite %
12:30 PM	30	15	45	17	38
1:30 PM	34	17	51	9	41
2:45 PM	32	17	49	13	38
3:30 PM	35	17	53	10	37
5:00 PM	38	19	56	4	39
6:00 PM	40	15	55	11	34
9:30 PM	40	18	58	6	36

Storm 2
5/30/96

Time (DST)	Clay %	Quartz %	Clastic %	Calcite %	Dolomite %
12:45 PM	32	9	40	31	29
1:45 PM	29	13	43	30	27
2:45 PM	30	11	42	30	27
3:45 PM	37	12	49	14	37
4:45 PM	41	13	55	9	36
5:45 PM	34	13	48	11	41
6:45 PM	38	13	51	7	42
7:45 PM	40	14	54	11	35
8:45 PM	43	13	57	10	33
9:45 PM	44	13	58	12	30
10:45 PM	54	12	68	10	22

Appendix D. Aqueous Chemistry of Barton Springs Water Samples

Storm 1 date	time	T	log IAP/KT	pH	cond (u-siemens/cm)	turb (NTU)	DO (mg/l)	HCO3 (mg/l)	HCO3 M
11/1/95	8:10 AM		-0.19					316.38	5.19E-03
	9:05 AM		-0.21					300.12	4.92E-03
	10:30 AM		-0.21					303.04	4.97E-03
	11:35 AM	21.30	-0.19	6.93	570.00	13.00	5.90	298.11	4.89E-03
	12:35 PM	21.30	-0.22	6.89	567.00	15.00	6.16	302.54	4.96E-03
	1:30 PM	21.40	-0.15	6.97	564.00	18.00	6.18	297.86	4.88E-03
	2:40 PM	21.40	-0.16	6.97	558.00	21.00	6.04	294.54	4.83E-03
	3:30 PM	21.40	-0.20	6.93	556.00	22.00	6.11	293.96	4.82E-03
	4:55 PM	21.50	-0.11	7.02	632.00	21.00	5.99	293.93	4.82E-03
	6:05 PM	21.30	-0.26	6.87	556.00	17.00	6.10	292.1	4.79E-03
	9:30 PM		-0.24					291.22	4.77E-03
11/2/95	8:30 AM		-0.23					293.49	4.81E-03

SI calculated using an estimated pH of 6.9 for first three and last 2 samples

Storm 1 cont. time	Al (mg/l)	Al M	Ba (mg/l)	Ba M	Ca (mg/l)	Ca M	Cr (mg/l)	Cr M
8:10 AM			0.07	6.48E-06	90.46	2.26E-03	<0.01	
9:05 AM			0.06	5.55E-06	89.65	2.24E-03	<0.01	
10:30 AM			0.06	5.55E-06	89.15	2.22E-03	<0.01	
11:35 AM			0.06	5.55E-06	88.35	2.20E-03	<0.01	
12:35 PM			0.06	5.55E-06	87.99	2.20E-03	<0.01	
1:30 PM			0.06	5.55E-06	88.07	2.20E-03	<0.01	
2:40 PM			0.06	5.55E-06	86.74	2.16E-03	<0.01	
3:30 PM			0.06	5.55E-06	86.38	2.16E-03	<0.01	
4:55 PM			0.06	5.55E-06	86.27	2.15E-03	<0.01	
6:05 PM			0.06	5.55E-06	86.14	2.15E-03	<0.01	
9:30 PM			0.05	4.63E-06	85.53	2.13E-03	<0.01	
8:30 AM			0.05	4.63E-06	87.04	2.17E-03	0.01	

Storm 1 cont. time	Mg (mg/l)	Mg M	Ni (mg/l)	Ni M	Pb (mg/l)	Pb M	Sr (mg/l)	Sr M
8:10 AM	24.04	9.89E-04	<0.01		0.07	3.38E-07	1.41	1.61E-05
9:05 AM	23.32	9.60E-04	<0.01		0.06	2.90E-07	1.39	1.59E-05
10:30 AM	22.65	9.32E-04	<0.01		0.08	3.86E-07	1.36	1.55E-05
11:35 AM	22.12	9.10E-04	<0.01		0.08	3.86E-07	1.33	1.52E-05
12:35 PM	21.67	8.92E-04	<0.01		0.06	2.90E-07	1.3	1.48E-05
1:30 PM	21.44	8.82E-04	<0.01		0.07	3.38E-07	1.29	1.47E-05
2:40 PM	21.17	8.71E-04	<0.01		0.06	2.90E-07	1.28	1.46E-05
3:30 PM	21.08	8.67E-04	<0.01		0.05	2.41E-07	1.26	1.44E-05
4:55 PM	21.14	8.70E-04	<0.01		0.05	2.41E-07	1.26	1.44E-05
6:05 PM	21.18	8.72E-04	<0.01		0.05	2.41E-07	1.25	1.43E-05
9:30 PM	20.86	8.58E-04	<0.01		0.03	1.45E-07	1.19	1.36E-05
8:30 AM	20.69	8.51E-04	<0.01		0.05	2.41E-07	1.13	1.29E-05

Storm 1 cont. time	Na (mg/l)	Na M	Si (mg/l)	Si M	B (mg/l)	B M	K (mg/l)	K M
8:10 AM	18.06	7.86E-04	5.83	2.08E-04	0.05	4.63E-06		
9:05 AM	16.8	7.31E-04	5.37	1.91E-04	0.05	4.63E-06		
10:30 AM	15.29	6.65E-04	5.28	1.88E-04	0.04	3.70E-06		
11:35 AM	14.99	6.52E-04	5.19	1.85E-04	0.04	3.70E-06		
12:35 PM	14.47	6.29E-04	5.14	1.83E-04	0.04	3.70E-06		
1:30 PM	13.96	6.07E-04	5.08	1.81E-04	0.04	3.70E-06		
2:40 PM	13.78	5.99E-04	5.03	1.79E-04	0.04	3.70E-06		
3:30 PM	13.76	5.99E-04	5.06	1.80E-04	0.04	3.70E-06		
4:55 PM	13.94	6.06E-04	5.01	1.78E-04	0.04	3.70E-06		
6:05 PM	13.77	5.99E-04	5.05	1.80E-04	0.04	3.70E-06		
9:30 PM	13.83	6.02E-04	5.05	1.80E-04	0.04	3.70E-06		
8:30 AM	14.91	6.49E-04	5.08	1.81E-04	0.04	3.70E-06		

Storm 1 (cont.) time	Li (mg/l)	Li M	Cl (mg/l)	Cl M	NO3 (mg/l)	NO3 M	SO4 (mg/l)	SO4 M	TSS (mg/l)
8:10 AM			28.52	8.04E-04	6.2	1.00E-04	25.95	2.98E-04	0.95
9:05 AM			26.81	7.56E-04	5.49	8.85E-05	24.74	2.84E-04	2.65
10:30 AM			23.28	6.57E-04	5.54	8.94E-05	25.81	2.97E-04	3.15
11:35 AM			23.92	6.75E-04	5.65	9.11E-05	24.5	2.82E-04	2.55
12:35 PM			23.24	6.56E-04	5.99	9.66E-05	23.64	2.72E-04	11.25
1:30 PM			23.48	6.62E-04	6.11	9.85E-05	24.52	2.82E-04	11.45
2:40 PM			23.11	6.52E-04	5.33	8.60E-05	22.24	2.56E-04	13.35
3:30 PM			23.84	6.72E-04	5.77	9.31E-05	23	2.64E-04	13.1
4:55 PM			21.84	6.16E-04	5.85	9.44E-05	23.29	2.68E-04	12.95
6:05 PM			22.53	6.35E-04	5.88	9.48E-05	21.81	2.51E-04	8.05
9:30 PM			22.05	6.22E-04	5.53	8.92E-05	22.37	2.57E-04	4.45
8:30 AM			23.74	6.70E-04	5.47	8.82E-05	23.72	2.73E-04	1.5

Storm 2 date	time (DST)	T	log IAP/KT	pH	cond (u-siemens/cm)	turb (NTU)	DO (mg/l)	HCO3 (mg/l)	HCO3 M
5/30/96	7:00 AM							283.02	4.64E-03
	11:45 AM	21.6	0	7.1	680	8	4.6	329.4	5.40E-03
	12:45 PM	21.5	-0.205	6.93	680	11	4.77	300.12	4.92E-03
	1:45 PM	21.5	-0.03	7.1	693	14	4.61	302.54	4.96E-03
	2:45 PM	21.5	-0.024	7.11	697	20	4.54	300.12	4.92E-03
	3:45 PM	21.5	-0.011	7.12	698	29	4.78	303.72	4.98E-03
	4:45 PM	21.5	-0.027	7.11	698	41	4.64	297.66	4.88E-03
	5:45 PM	21.5	-0.02	7.1	702	39	4.52	310.124	5.08E-03
	6:45 PM	21.5	-0.025	7.11	719	41	4.62	302.02	4.95E-03
	7:45 PM	21.5	-0.034	7.12	714	43	4.27	295.24	4.84E-03
	8:45 PM	21.4	-0.034	7.13	709	45	4.43	290.36	4.76E-03
	9:45 PM	21.4	-0.022	7.15	701	36	4.54	288.48	4.73E-03
	10:45 PM	21.4	-0.025	7.16	697	23	4.95	278.12	4.56E-03
5/31/96	5:20 AM	21.60	-0.09	7.09	683.00	8.00	4.76	278.12	4.56E-03
	7:30 AM	21.5	-0.098	7.11	685	8	4.3	264.008	4.33E-03

Storm 2 (cont.)

time	Al (mg/l)	Al M	Ba (mg/l)	Ba M	Ca (mg/l)	Ca M	Cr (mg/l)	Cr M
7:00 AM	4.00E-02	1.48E-06	0.06	5.55E-06	83.17	2.08E-03	0.01	1.92E-07
11:45 AM	6.00E-02	2.22E-06	0.07	6.48E-06	84.94	2.12E-03	0.02	3.85E-07
12:45 PM	5.00E-02	1.85E-06	0.07	6.48E-06	85.95	2.14E-03	0.02	3.85E-07
1:45 PM	5.00E-02	1.85E-06	0.07	6.48E-06	86.61	2.16E-03	0.01	1.92E-07
2:45 PM	7.00E-02	2.59E-06	0.07	6.48E-06	86.49	2.16E-03	0.02	3.85E-07
3:45 PM	6.00E-02	2.22E-06	0.07	6.48E-06	86.27	2.15E-03	0.02	3.85E-07
4:45 PM	5.00E-02	1.85E-06	0.07	6.48E-06	86.5	2.16E-03	0.01	1.92E-07
5:45 PM	6.00E-02	2.22E-06	0.07	6.48E-06	86.71	2.16E-03	0.02	3.85E-07
6:45 PM	6.00E-02	2.22E-06	0.07	6.48E-06	86	2.15E-03	0.02	3.85E-07
7:45 PM	6.00E-02	2.22E-06	0.07	6.48E-06	84.02	2.10E-03	0.02	3.85E-07
8:45 PM	5.00E-02	1.85E-06	0.07	6.48E-06	83.6	2.09E-03	0.01	1.92E-07
9:45 PM	5.00E-02	1.85E-06	0.07	6.48E-06	82.8	2.07E-03	0.02	3.85E-07
10:45 PM	6.00E-02	2.22E-06	0.06	5.55E-06	82.94	2.07E-03	0.02	3.85E-07
5:20 AM	5.00E-02	1.85E-06	0.06	5.55E-06	82.66	2.06E-03	0.01	1.92E-07
7:30 AM	5.00E-02	1.85E-06	0.06	5.55E-06	81.66	2.04E-03	0.01	1.92E-07

Storm 2 (cont.) time	Mg (mg/l)	Mg M	Ni (mg/l)	Ni M	Pb (mg/l)	Pb M	Sr (mg/l)	Sr M
7:00 AM	23.45	9.65E-04	0.03	5.11E-07	0.13	6.27E-07	2.74	3.13E-05
11:45 AM	23.97	9.86E-04	0.03	5.11E-07	0.14	6.76E-07	2.66	3.04E-05
12:45 PM	24.3	1.00E-03	0.03	5.11E-07	0.13	6.27E-07	2.68	3.06E-05
1:45 PM	24.47	1.01E-03	0.03	5.11E-07	0.14	6.76E-07	2.68	3.06E-05
2:45 PM	24.68	1.02E-03	0.03	5.11E-07	0.15	7.24E-07	2.66	3.04E-05
3:45 PM	24.52	1.01E-03	0.03	5.11E-07	0.16	7.72E-07	2.65	3.02E-05
4:45 PM	24.54	1.01E-03	0.03	5.11E-07	0.15	7.24E-07	2.64	3.01E-05
5:45 PM	24.5	1.01E-03	0.03	5.11E-07	0.15	7.24E-07	2.64	3.01E-05
6:45 PM	24.39	1.00E-03	0.03	5.11E-07	0.15	7.24E-07	2.65	3.02E-05
7:45 PM	23.68	9.74E-04	0.03	5.11E-07	0.15	7.24E-07	2.64	3.01E-05
8:45 PM	23.49	9.67E-04	0.03	5.11E-07	0.15	7.24E-07	2.67	3.05E-05
9:45 PM	25.62	1.05E-03	0.03	5.11E-07	0.14	6.76E-07	2.67	3.05E-05
10:45 PM	23.24	9.56E-04	0.03	5.11E-07	0.14	6.76E-07	2.7	3.08E-05
5:20 AM	23.04	9.48E-04	0.03	5.11E-07	0.14	6.76E-07	2.72	3.10E-05
7:30 AM	22.77	9.37E-04	0.03	5.11E-07	0.13	6.27E-07	2.69	3.07E-05

Storm 2 (cont.)

time	Na (mg/l)	Na M	Si (mg/l)	Si M	B (mg/l)	B M	K (mg/l)	K M
7:00 AM	26.85	1.17E-03	5.06	1.80E-04			1.63	4.17E-05
11:45 AM	25.84	1.12E-03	5.18	1.84E-04			1.31	3.35E-05
12:45 PM	26.09	1.13E-03	5.25	1.87E-04			1.47	3.76E-05
1:45 PM	26.92	1.17E-03	5.26	1.87E-04			1.76	4.50E-05
2:45 PM	27.41	1.19E-03	5.27	1.88E-04			2.08	5.32E-05
3:45 PM	27.07	1.18E-03	5.25	1.87E-04			1.63	4.17E-05
4:45 PM	27.3	1.19E-03	5.26	1.87E-04			1.79	4.58E-05
5:45 PM	27.96	1.22E-03	5.34	1.90E-04			1.47	3.76E-05
6:45 PM	31.27	1.36E-03	5.29	1.88E-04			1.63	4.17E-05
7:45 PM	32.13	1.40E-03	5.12	1.82E-04			1.53	3.91E-05
8:45 PM	32.16	1.40E-03	5.04	1.79E-04			1.63	4.17E-05
9:45 PM	31.68	1.38E-03	4.99	1.78E-04			1.76	4.50E-05
10:45 PM	31.51	1.37E-03	4.95	1.76E-04			2.2	5.63E-05
5:20 AM	29.7	1.29E-03	4.94	1.76E-04			1.72	4.40E-05
7:30 AM	29.6	1.29E-03	4.97	1.77E-04			1.12	2.86E-05

Storm 2 (cont.)

time	Li	Li	Cl	Cl	NO3	NO3	SO4	SO4	TSS
time	(mg/l)	M	(mg/l)	M	(mg/l)	M	(mg/l)	M	(mg/l)
7:00 AM	0.03	4.32E-06	41.68	1.18E-03	6.03	9.73E-05	34.02	3.91E-04	3.25
11:45 AM	0.02	2.88E-06	38.82	1.09E-03	5.81	9.37E-05	32.73	3.76E-04	3.25
12:45 PM	0.03	4.32E-06	39.12	1.10E-03	6.58	1.06E-04	35.51	4.08E-04	8.65
1:45 PM	0.03	4.32E-06	39.45	1.11E-03	5.74	9.26E-05	35.95	4.13E-04	8.05
2:45 PM	0.04	5.76E-06	41.31	1.17E-03	5.6	9.03E-05	35.86	4.12E-04	13.05
3:45 PM	0.03	4.32E-06	41.01	1.16E-03	5.59	9.02E-05	37.26	4.28E-04	16.25
4:45 PM	0.03	4.32E-06	41.35	1.17E-03	5.92	9.55E-05	36.45	4.19E-04	18.15
5:45 PM	0.03	4.32E-06	43.48	1.23E-03	5.47	8.82E-05	37.06	4.26E-04	18.75
6:45 PM	0.04	5.76E-06	46.19	1.30E-03	6.03	9.73E-05	37.36	4.29E-04	20.15
7:45 PM	0.03	4.32E-06	49.26	1.39E-03	6.19	9.98E-05	38.07	4.38E-04	16.95
8:45 PM	0.04	5.76E-06	49.54	1.40E-03	5.54	8.94E-05	38.96	4.48E-04	10.55
9:45 PM	0.03	4.32E-06	49.19	1.39E-03	5.38	8.68E-05	39.51	4.54E-04	10.45
10:45 PM	0.05	7.21E-06	48.75	1.38E-03	5.52	8.90E-05	39.46	4.54E-04	10.95
5:20 AM	0.03	4.32E-06	46.85	1.32E-03	5.6	9.03E-05	36.4	4.18E-04	5.55
7:30 AM	0.03	4.32E-06	47.41	1.34E-03	5.71	9.21E-05	37.25	4.28E-04	4.15

Drawdown date	time	T	log IAP/KT	pH	cond (u-siemens/cm)	turb (NTU)	DO (mg/l)	HCO3 (mg/l)	HCO3 M
7/18/96	7:45 PM	21.7	-0.153	6.98	720	3	5.45	292.8	4.80E-03
	8:45 PM	21.5	-0.178	6.95	734	3	4.9	300.1	4.92E-03
	9:45 PM	21.5	-0.141	6.99	733	3	5.1	297.7	4.88E-03
	10:45 PM	21.7	-0.232	6.98	732	3	5.3	323.9	5.31E-03
	11:45 PM	21.5	-0.163	6.97	733	3	4.9	298.6	4.90E-03
7/19/96	12:45 AM	21.5	-0.197	6.96	739	2	4.95	287.1	4.71E-03
	1:45 AM	21.5	-0.232	6.91	742	2	4	297.9	4.88E-03
	2:45 AM	21.5	-0.252	6.89	743	2	4.55	297.7	4.88E-03
	3:45 AM	21.5	-0.183	6.95	741	2	5.5	302.5	4.96E-03
	4:45 AM	21.5	-0.221	6.92	741	3	5.4	298.2	4.89E-03
	5:45 AM	21.5	-0.168	6.96	741	2	5.35	300.1	4.92E-03
	6:45 AM	21.5	-0.113	7.02	751	2	5.15	293.4	4.81E-03
	7:56 AM	21.5	-0.122	7.01	777	2	4.95	302.5	4.96E-03
	8:30 AM	21.5	-0.132	7.01	800	2	4.85	295.2	4.84E-03
	9:00 AM	21.5	-0.137	7	808	2	4.8	297.7	4.88E-03
	10:30 AM	21.5		6.84	817	2	5.05	301.2	4.94E-03
	11:30 AM	21.5	-0.174	6.94	819	2	4.9	316.7	5.19E-03
	12:30 PM	21.5		6.85	815	2	4.85	307.4	5.04E-03
	1:30 PM	21.6	-0.35	6.79	808	2	4.5	290.4	4.76E-03
	2:30 PM	21.6	-0.28	6.84	795	2		307.4	5.04E-03
	3:30 PM	21.6	-0.32	6.81	774	2		301.2	4.94E-03
	4:30 PM	21.5	-0.303	6.82	761	3		304.2	4.99E-03
	5:30 PM	21.6	-0.342	6.78	749	3		301.3	4.94E-03
	6:30 PM	21.6	-0.314	6.81	743	2		301.4	4.94E-03

Drawdown (cont.) time	Al (mg/l)	Al M	Ba (mg/l)	Ba M	Ca (mg/l)	Ca M	Cr (mg/l)	Cr M
7:45 PM	0.04	1.48E-06	0.07	6.48E-06	90.03	2.25E-03	0.02	3.85E-07
8:45 PM	0.04	1.48E-06	0.07	6.48E-06	89.25	2.23E-03	0.01	1.92E-07
9:45 PM	0.05	1.85E-06	0.07	6.48E-06	89.59	2.24E-03	0.02	3.85E-07
10:45 PM	0.05	1.85E-06	0.05	4.63E-06	65.92	1.64E-03	0.01	1.92E-07
11:45 PM	0.06	2.22E-06	0.07	6.48E-06	89.33	2.23E-03	0.02	3.85E-07
12:45 AM	0.02	7.41E-07	0.07	6.48E-06	86.23	2.15E-03	0.01	1.92E-07
1:45 AM	0.02	7.41E-07	0.07	6.48E-06	86.5	2.16E-03	0.01	1.92E-07
2:45 AM	0.03	1.11E-06	0.07	6.48E-06	86.63	2.16E-03	0.01	1.92E-07
3:45 AM	0.03	1.11E-06	0.07	6.48E-06	86.9	2.17E-03	0.02	3.85E-07
4:45 AM	0.03	1.11E-06	0.07	6.48E-06	86.7	2.16E-03	0.01	1.92E-07
5:45 AM	0.03	1.11E-06	0.07	6.48E-06	89.12	2.22E-03	0.01	1.92E-07
6:45 AM	0.03	1.11E-06	0.07	6.48E-06	90.12	2.25E-03	0.01	1.92E-07
7:56 AM	0.02	7.41E-07	0.07	6.48E-06	88.15	2.20E-03	0.01	1.92E-07
8:30 AM	0.02	7.41E-07	0.07	6.48E-06	88.59	2.21E-03	0.01	1.92E-07
9:00 AM	0.03	1.11E-06	0.07	6.48E-06	89.35	2.23E-03	0.02	3.85E-07
10:30 AM	0.03	1.11E-06	0.07	6.48E-06	89.84	2.24E-03	0.02	3.85E-07
11:30 AM	0.03	1.11E-06	0.07	6.48E-06	88.92	2.22E-03	0.02	3.85E-07
12:30 PM	0.04	1.48E-06	0.07	6.48E-06	89.76	2.24E-03	0.02	3.85E-07
1:30 PM	0.05	1.85E-06	0.07	6.48E-06	90.4	2.26E-03	0.02	3.85E-07
2:30 PM	0.05	1.85E-06	0.07	6.48E-06	89.57	2.23E-03	0.02	3.85E-07
3:30 PM	0.04	1.48E-06	0.07	6.48E-06	89	2.22E-03	0.02	3.85E-07
4:30 PM	0.04	1.48E-06	0.07	6.48E-06	89.69	2.24E-03	0.02	3.85E-07
5:30 PM	0.06	2.22E-06	0.07	6.48E-06	90.18	2.25E-03	0.02	3.85E-07
6:30 PM	0.04	1.48E-06	0.07	6.48E-06	89.81	2.24E-03	0.01	1.92E-07

Drawdown (cont.) time	Mg (mg/l)	Mg M	Ni (mg/l)	Ni M	Pb (mg/l)	Pb M	Sr (mg/l)	Sr M
7:45 PM	26.71	1.10E-03	0.03	5.11E-07	0.15	7.24E-07	3.33	3.80E-05
8:45 PM	26.59	1.09E-03	0.03	5.11E-07	0.14	6.76E-07	3.32	3.79E-05
9:45 PM	26.63	1.10E-03	0.03	5.11E-07	0.15	7.24E-07	3.31	3.78E-05
10:45 PM	20.17	8.30E-04	0.02	3.41E-07	0.12	5.79E-07	2.44	2.78E-05
11:45 PM	26.56	1.09E-03	0.03	5.11E-07	0.15	7.24E-07	3.25	3.71E-05
12:45 AM	26.1	1.07E-03	0.03	5.11E-07	0.13	6.27E-07	3.23	3.69E-05
1:45 AM	26.13	1.08E-03	0.02	3.41E-07	0.11	5.31E-07	3.21	3.66E-05
2:45 AM	26.08	1.07E-03	0.03	5.11E-07	0.13	6.27E-07	3.19	3.64E-05
3:45 AM	26.1	1.07E-03	0.03	5.11E-07	0.13	6.27E-07	3.17	3.62E-05
4:45 AM	25.99	1.07E-03	0.03	5.11E-07	0.13	6.27E-07	3.15	3.60E-05
5:45 AM	26.55	1.09E-03	0.02	3.41E-07	0.12	5.79E-07	3.2	3.65E-05
6:45 AM	26.85	1.10E-03	0.02	3.41E-07	0.13	6.27E-07	3.24	3.70E-05
7:56 AM	26.51	1.09E-03	0.03	5.11E-07	0.14	6.76E-07	3.22	3.67E-05
8:30 AM	26.85	1.10E-03	0.02	3.41E-07	0.13	6.27E-07	3.25	3.71E-05
9:00 AM	26.96	1.11E-03	0.02	3.41E-07	0.13	6.27E-07	3.28	3.74E-05
10:30 AM	27.28	1.12E-03	0.03	5.11E-07	0.13	6.27E-07	3.34	3.81E-05
11:30 AM	27.06	1.11E-03	0.03	5.11E-07	0.13	6.27E-07	3.32	3.79E-05
12:30 PM	27.3	1.12E-03	0.03	5.11E-07	0.14	6.76E-07	3.37	3.85E-05
1:30 PM	27.46	1.13E-03	0.03	5.11E-07	0.14	6.76E-07	3.4	3.88E-05
2:30 PM	27.18	1.12E-03	0.03	5.11E-07	0.14	6.76E-07	3.36	3.83E-05
3:30 PM	26.96	1.11E-03	0.03	5.11E-07	0.14	6.76E-07	3.33	3.80E-05
4:30 PM	26.94	1.11E-03	0.03	5.11E-07	0.14	6.76E-07	3.34	3.81E-05
5:30 PM	26.94	1.11E-03	0.03	5.11E-07	0.14	6.76E-07	3.33	3.80E-05
6:30 PM	26.79	1.10E-03	0.03	5.11E-07	0.13	6.27E-07	3.33	3.80E-05

Drawdown (cont.) time	Na (mg/l)	Na M	Si (mg/l)	Si M	B (mg/l)	B M	K (mg/l)	K M
7:45 PM	31.25	1.36E-03	5.21	1.85E-04			1.84	4.71E-05
8:45 PM	31.7	1.38E-03	5.13	1.83E-04			1.6	4.09E-05
9:45 PM	31.64	1.38E-03	5.07	1.80E-04			1.57	4.02E-05
10:45 PM	23.46	1.02E-03	3.64	1.30E-04			1.48	3.79E-05
11:45 PM	31.99	1.39E-03	5.07	1.80E-04			1.29	3.30E-05
12:45 AM	32.59	1.42E-03	5.16	1.84E-04			1.08	2.76E-05
1:45 AM	33.34	1.45E-03	4.85	1.73E-04			1.51	3.86E-05
2:45 AM	33.4	1.45E-03	4.81	1.71E-04			1.44	3.68E-05
3:45 AM	32.99	1.43E-03	4.81	1.71E-04			0.56	1.43E-05
4:45 AM	33.09	1.44E-03	4.77	1.70E-04			0.68	1.74E-05
5:45 AM	33.17	1.44E-03	5.22	1.86E-04			1.11	2.84E-05
6:45 AM	34.61	1.51E-03	5.17	1.84E-04			1.23	3.15E-05
7:56 AM	38.36	1.67E-03	5.01	1.78E-04			0.68	1.74E-05
8:30 AM	42.05	1.83E-03	5.04	1.79E-04			0.99	2.53E-05
9:00 AM	43.89	1.91E-03	4.99	1.78E-04			1.17	2.99E-05
10:30 AM	45.86	1.99E-03	5.01	1.78E-04			1.57	4.02E-05
11:30 AM	45.38	1.97E-03	4.93	1.76E-04			1.54	3.94E-05
12:30 PM	45.23	1.97E-03	4.96	1.77E-04			1.44	3.68E-05
1:30 PM	44.52	1.94E-03	4.97	1.77E-04			2.06	5.27E-05
2:30 PM	42.25	1.84E-03	5.25	1.87E-04			2.03	5.19E-05
3:30 PM	38.89	1.69E-03	5.13	1.83E-04			2.42	6.19E-05
4:30 PM	36.52	1.59E-03	5.06	1.80E-04			2.64	6.75E-05
5:30 PM	35	1.52E-03	5.06	1.80E-04			2.61	6.68E-05
6:30 PM	33.66	1.46E-03	5.05	1.80E-04			2.39	6.11E-05

Drawdown (cont.) (cont.) time	Li (mg/l)	Li M	Cl (mg/l)	Cl M	NO3 (mg/l)	NO3 M	SO4 (mg/l)	SO4 M	TSS (mg/l)
7:45 PM	0.03	4.32E-06	54.53	1.54E-03	6.82	1.10E-04	46.96	5.40E-04	
8:45 PM	0.04	5.76E-06	54.8	1.55E-03	5.98	9.65E-05	46.12	5.30E-04	
9:45 PM	0.03	4.32E-06	56.22	1.59E-03	7.31	1.18E-04	47.93	5.51E-04	
10:45 PM	0.03	4.32E-06	56.53	1.59E-03	8.41	1.36E-04	48.62	5.59E-04	
11:45 PM	0.03	4.32E-06	58.4	1.65E-03	8.02	1.29E-04	50.66	5.82E-04	
12:45 AM	0.03	4.32E-06	49.61	1.40E-03	6.47	1.04E-04	40.84	4.69E-04	
1:45 AM	0.03	4.32E-06	49.57	1.40E-03	6.21	1.00E-04	42.33	4.87E-04	
2:45 AM	0.02	2.88E-06	51.06	1.44E-03	6.8	1.10E-04	43.71	5.02E-04	
3:45 AM	0.01	1.44E-06	49.68	1.40E-03	6.08	9.81E-05	41.7	4.79E-04	
4:45 AM	0.02	2.88E-06	50.62	1.43E-03	6.69	1.08E-04	43.68	5.02E-04	
5:45 AM	0.03	4.32E-06	50.23	1.42E-03	6.69	1.08E-04	42.9	4.93E-04	
6:45 AM	0.03	4.32E-06	53.08	1.50E-03	6.11	9.85E-05	43.32	4.98E-04	
7:56 AM	0.02	2.88E-06	57.74	1.63E-03	6.56	1.06E-04	45.45	5.22E-04	
8:30 AM	0.03	4.32E-06	63.21	1.78E-03	7.11	1.15E-04	47.34	5.44E-04	
9:00 AM	0.04	5.76E-06	65.71	1.85E-03	6.29	1.01E-04	51.74	5.95E-04	
10:30 AM	0.04	5.76E-06	67.11	1.89E-03	5.98	9.65E-05	50.86	5.85E-04	
11:30 AM	0.04	5.76E-06	68.07	1.92E-03	6.65	1.07E-04	51.49	5.92E-04	
12:30 PM	0.04	5.76E-06	67.93	1.92E-03	6.61	1.07E-04	51.36	5.90E-04	
1:30 PM	0.05	7.21E-06	67.68	1.91E-03	5.88	9.48E-05	50.75	5.83E-04	
2:30 PM	0.05	7.21E-06	64.52	1.82E-03	5.94	9.58E-05	49.81	5.73E-04	
3:30 PM	0.05	7.21E-06	62.33	1.76E-03	6.71	1.08E-04	48.22	5.54E-04	
4:30 PM	0.05	7.21E-06	58.36	1.65E-03	6.66	1.07E-04	47.32	5.44E-04	
5:30 PM	0.05	7.21E-06	56.8	1.60E-03	6.14	9.90E-05	46.24	5.32E-04	
6:30 PM	0.05	7.21E-06	54.54	1.54E-03	6.87	1.11E-04	49.42	5.68E-04	

Bibliography

Adb-Elfattah, A., and Wada, K., 1981, Adsorption of lead, copper, zinc, cobalt and cadmium by soils that differ in cation-exchange materials: J. Soil Sci., v. 32, p. 271-283.

Aldrich, D.G., and Buchanan, J.R., 1958, Anomalies in techniques for preparing H-Bentonites: Soil Science Society of America Proceedings, v. 22, p. 281-285.

Aley, T., and Fletcher, M.W., 1976, Water tracer's cookbook: Journal of the Missouri Speleological Survey, v. 16.

Allen-King, R.M., Groenevelt, H., Warren, C.J., and Mackay, D.M., 1996, Non-linear chlorinated-solvent sorption in four aquitards: Journal of Contaminant Hydrology, v. 22, p. 203-221.

Arnold, C.L., Jr., and Gibbons, C.J., 1996, Impervious surface coverage: the emergence of a key environmental indicator: Journal of the American Planning Association, v. 62, p. 243-258.

Atkinson, T.C., Smith, D.I., Lavis, J.J., and Whitaker, R.J., 1973, Experiments in tracing underground waters in limestones: Journal of Hydrology, v. 19, p. 323-349.

Austin, City of, 1994, Unpublished data.

Bettis, R., 1996, personal communication.

Bögli, A., 1980, Karst Hydrology and Physical Speleology: New York, Springer-Verlag.

Bretz, J.H., 1942, Vadose and phreatic features of limestone caves: Journal of Geology, v. L, p. 675-811.

Brune, G., 1981, Springs of Texas: Fort Worth, Branch-Smith Inc., 566 p.

Bruque, S., Mozas, T., and Rodriguez, A., 1980, Factors influencing retention of lanthanide ions by montmorillonite: Clay Minerals, v. 15, p. 413-420.

Buller, A.T., and McManus, J., 1972, Simple metric sedimentary statistics used to recognize different environments: Sedimentology, v. 18, p. 1-21.

Cantrell, K.J., and Byrne, R.H., 1987, Rare earth element complexation by carbonate and oxalate ions: Geochim. Cosmochim. Acta, v. 51, p. 597-605.

Carey, D.A., 1989, Fluorometric detection of tracer particles used to study animal-particle dynamics: Limnol. Oceanogr., v. 34, p. 630-635.

Cassidy, R.M., 1988, Determination of rare-earth elements in rocks by liquid chromatography: Chemical Geology, v. 67, p. 185-195.

Dahl, S.L., 1990, Hydrogeology and Stream Interactions of the Edwards Aquifer in the Salado Creek Basin, Bell and Williamson Counties, Central Texas [Masters thesis]: Waco, Baylor University.

Davis, J.C., 1973, Statistics and Data Analysis in Geology: New York, John Wiley & Sons, 550 p.

Davis, S.N., Campbell, D.J., Bentley, H.W., and Flynn, T.J., 1985, Ground-water Tracers: Ada, Oklahoma, U.S. Environmental Protection Agency, 200 p.

Dreiss, S.J., 1989, Regional scale transport in a karst aquifer 1. Component separation of spring flow hydrographs: Water Resources Research, v. 25, p. 117-125.

Drew, D.P., and Smith, D.I., 1969, Techniques for the tracing of subterranean drainage, Br. Geomorphol. Res. Group Tech. Bulletin, v.2, 36 p.

Dzombak, D.A., and Morel, F.M.M., 1990, Surface Complexation Modeling: New York, J. Wiley and Sons.

Elchuk, S., and Cassidy, R.M., 1979, Separation of the lanthanides on high-efficiency bonded phases an conventional ion-exchange resins: Analytical Chemistry, v. 51, p. 1434-1450.

Erel, Y., and Morgan, J.J., 1991, The effect of surface reactions on the relative abundances of trace metals in deep-sea water: Geochimica et Cosmochimica Acta, v. 55, p. 1807-1813.

Fisher, W.L., and Rodda, P.U., 1969, Edwards Formation (Lower Cretaceous), Texas: dolomitization in a carbonate platform system: AAPG Bulletin, v. 53, p. 55-72.

Folk, R.L., 1980, Petrology of Sedimentary Rocks: Austin, Hemphill Publishing Co., 184 p.

Folk, R.L., and Land, L.S., 1975, Mg/Ca ratio and salinity: two controls over crystallization of dolomite: AAPG Bulletin, v. 59, p. 60-68.

Folk, R.L., and Siedlecka, A., 1974, The "schizohaline" environment: its sedimentary and diagenetic fabrics as exemplified by Late Paleozoic rocks of Bear Island, Svalbard: Sedimentary Geology, v. 11, p. 1-15.

Ford, D.C., and Williams, P.W., 1989, Karst Geomorphology and Hydrology: London, Unwin Hyman Ltd.

Frank, R., 1969, The clastic sediments of Douglas Cave, Stuart Town, New South Wales: Helectite, v. January, p. 3-13.

Frank, R.M., 1965, Petrologic study of sediments from selected Central Texas caves [Masters thesis]: Austin, University of Texas at Austin.

Freedman, Y.E., Magaritz, M., Long, G.L., and Ronen, D., 1994, Interaction of metals with mineral surfaces in a natural groundwater environment: Chemical Geology, v. 116, p. 111-121.

Gale, S.J., 1984, The hydraulics of conduit flow in carbonate aquifers: Journal of Hydrology, v. 70, p. 309-327.

Gerino, M., 1990, The effects of bioturbation on particle redistribution in Mediterranean coastal sediment. Preliminary results: Hydrobiologia, v. 207, p. 251-258.

Goldstein, S.J., and Jacobsen, S.B., 1988, Rare earth elements in river waters: Earth and Planetary Science Letters, v. 89, p. 35-47.

Griffin, R.A., and Shimp, N.F., 1976, Effect of pH on exchange-adsorption or precipitation of lead from landfill leachates by clay minerals: Environ. Sci. Technol., v. 10, p. 1256-1261.

Gupta, S.K., and Chen, K.Y., 1978, Arsenic removal of adsorption: J. Water Pollut. Control Fed. J., v. 50, p. 493-506.

Haskin, L.A., Frey, F.A., Schmitt, R.A., and Smith, R.H., 1966, Meteoric, solar, and terrestrial rare earth distributions, *in* Ahrens, L.H., Press, F., Runcorn,

S.K., and Urey, H.C., eds., Physics and Chemistry of the Earth, Volume 7: Oxford, Pergamon Press, p. 169-321.

Hauwert, N., 1996, personal communication.

Hauwert, N.M., 1995, Localization of sediment and trace metals along a karst conduit flow route in the Barton Springs segment of the Edwards Aquifer, *in* Hauwert, N.M., and Hanson, J.A., eds., A Look at the Hydrostratigraphic Members of the Edwards Aquifer in Travis and Hays Counties, Texas: Austin Geological Society Guidebook: Austin, Austin Geological Society, p. 39-51.

Hauwert, N., and Vickers, S., 1994, Barton Springs/Edwards Aquifer Hydrogeology and Groundwater Quality, submitted by the Barton Springs/Edwards Aquifer Conservation District to the Texas Water Development Board.

Hess, J.W., and White, W.B., 1988, Storm response of the karstic carbonate aquifer of southcentral Kentucky: Journal of Hydrology, v. 99, p. 235-252.

Ingle, J.C., Jr., 1966, The Movement of Beach Sand, Developments in Sedimentology, v.5: New York, Elsevier, 266 p.

Jacobson, R.L., and Langmuir, D., 1974, Controls on the quality variations of some carbonate spring waters: Journal of Hydrology, v. 23, p. 247-265.

Jarvis, J.C., Wildeman, T.R., and Banks, N.G., 1975, Rare earths in the leadville limestone and its marble derivates: Chemical Geology, v. 16, p. 27-37.

Kennedy, V.C., and Kouba, D.L., 1970, Fluorescent Sand as a Tracer of Fluvial Sediment, U.S. Geological Survey Professional Paper 562-E.

Krezoski, J.R., 1989, Sediment reworking and transport in eastern Lake Superior: *in situ* rare earth element tracer studies: Journal of Great Lakes Research, v. 15, p. 26-33.

Loveland, W., 1989, Environmental Sciences, *in* Bünzli, J.-C.G., and Choppin, G.R., eds., Lanthanide Probes in Life, Chemical and Earth Sciences: Theory and Practice: Amsterdam, Elsevier, p. 391-411.

Lynch, F.L., 1994, The effects of depositional environment and formation water chemistry on the diagenesis of Frio formation (Oligocene) standstones and shales, Aransas, Nueces, and San Patricio Counties, Texas [Ph.D. thesis]: Austin, University of Texas at Austin.

Maclay, R.W., and Small, T.A., 1984, Carbonate Geology and Hydrology of the Edwards Aquifer in the San Antonio Area, Texas, U.S. Geological Survey Open-File Report 83-537.

Mahaut, M.L., and Graf, G., 1987, A luminophore tracer technique for bioturbation studies: Oceanol. Acta., v. 10, p. 323-328.

McCarthy, J.F., and Zachara, J.M., 1989, Subsurface transport of contaminants: Environ. Sci. Technol., v. 23, p. 496-502.

McCarty, P.L., Reinhard, M., and Rittman, B.E., 1981, Trace organics in groundwater: Environ. Sci. Technol., v. 15, p. 40-51.

Millipore Corporation, 1989, Waters Ion Chromatography Cookbook, Volume Manual No. 20195, Revision 1.0.

Mull, D.S., Liebermann, T.D., Smoot, J.L., and Woosley, L.H., 1988, Application of dye-tracing techniques for determining solute-transport characteristics

of ground water in karst terranes: Atlanta, U.S. Environmental Protection Agency, EPA 904/6-88-001.

Muñoz-Páez, A., Alba, M.D., Castro, M.A., Alvero, R., and Trillo, J.M., 1994, Geometric structures of lanthanide ions within layered clays as determined by EXAFS: From the Lu(III) hydrate to the disilicate: Journal of Physical Chemistry, v. 98, p. 9850-9860.

Olmez, I., Pink, F.X., and Wheatcroft, R.A., 1994, New particle-labeling technique for use in biological and physical transport studies: Environmental Science and Technology, v. 28, p. 1487-1490.

Onishi, Y., 1981, Sediment-contaminant transport model: Journal of the Hydraulic Division, Proceedings of the American Society of Civil Engineers, v. 107, p. 1089-1107.

Paecht-Horowitz, M., and Eirich, F.R., 1988, The polymerization of amino acid adenylates on sodium-montmorillonite with preadsorbed polypeptides: Origins of Life and Evolution of the Biosphere, v. 18, p. 359-387.

Pankow, J.F., and McKenzie, S.W., 1991, Parameterizing the equilibrium distribution of chemicals between the dissolved, solid particulate matter, and colloidal matter compartments in aqueous systems: Environ. Sci. and Technol., v. 25, p. 2046-2054.

Papenguth, H.W., 1995, Metal sorption on dolomite surfaces: GSA Abstracts with Programs, p. A-198.

Plummer, L.N., Jones, B.F., and Truesdell, A.H., 1976, WATEQF: A FORTRAN IV version of WATEQ, a computer program for calculating chemical

equilibrium of Natural Waters, user's guide: Reston, U.S. Geological Survey WRI 76-13.

Rathbun, R.E., Kennedy, V.C., and Culbertson, J.K., 1971, Transport and dispersion of fluorescent tracer particles for the flat-bed condition, Rio Grande conveyance channel, near Bernardo, New Mexico, U.S. Geological Survey Professional Paper PO 562-I.

Reimus, P.W., Robinson, B.A., Nuttall, H.E., and Kale, R., 1996, Simultaneous transport of synthetic colloids and a nonsorbing solute through single saturated natural fractures, Volume 383: Mat. Res. Soc. Symp. Proc., Materials Research Society, p. 363-370.

Rose, P.R., 1972, Edwards group, surface and subsurface, Central Texas, Bureau of Economic Geology Report of Investigations 74.

Russell, W.H., 1996, Environmental evaluation of Blowing Sink Cave: The Texas Caver, v. 3, p. 3-16.

Ryan, M., and Meiman, J., 1996, An examination of short-term variations in water quality at a karst spring in Kentucky: Ground Water, v. 34, p. 23-30.

Saiers, J.E., and Hornberger, G.M., 1994, First- and second-order kinetics approaches for modeling the transport of colloidal particles in porous media: Water Resources Res., v. 30, p. 2499-2506.

Sayre, W.W., and Hubbell, D.W., 1965, Transport and dispersion of labeled bed material, North Loup River, Nebraska, U.S. Geological Survey Professional Paper PO 0433-C.

Schwarzenbach, R.P., Gschwend, P.M., and Imboden, D.M., 1993, Environmental Organic Chemistry: New York, John Wiley and Sons, Inc., 681 p.

Senger, R.K., 1983, Hydrogeology of Barton Springs, Austin, Texas [Masters thesis]: Austin, University of Texas at Austin.

Shuster, E.T., and White, W.B., 1971, Seasonal fluctuations in the chemistry of limestone springs: a possible means for characterizing carbonate aquifers: Journal of Hydrology, v. 14, p. 93-128.

Singh, B., and Sekhon, G.S., 1977, Adsorption, desorption and solubility relationships of lead and cadmium in some alkaline soils: J. Soil. Sci., v. 28, p. 271-275.

Slade, R.M., Jr., 1991, unpublished data.

Slade, R.M., Jr., Dorsey, M., and Stewart, S., 1986, Hydrology and water quality of the Edwards Aquifer associated with Barton Springs in the Austin Area, Texas, U.S. Geological Survey, WRI 86-4036.

Small, T.A., Hanson, J.A., and Hauwert, N.M., 1996, Geologic framework and hydrogeologic characteristics of the Edwards Aquifer outcrop (Barton Springs segment), Northeastern Hays and Southwestern Travis Counties, Texas, U.S. Geological Survey, WRI 96-4306.

Smith, J.A., Witkowski, P.J., and Fusillo, T.V., 1988, Manmade organic compounds in the surface waters of the United States--a review of current understanding: Denver, U.S. Geological Survey Circular 1007.

Stumm, W., and Morgan, J.J., 1981, Aquatic Chemistry: New York, John Wiley and Sons, 780 p.

Taylor, S.R., and McLennan, S.M., 1988, The significance of the rare earths in geochemistry and cosmochemistry, *in* Gschneidner, K.A., Jr., and Eyring, L., eds., Handbook on the Physics and Chemistry of Rare Earths, Volume 11: New York, Elsevier, p. 485-578.

Thrailkill, J., 1989, Shallow conduit-flow carbonate aquifers: conceptual models and parameter evaluation, *in* Moore, J.E., Zaporozec, A.A., Csallany, S.C., and Varney, T.C., eds., Recent Advances in Ground-water Hydrology, American Institute of Hydrology, p. 153-159.

Thurman, E.M., 1985, Organic geochemistry of natural waters: Dordrecht, Martinus Nijhoff/Dr W. Junk, 497 p.

Turner, D.R., Whitfield, M., and Dickson, A.G., 1981, The equilibrium speciation of dissolved components in freshwater and sea water at 25° C and 1 atm pressure: Geochim. Cosmochim. Acta, v. 45, p. 855-881.

United States Fish and Wildlife Service, 1994, Proposal to list the Barton Springs Salamander as endangered: Federal Register, v. 59, p. 7968-7978.

Veni, G., 1988, Implications of aquifer hydraulics on conduit development in karst regions, Karst Hydrogeology and Karst Environment Protection: IAH 21st Congress: Guilin, China, IAH, p. 417-420.

Wheatcroft, R.A., 1991, Conservative tracer study of horizontal sediment mixing rates in a bathyal basin, California borderland: Journal of Marine Research, v. 49, p. 565-588.

Wheatcroft, R.A., 1992, Experimental tests for particle size-dependent bioturbation in the deep ocean: Limnol. Oceanogr., v. 37, p. 90-104.

Wheatcroft, R.A., Olmez, I., and Pink, F.X., 1994, Particle bioturbation in Massachusetts Bay: Preliminary results using a new deliberate tracer technique: Journal of Marine Research, v. 52, p. 1129-1150.

White, E.L., and White, W.B., 1968, Dynamics of sediment transport in limestone caves: National Speleological Society Bulletin, v. 30, p. 115-129.

White, W.B., 1977, Characterization of karst soils by near infrared spectroscopy: The National Speleological Society Bulletin, v. 39, p. 27-31.

White, W.B., 1988, Geomorphology and Hydrology of Karst Terrains: New York, Oxford University Press, 464 p.

Wood, S.A., 1990, The aqueous geochemistry of the rare-earth elements and yttrium: Chemical Geology, v. 82, p. 159-186.

Wood, W.W., and Ehrlich, G.G., 1978, Use of baker's yeast to trace microbial movement in ground water: Ground Water, v. 16, p. 398-403.

Wu, S.-c., and Gschwend, P.M., 1988, Numerical modeling of sorption kinetics of organic compounds to soil and sediment particles: Water Resources Res., v. 24, p. 1373-1383.

Yevjevich, V., 1981, Introduction, Karst Water Research Needs: Littleton, CO, Water Research Publications.

The vita has been removed from the digitized version of this document.